JRC Scientific and Technical Reports

Impact Study of Unintentional Interference on GNSS Receivers

M. Wildemeersch, E. Cano Pons,
A. Rabbachin and J. Fortuny Guasch
EC Joint Research Centre
Security Technology Assessment Unit

EUR 24742 EN

JRC
EUROPEAN COMMISSION

ipsc
Institute for the Protection and Security of the Citizen

The mission of the IPSC is to provide research results and to support EU policy-makers in their effort towards global security and towards protection of European citizens from accidents, deliberate attacks, fraud and illegal actions against EU policies

European Commission
Joint Research Centre
Institute for the Protection and Security of the Citizen

Contact information
Address: Centro Comune di Ricerca
Via E. Fermi 2749, 21027 Ispra (VA), Italy

E-mail: Joaquim.Fortuny@jrc.ec.europa.eu
Tel.: +39 0332 785104
Fax: +39 0332 786565

http://www.jrc.ec.europa.eu

JRC62607

EUR 24742 EN
ISBN 978-92-79-19523-5
ISSN 1018-5593
doi:10.2788/57794

Luxembourg: Publications Office of the European Union

Printed in Italy

Executive Summary

This work has been performed in the context of an Administrative Arrangement for DG HOME. The overall scope is to perform an impact assessment of radio frequency (RF) interference on critical infrastructures relying on GNSS-services for timing and synchronization purposes. In WP3, the analysis has been divided into the impact of intentional interference on critical infrastructures presented in WP3.1 and the analysis of unintentional interference, covered in this report. DVB-T has been identified as the most important source of unintentional interference in the GNSS frequency bands and therefore a special attention is paid to this interference source.

The main motivation to assess the performance reduction of receivers due to unintentional interference, is related to the high probability of these events. Unintentional interference stems from out-of-band emissions or spurious transmissions. Four different scenarios have been considered in this work, covering (i) additive white Gaussian noise, (ii) continuous wave interference, (iii) pulsed continuous wave interference and (iv) interference that stems from the third harmonic of DVB-T transmissions. All these scenarios are highly relevant and are frequently observed in realistic signal conditions. The scenario of DVB-T interference receives most of the attention in this work, since DVB-T has become the most widely adopted digital terrestrial television broadcasting standard in the world. Harmonics of the DVB-T signal could possibly fall together with the GPS L1 or Galileo E1 bands and as such become a threat. DVB-T services are operational in more than 40 countries, with more than 75% of the deployment in Europe. In the coming years, DVB-T is expected to be deployed in more than 100 countries.

In the frame of this work, different tools have been developed to quantify the impact of unintentional interference. First, a laboratory testbed has been set up, that allows to take real GPS L1 signals, combine them with synthetic interfering signals and test the robustness of different commercial and professional receivers. Further, in order to have a full control of the signal characteristics and the implementation details of the receiver, a simulation platform has been developed. This simulation tool generates GNSS as well as interfering signals, and observes consequently the impact on the acquisition or tracking performance for different receiver implementations. Finally, since it is difficult to reach statistical significance for the acquisition performance, an analytical tool has been developed allowing to evaluate the effects of interference.

This report summarises the relevant results for the four considered scenarios. For the assessment of the acquisition performance the analytical tool and the simulation platform have been used. In order to evaluate the tracking performance, experimental work has been conducted with real receivers and simulations have been performed. For the acquisition, the report quantifies how much the probability of detection and the probability of false alarm are affected by the presence of interference. For the tracking, the main result of this report is the quantification of the signal degradation in terms of C/N_0 and in terms of the variance of the position solution. In the scenario of DVB-T

interference, the degradation of the signal quality has been determined as a function of the DVB-T third harmonic power and the distance between the victim receiver and the DVB-T base station.

Contents

1 Outline

The Institute for the Protection and Security of the Citizen of the EC Joint Research Centre (IPSC-JRC) has been mandated, in the context of the AA for DG HOME, to perform a study on the Radio Frequency (RF) threat against telecommunications and ICT control systems. The study consist of 3 work packages:

WP1 - Study on European capabilities encompasses an inventory of existing European capabilities (theoretical and practical) for the analysis of RF threats in the EU Member States. This overview covers EM immunity tests, simulation of jamming, current detection-, localisation- and mitigation methods for threat agents.

WP2 - Preliminary RF risk and threat assessment covers a risk and threat assessment of some significant RF threats to telecommunications and ICT control systems. In this WP distinction will be made between high and low energy RF threats.

- ☑ WP2.1 covers the first group of HERF threats. To this group belong the electromagnetic pulses (EMP), inducing physical damage to all types of conducting networks.
- ☑ WP2.2 deals with low energy RF threats and focuses on Global Navigation Satellite Systems and the consequences of service disruption.

WP3 - RF threats technical analysis builds further on WP2.2 and combines theoretical analysis, simulation and experimental work, related to the RF interference on Global Navigation Satellite Systems (GNSS) receivers. The following activities are covered:

- ☑ WP3.1 focuses on the time and synchronisation applications that make use of GNSS signals. The study starts with the identification of the critical infrastructures relying on GNSS signals for timing and synchronisation. The impact of denial of GNSS service is assessed for those critical infrastructures. Moreover, some preliminary results on timing drift are presented and an outline is given of the future activities on timing and synchronisation.
- ☑ WP3.2 discusses the robustness of GNSS receivers with regard to unintentional interference. The standards and services that could possibly deteriorate the receiver performance are first identified. The theoretical analysis focuses on the acquisition of GNSS signals. We dedicate special attention to the case study of GNSS signals in presence of DVB-T. The performance analysis is also conducted by simulation. An emulator of a complete GNSS system is presented. The emulator comprises a signal generator for GNSS and interfering signals, a channel model, a receiver front-end and a SW defined receiver, performing the signal demodulation, decorrelation and performance analysis. The performance degradation in different interference scenarios is discussed. Finally,

results of an extensive measurement campaign are presented by comparing the interference impact on commercial and professional receivers.

This document covers WP3.2.

2 Problem Statement

The GNSS signal power is extremely low, due to the long satellite-receiver distance. Consequently, it is fairly easy to disturb the signal detection and tracking. Nonetheless, GNSS signals are used in a wide variety of critical infrastructures for applications related to navigation, but as well for applications related to timing and synchronisation.

GNSS can be considered as a critical infrastructure on itself and has a cascading effect on other critical infrastructures. Within the field of navigation, there are critical applications for emergency services, the tracking of hazardous goods and law enforcement. In order to emphasise the relevance of a vulnerability assessment on navigation applications, we consider in more detail the fisheries Vessel Monitoring System (VMS). In this system, a tracking system records and reports nearly real-time its position. Nearly all trackers are composed of a GNSS receiver module and a communications module for transmission of the positions to a public or commercial organisation. Every such GNSS-based tracker is vulnerable to tampering. The financial profit deriving from the tampering depends largely on the application domain. In [1], the hardening techniques for GNSS-based trackers for fisheries monitoring are discussed. In the context of over-fishing, vessels are equipped with a VMS unit to enforce fishermen to respect the regulated fishing areas. The report mentions a profit from illegal fishing for a large vessel of 3.4 million GBP over two years. While the unsophisticated adversary may use a metal barrier to block radiofrequency wave reception and emission, a more sophisticated attack could be set up introducing real looking but falsified tracking information. The technical and time requirements to develop a GPS spoofer on a Software Defined Radio (SDR) or FPGA platform are not unsurmountable. This spoofer could circumvent classical GPS receiver integrity checks and the falsified position information consequently impairs the authenticity of the tracker outgoing message.

In WP3.1 a preliminary study has been performed on the vulnerability of the timing and synchronisation applications based on GNSS. In this study, the focus was clearly on intentional interference, stemming from a jamming or a spoofing attack. While deliberate jamming is definitely a realistic and feasible interference scenario, a sophisticated spoofing attack is still considered as a low probability event. In [2] for instance, the authors did an informal survey with several high quality GPS receiver manufacturers. They recognised the spoofing vulnerability, but at the same time they appeared very skeptical about the spoofing threat.

As stated before, the likeliness of an intentional jamming attack is relatively high while the probability of a spoofing attack remains relatively low. Yet, both forms of intentional interference could have serious effects on critical infrastructures. In spite of that, unintentional interference is ubiquitous and thus, a high probability event. This report aims to assess the impact of unintentional interference. Unintentional interference can originate from spurious emissions or out-of-band emissions. Spurious emissions can be consist of harmonics, parasitic emissions or intermodulation products. The most

simple case of spurious emission is a single continuous wave interference (CWI). Further, we consider the impact of pulsed CWI (PCWI) and Digital Video Broadcasting (DVB-T). The report consists of three parts that cover all steps in the GNSS signal processing. In Section 3 the impact of interference on the acquisition is discussed. In the remaining part of the report the tracking is discussed. In Section 4 the deleterious effects of interference on the signal quality are monitored for real GPS receivers, while in Section 5 the interference effects are simulated.

3 Detailed analysis of the acquisition of GNSS signals

The objective of this section is to assess the robustness of the acquisition process for GNSS receivers in the presence of interference. The acquisition of GNSS signals yields the necessary information to start the tracking of the signals. The acquisition is a process that is performed continuously in real receivers, in parallel with the tracking of the signals. That is, satellites can get out of view for a number of reasons. The satellites con disappear behind the horizon, in urban canyon there can be signal blockage or the entire constellation can disappear when a receiver is used indoors or in a tunnel. The acquisition process is fundamental to allow the receiver operation and thus, it is very relevant to study the impact that interference can have on the acquisition.

It is however not trivial to test the acquisition performance of real receivers. The acquisition is a probabilistic problem and it is extremely cumbersome to reach statistical significance. Moreover, in a realistic environment, all parameters that are estimated by the acquisition process vary, which could possibly lead to biased results. Therefore, we assess the acquisition performance by means of theoretical analysis and by simulation. This approach allows to have a full control of the testing environment and further, it allows as well to reach statistical significance.

In the following sections, we discuss different interference scenarios. We start the analysis with the case of white noise. Further, narrowband interference is considered as a single tone. Finally, we discuss wideband interference originating from Digital Video Broadcasting (DVB-T), which is largely deployed in Europe.

3.1 Acquisition: a classical detection problem

The theoretical analysis that will be presented hereafter covers the acquisition process within a GNSS receiver. The acquisition of a GNSS signal can be considered as a classical detection problem, where the signal of interest is buried in noise. The outcome of the acquisition process is twofold. First a decision is made on the presence or absence of the signal of interest. In case the signal is present, a rough estimate is returned of the code phase and carrier frequency of the signal of interest. The incoming signal is impaired by noise and interference and gets processed, yielding a decision variable (Figure 1). This decision statistic is calculated by downconverting the incoming signal and by correlating the downconverted signal with a local replica of the code. The resulting decision variable is a random variable and is subsequently compared with a threshold, thus determining the presence of the signal. The probability that the decision variable passes the threshold is called the detection probability if the signal is present; it is called the false alarm probability if the signal is absent. The probability density functions (pdf) of the decision variable (in presence and absence of the signal of interest) determine the overall performance of the detection process. The performance of the acquisition process is often studied in terms of receiver operating curves (ROC) [3]. The receiver operating characteristic completely defines the performance of the decision test, i.e. of the acquisition

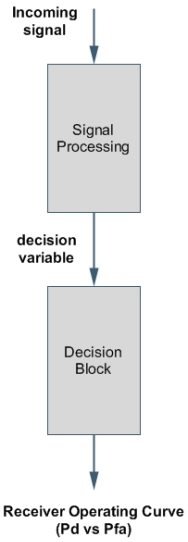

Figure 1: acquisition as a classical detection problem

process. It puts the probability detection as a function of the probability of false alarm. It is important to define clearly those 2 concepts. Therefore, two hypothesis are defined:

1. H0: the signal is not present, or the signal is not aligned correctly with the local replica and the carrier. Under this hypothesis, the probability of false alarm is defined as follows

$$P_{fa}(\beta) = P(S > \beta | H_0) = P(S > \beta | \tau \neq \tau_0 \cup f_d \neq f_{d,0}) \tag{1}$$

2. H1: the signal is present and the local replica and the carrier are correctly aligned. Under this hypothesis, the probability of detection is defined as the probability that the decision variable is bigger than a defined threshold.

$$P_d(\beta) = P(S > \beta | H_1) = P(S > \beta | \tau = \tau_0 \cap f_d = f_{d,0}) \tag{2}$$

Goal of the analysis that will be presented hereafter, is to get an expression of the probability of detection and the probability of false alarm in different scenarios. GNSS signal will be considered in the presence of noise and different types of interference.

3.2 System Model

In this section, we present the signal model for the GNSS signal and the interference. The widespread use of software-defined receivers suggests the use of a discrete signal model. As has been explained in Section 3.1, the incoming signal is first digitised, down-converted and subsequently passed through a correlator block. The signal presented at

the acquisition block has the following form:

$$s[n] = \sum_{i=1}^{N_{sat}} r_i[n] + i[n] + \eta[n]. \tag{3}$$

We notice that the incoming signal is composed of 3 terms: the sum of N_{sat} satellite signals $r_i[n]$, the interference $i[n]$ and additive white Gaussian noise $\eta[n]$.

3.2.1 GNSS Signal Model

The signal received from a single satellite can be represented as

$$r_i[n] = \sqrt{2C_i}c_i[n-\tau_i]d_i[n-\tau_i]\cos[2\pi(f_{IF} + f_{d,i})n + \phi_i], \tag{4}$$

where C_i is the GNSS signal power, c_i is the code with corresponding phase delay τ_i, f_{IF} and $f_{d,i}$ are the discrete equivalents of the intermediate frequency and the doppler frequency, ϕ_i is the carrier phase delay introduced by transmission.

3.2.2 Noise Model

Additive White Gaussian Noise (AWGN) has a variance of $\sigma_n^2 = \frac{N_0 f_s}{2}$, with $N_0/2$ the power spectral density (PSD) of the noise and f_s the sampling frequency.

3.2.3 Interference Model

In this report, different types of interference will be discussed. Concerning the acquisition, the interference study will be limited to continuous wave interference (CWI) and Digital Video Broadcasting - Terrestrial (DVB-T). The interference models will be introduced in the corresponding sections.

3.3 Acquisition Performance in the Presence of AWGN

The decision statistic $X(\tau, f_d)$ is a bi-dimensional function over the codephase τ and the doppler frequency f_d. For direct sequence spread spectrum (DSSS) systems, literature gives expressions for the probability of false alarm and the probability of missed detection in the case of serial search techniques, maximum search techniques or hybrid forms [3, 4]. Specific expressions for the scenario of GNSS signals have as well been studied [5]. The incoming signal at the receiver can be represented as

$$s[n] = \sqrt{2C}c[n-\tau_0]d[n-\tau_0]cos(2\pi f_{d,0}n + \phi_0) + i[n] + \eta[n] \tag{5}$$

where the first term is the signal of interest, consisting of the code (c), the data bit(d) and the carrier. Further, I_{IF} is the interference term and N_{IF} represents Additive White

Gaussian Noise (AWGN). In the detector block (Figure 2), the incoming signal is first multiplied with a local oscillator

$$s_I[n] = s[n]cos(2\pi F_D n) \quad (6)$$

$$s_Q[n] = s[n]sin(2\pi F_D n) \quad (7)$$

Subsequently the downconverted signal is decorrelated, i.e. a multiplication with a local

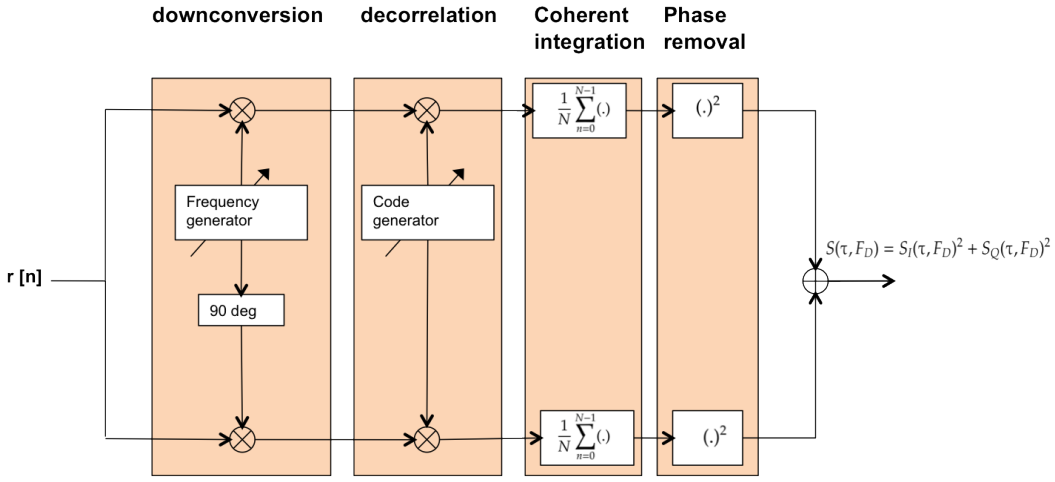

Figure 2: detector block

replica of the CDMA code, followed by a sum-and-dump operation. This is expressed as follows

$$S_I(\tau, F_D) = \frac{1}{N}\sum_{n=0}^{N-1} s_I[n]c[n-\tau] = s_I[\tau] \otimes h_c[\tau] \quad (8)$$

$$S_Q(\tau, F_D) = \frac{1}{N}\sum_{n=0}^{N-1} s_Q[n]c[n-\tau] = s_Q[\tau] \otimes h_c[\tau] \quad (9)$$

Finally, by removing the dependency of the carrier phase, the decision statistic is defined

$$S_{I,Q}(\tau_0, f_{d,0}) = S_I(\tau_0, f_{d,0}) + jS_Q(\tau_0, f_{d,0}) \quad (10)$$

$$S(\tau, f_d) = S_I(\tau, f_d)^2 + S_Q(\tau, f_d)^2 = S_s + S_N \quad (11)$$

Since all operations in the detector block are linear, the three components (useful signal, interference and noise) can be discussed separately. First, the useful signal and the noise will be treated. The useful signal is supposed to be deterministic. Hence, the input of the squaring action, $S_{I,Q}$, is a Gaussian random variable. In [5], the author shows that under the null hypothesis, we found a Gaussian random variable with mean equal to zero

$$H_0 : \begin{cases} E[S(\tau, f_d)] = 0 \\ Var[S_I(\tau, f_d)] = Var[S_Q(\tau, f_d)] = \sigma^2 \end{cases} \quad (12)$$

The square of this variable has a Chi-square distribution with two degrees of freedom, i.e. an exponential distribution

$$f_0(S(\tau, f_d)) = \begin{cases} \frac{1}{2\sigma^2}\exp(-\frac{S}{2\sigma^2}) & S > 0 \\ 0 & S \leq 0 \end{cases} \tag{13}$$

which leads to the expression of the probability of false alarm

$$P_{fa}(\beta) = \int_{\beta}^{+\infty} f_0(S)dS = exp\Big(-\frac{\beta}{2\sigma^2}\Big) \tag{14}$$

Under the H1 hypothesis, $S_I(\tau, f_d)$ and $S_Q(\tau, f_d)$ are no longer zero mean variables; instead, we have

$$H_1 : \begin{cases} E[S_I(\tau, f_d)] &= \frac{A}{2}cos(\phi_0) \\ E[S_Q(\tau, f_d)] &= \frac{A}{2}sin(\phi_0) \\ Var[S_I(\tau, f_d)] &= Var[S_Q(\tau, f_d)] = \sigma^2 \end{cases} \tag{15}$$

which leads to the expression of the distribution of the decision statistic, a non-central chi-square distribution with non-centrality parameter μ

$$f_1(S(\tau, f_d)) = \begin{cases} \frac{1}{2\sigma^2}exp\Big(-\frac{S+\mu}{2\sigma^2}\Big)I_0\Big(\frac{\sqrt{S\mu}}{\sigma^2}\Big) & S > 0 \\ 0 & S \leq 0 \end{cases} \tag{16}$$

Finally, integration of this distribution from the threshold to infinity, yields the probability of detection.

$$P_d(\beta) = Q_1\Big(\sqrt{\frac{\mu}{\sigma^2}}, \sqrt{\frac{\beta}{\sigma^2}}\Big) \tag{17}$$

The performance of the detector block can now be appreciated in Figure 3.

3.4 Acquisition Performance in the Presence of CWI

In [6], a theoretical study on the acquisition performance in the presence of CWI is presented. We are not going to repeat this theoretical analysis, but instead we present here the simulation results of the impact of CWI on the acquisition process. A simulator has been developed which consists of a signal generator, a channel model, a front-end and a SW defined receiver that performs acquisition, tracking and performance analysis.

The acquisition has been processed by Monte Carlo simulations. In order to quantify the probability of detection, a GNSS signal has been generated after which the receiver calculates the decision statistic. Every time a signal is generated, a data bit is created randomly and a different realisation of the noise and the interference is used. This process has been repeated 10000 times. The obtained values of the decision statistic are subsequently compared with different threshold values, yielding the probability of detection as a function of the threshold. For calculating the probability of false alarm, a signal is generated consisting again of a useful signal, noise and interference. During acquisition, the incoming signal is correlated with a local replica of a code different than

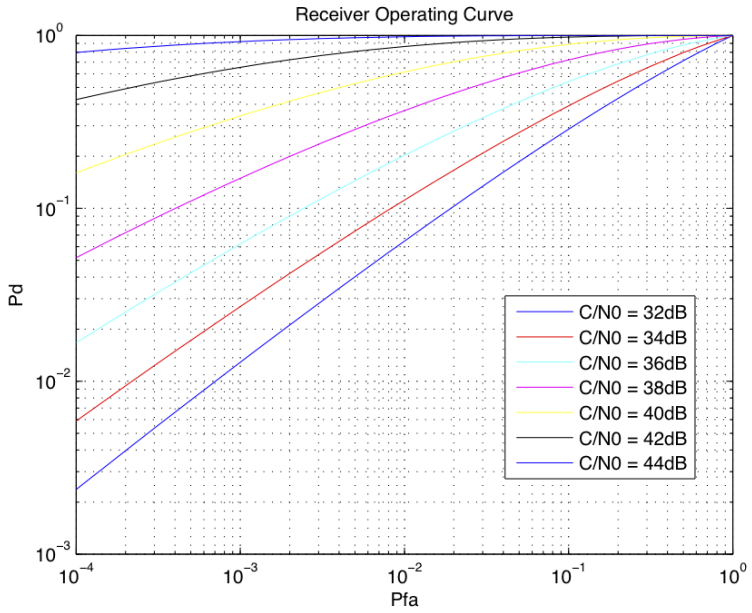

Figure 3: ROC curve of GPS signal in presence of white noise

the one of the generated signal. The decision statistic is again calculated and compared with different values of the threshold, yielding the probability of false alarm as a function of the threshold. It is possible that this approach underestimates the probability of false alarm, since only one satellite signal is considered in this scenario. Another approach could be a scenario where the decision statistic is calculated using a signal only containing noise. We chose however a scenario that approximates realistic signal conditions, that is, the signal conditions are simulated corresponding with open sky-view where there are always several satellites in view. A constellation of 8 satellites is generated. In this case the probability of false alarm is a function of the sum of the cross-correlations with the different PRN's that correspond to the satellites in view.

In the theoretical analysis of section 3.3, only one decision statistic has been used, being the maximum value of the search space. This reduced the mathematical complexity to a large extent. In this section however, we introduce also another decision statistic and the simulations will be repeated correspondingly. Decision statistics can differ from the correlation peak over the search space, for instance by referring the correlation peak to the noise level, or to other peak values in the search domain. Also other parameters have an impact on the acquisition performance, as for instance the coherent integration time.

Three scenarios have been simulated, that can be summarised as follows:

1. CW interference fixed, changing the value of C/N_0
2. C/N_0 fixed, changing the frequency of the CW interference

3. refer decision variable to second highest peak in the search domain

3.4.1 Acquisition with Changing Signal Quality

In the first scenario, a signal is generated containing the useful signal (PRN 15), noise and CW interference at the worst line. For this PRN code this means that the CW interference is added at the central frequency + 69kHz; the power of the interfering signal is set at -150dBW; every cell of the bi-dimensional search space is defined as $S(\tau, F_D) = S_I(\tau, F_D)^2 + S_Q(\tau, F_D)^2$, and let the decision statistic be defined by $\max\{S(\tau, F_D)\}$, as defined in section 3.3. The results are gathered in Figure 4. The ROC curve illustrates that a reduction of the signal quality leads to a considerable reduction of the acquisition performance.

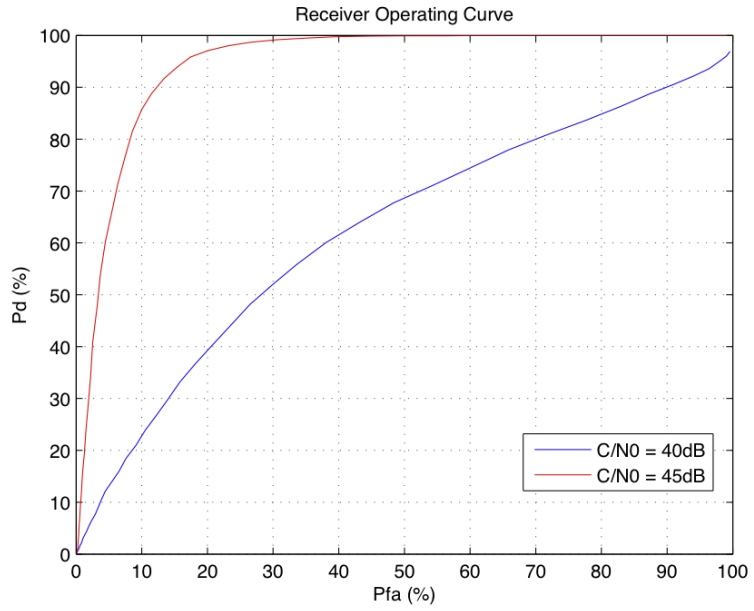

Figure 4: ROC curve - changing signal quality

3.4.2 Acquisition changing the frequency of the CWI

In this scenario, a signal is generated consisting of the useful signal, noise and CW interference term. The interference power is set at -150 dBW, while the frequency is fixed at (i) the worst line of the line spectrum of the considered PRN code, (ii) at half the main lobe of the GNSS signal, and (iii) at the first null. Simulation results are gathered in Figures 5 and 6, illustrating the probability of detection as a function of the threshold and the ROC curve, respectively. In Figure 5, the threshold has been normalised in order to compare the different results. We note that the probability of detection decreases faster

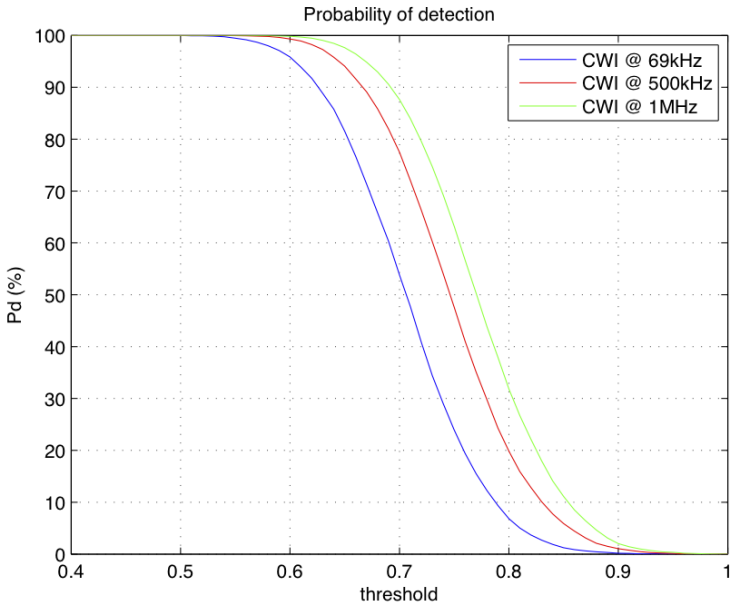

Figure 5: simulating changing frequency CWI

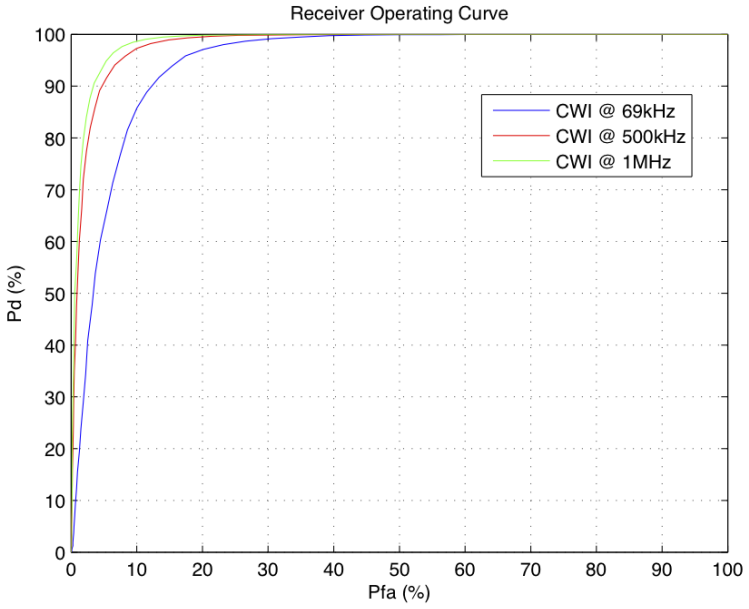

Figure 6: ROC curve - changing frequency CWI

when the interference is positioned at the highest spectral line of the PRN code under test. In Figure 6, one can appreciate again the reduction of the acquisition performance

when the CWI is positioned at the strongest line of the considered PRN. Moreover, we can quantify how much the acquisition performance is affected by the CW interference.

3.4.3 Acquisition with a different decision statistic

In literature however, a decision statistic that is frequently used is the ratio between the largest and the second largest correlation peak in the search domain [7, 8]. The idea was introduced as a detection confidence measure in [9]. Setting threshold levels in a changing RF environment can be very challenging. It can be shown that the false alarm probability is independent of the noise power spectral density, when the ratio of correlation peak values is used. Thus, the choice of this decision statistic allows a fixed setting of the threshold.

In this scenario, a signal is generated consisting of a useful signal and noise. The decision statistic used in this analysis is represented by

$$S(\tau, f_d) = \frac{S_I(\tau_1, f_{d,1})^2 + S_Q(\tau_1, f_{d,1})^2}{S_I(\tau_2, f_{d,2})^2 + S_Q(\tau_2, f_{d,2})^2} \tag{18}$$

where the index 1 and 2 indicate the codephase and the doppler frequency corresponding to the highest and the second highest peak in the search space. The coherent integration time is set to 10ms. The results have been plotted for different values of the signal quality and are illustrated in Figure 7. This figure illustrates in the first place the effect

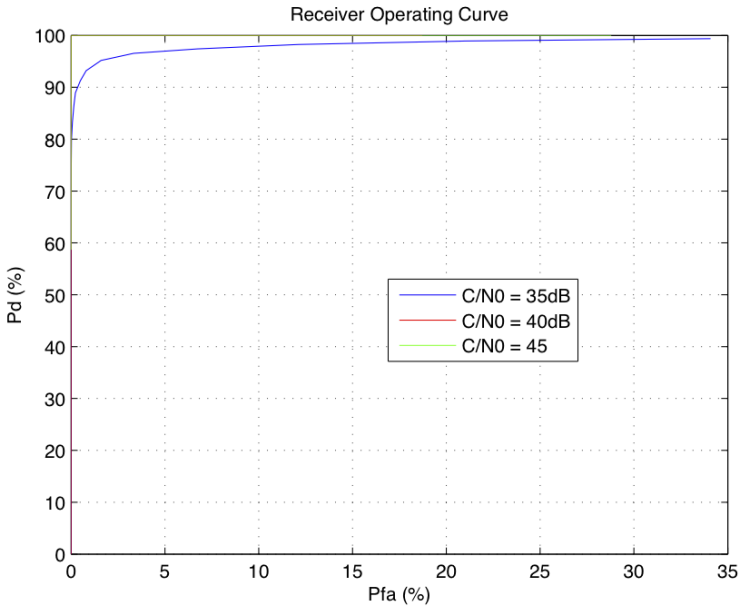

Figure 7: ROC curve - altering the decision statistic

of the increased integration time and corresponding processing gain, rather than the

effect of the decision variable. The reason to use this decision metric is most probably related to the fact that a preliminary noise estimation does not have to be performed, and that a fixed threshold can be set. However, there is no indication that the ratio of correlation values performs better than the maximum likelihood estimation [3].

3.5 Acquisition Performance in the Presence of DVB-T

In this analysis we study the acquisition performance in the presence of terrestrial Digital Video Broadcasting (DVB-T) signals [10]. DVB-T is the European standard for the broadcasting of digital terrestrial television and has been adopted in many countries, mainly in Europe, Asia and Australia. The standard uses an OFDM modulation and the frequency bands are indicated in the VHF III (174-230MHz), UHF IV (470-582 MHz) and UHF V (582-862MHz) band. None of those frequency bands fall together with the frequency bands allocated for GNSS signals. However, the second harmonics of UHF IV and the third harmonics of UHF V could coincide with the GPS L1 or Galileo E1 band and could form a real threat.

3.5.1 Equivalence between DVB-T and AWGN

There are different kinds of implementations of the DVB-T signal, basically changing the number of subcarriers and the bandwidth. The DVB-T signal and its harmonics can be written as [11]

$$s_{k,p}[n] = \left\{ \frac{1}{\sqrt{M}} \sum_{i=0}^{M-1} S_{k,i} exp\left(j2\pi \frac{in}{M}\right) \right\}^p; \quad p = 1, 2, 3 \tag{19}$$

where k represents the number of the OFDM symbol, n denotes the sample within the symbol k, i is the subcarrier, $S_{k,i}$ represents the constellation point and the power p is the order of the harmonic.

In [12], the spectral separation coefficient (SSC) has been introduced as a reliable measure to account for the interaction between the interference and the correlator in the acquisition block. The SSC is a power independent metric, that can be described as

$$\rho = \int_{-B/2}^{B/2} G_{\mathrm{i}}(f) G_{\mathrm{s}}(f) df, \tag{20}$$

with B the front-end bandwidth, G_{i} the normalised power spectral density (PSD) of the interference and G_{s} the normalised PSD of the GNSS signal. The multiplication and integration with the local replica of the code can be represented by an equivalent filter. The Fourier transform of this equivalent filter is represented by $G_{\mathrm{s}}(f)$. Thus, the SSC characterises the interference impact, based on the spectral shape of the interference and the spectral shape of the equivalent filter of the correlator, which depends on the GNSS modulation. The second or the third harmonic of DVB-T can partially coincide or completely overlap with the GPS L1 or Galileo E1 band. It is important to determine and quantify the impact of DVB-T interference on different GNSS modulations. We want

to demonstrate that DVB-T has a very similar impact on different GNSS modulations. To that purpose, we present a case study that considers GPS BPSK and Galileo BOC(1,1). We evaluate the SSC for those two modulations, with an assumed front-end bandwidth of 10MHz. Figure 8 reports the SSC values for both GPS and Galileo. The x-axis represents the difference between the centre frequencies of the GNSS signal and the interference. In this case study the interference is the third harmonic of a DVB-T signal. The plot illus-

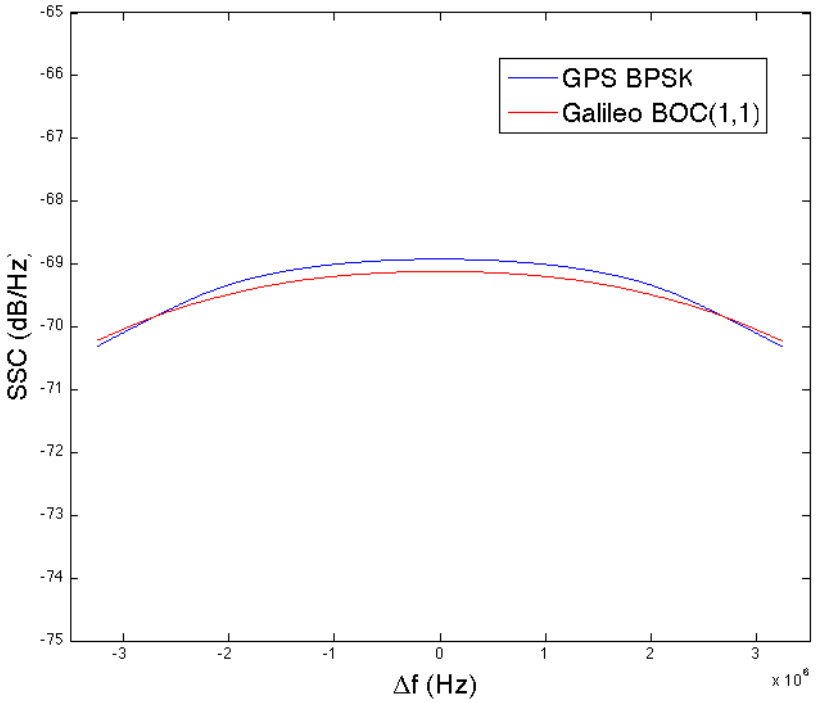

Figure 8: Spectral separation coefficient for GPS L1 CA and Galileo BOC(1,1)

trates that the third harmonic of DVB-T has almost equal values of the SSC for both the GPS and Galileo modulations. As a consequence, no differences are expected between GPS BPSK and Galileo BOC(1,1). In what follows, theoretical expressions are derived for a general GNSS signal model. We will compare analytical results and simulations for GPS L1 C/A signal. However, as indicated above, those results are valid as well for Galileo E1 BOC(1,1).

So far the performance of the acquisition has been discussed in the scenario where the signal of interest is impaired by the presence of white noise or by continuous wave interference. Here, we want to find how DVB-T interference contributes to the decision statistic. Since the DVB-T is composed of a large number of subcarriers, the signal can be modelled as a sum of continuous wave interference terms. An theoretical impact assessment of continuous wave interference on the GNSS acquisition performance

has been reported in [6]. One could try to expand this study to the case of the sum of CWI. However, the mathematical complexity increases dramatically, especially when the higher order harmonics are considered. Hence, the contribution of the DVB-T interference term has been determined experimentally. Figure 9 shows the histogram of the

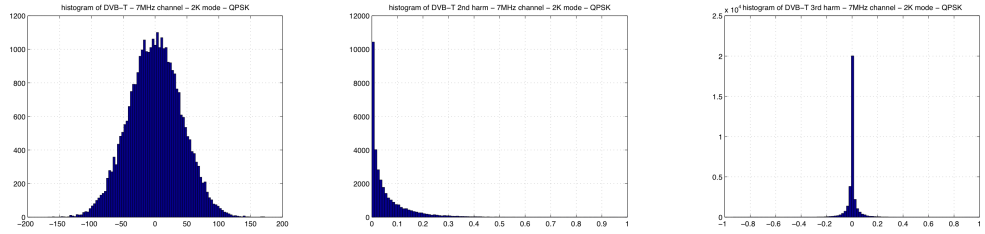

(a) DVB-T (b) 2nd harmonic (c) 3rd harmonic

Figure 9: Histogram of DVB-T and harmonics

DVB-T signal, its second and its third harmonic. While the DVB-T signal demonstrates a zero-mean normal distribution, this is not the case for the second and the third harmonic. The GNSS receiver is now fed with the DVB-T signal, its second and its third harmonic. Downconverting and decorrelating those signals yields the contribution of the DVB-T interference to the decision statistic, S_{int} in Formula 11. This is illustrated in Figure 10. The main conclusion is that while the second and third harmonic of the DVB-T signal do not feature a Gaussian distribution, the contribution to the decision statistic of the DVB-T signal and its second and third harmonic are distributed normally. This can be understood by the central limit theorem, since the integration in the correlator corresponds to the sum of a large number of independent, identically distributed variables, which yields a normal distributed random variable. This simplifies to a large extent the analysis. In

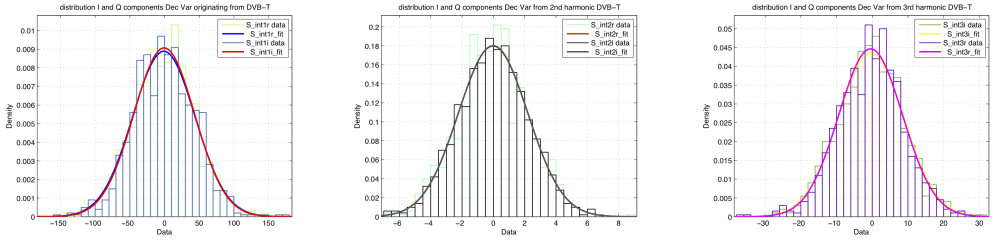

(a) DVB-T (b) 2nd harmonic (c) 3rd harmonic

Figure 10: Contribution to decision variable from DVB-T and harmonics

$S_{I,Q}(\tau, F_D) = S_{\text{s}} + S_{\text{int}} + S_{\text{N}}$, the contribution of the interference and the noise are both normally distributed, thus

$$S_{\text{int}} + S_N \sim \mathcal{N}_c(0, (\sigma_{int}^2 + \sigma_n^2) I_2) \tag{21}$$

and the analysis is reduced to the former case with the signal of interest corrupted by

white noise. Figure 11 illustrates the impact of a changing value of the signal-to-interference ratio (SIR). All curves start with a value of $C/N_0 = 40$dB, after which interference is

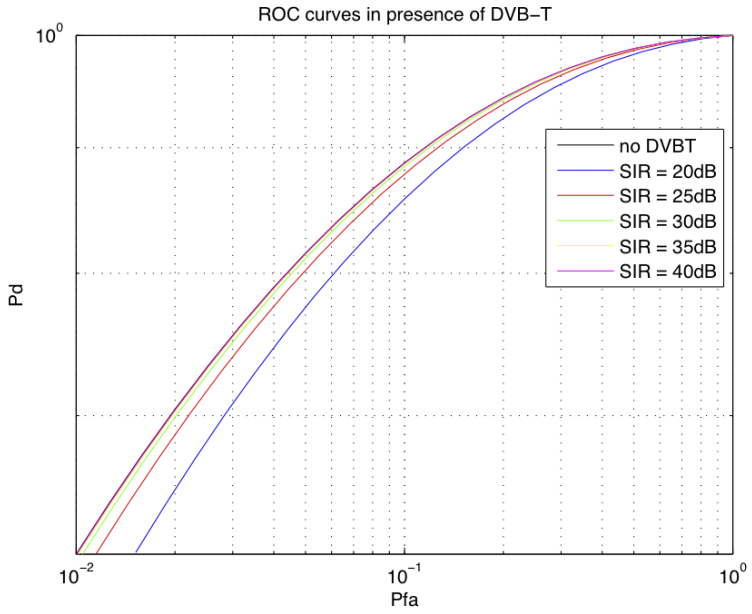

Figure 11: ROC curves for different SIR values

added. The figure visualises quantitatively the performance reduction of the acquisition process for different values of the SIR.

3.5.2 Adding Fading to the Acquisition Analysis

So far, the effect of the variations over time of the received signal power has not been taken into account. In this section, fading will be introduced on the signal of interest and on the interference. The acquisition performance depends on the probability distribution functions of the decision variable, under the two defined hypothesis. In 3.5, it has been shown that the DVB-T signal introduces an additional Gaussian contribution to the decision statistic

$$S = \left| \sqrt{h} S_s + \sqrt{A} S_{\text{int}} + S_N \right|^2, \tag{22}$$

with $S_{IN} = \sqrt{A} S_{\text{int}} + S_N \sim \mathcal{N}_c(0, \sigma^2_{IN|A})$ and $\sigma^2_{IN|A} = A\sigma^2_{\text{int}} + \sigma^2_N$. In order to derive an expression of the probability of false alarm and the probability of detection, we derive an expression of the decision statistic considering fading for both the GNSS signal and the interfering signal. The fading on the GNSS signal is represented by the random variable h, while the fading on the interfering signal is represented by A. Conditioning on the fading random variables related to the GNSS signal and the interference, the decision statistic

is a non-central Chi-square distribution, given by

$$S(\tau, F_D)_{|h,A} \sim \mathcal{X}\left(\frac{hS_s^2}{A\sigma_{\text{int}}^2 + \sigma_{\text{N}}^2}, 2\right). \tag{23}$$

The probability of detection can be derived, by making use of the characteristic function (CF) of the decision statistic. The CF of a Chi-square random variable can be expressed as [13]

$$\Psi_S(js|h, A) = \left(\frac{1}{1 - 2js\sigma_{\text{IN}}^2}\right) \exp\left\{\frac{jshS_s^2}{1 - 2js\sigma_{\text{IN}}^2}\right\} \tag{24}$$

Calculating the expectation value over h yields the CF of the decision statistic, conditioned on the random variable A

$$\Psi_S(js|A) = \mathbb{E}_h\left\{\Psi_S(js|h, A)\right\} = \left(\frac{1}{1 - 2js\sigma_{\text{IN}}^2}\right) \Psi_h\left(\frac{jsS_s^2}{1 - 2js\sigma_{\text{IN}}^2}\right) \tag{25}$$

Using the inversion theorem, the cumulative distribution function (CDF) can be calculated, leading to an expression of the probability of detection, conditioned on A.

$$P_{\text{d}}(\beta|A) = 1 - \left(\frac{1}{2} - \frac{1}{\pi}\int_0^\infty \frac{\Psi(-js|A)e^{js\beta} - \Psi(js|A)e^{-js\beta}}{js} ds\right) \tag{26}$$

This expression allows to separately study the effect of fading on the signal of interest and fading on the interfering signal. Integrating over a large number of values of A, the effect of fading on useful and interfering signal can be studied simultaneously.

We discuss now scenarios where the effects on fading are considered separately on the GNSS signal and on the interfering signal. In Figure 12 the effect of fading on the interfering signal is illustrated for different values of the signal-to-interference ratio (SIR). All curves are obtained with a $C/N_0 = 40\text{dB}$ and a coherent integration time equal to 1 ms. The curves in dashed lines consider Rayleigh fading, affecting the interfering signal. Rayleigh fading considers the case where there is no strong line of sight (LOS) component. By adding fading on the interfering signal, the performance of the acquisition process improves. In Figure 13, the interference has been studied for a single value of $\text{C/N}_0 = 40\text{dB}$ and $\text{SIR} = 10\text{dB}$. In this scenario, different fading distributions have been simulated. In the case of a Ricean distribution, there is a LOS component present. The value of the Rice factor k indicates the ratio between the power of the LOS component and the power of the remaining components. For low values of the Rice factor, the Ricean random variable reduces to a Rayleigh random variable. The figure illustrates that as the Rice factor increases, i.e. as the power of the LOS component becomes more important, the difference with regard to the scenario without fading gets smaller. In Figure 14, the impact of fading of the GNSS signal with regard to the acquisition performance is illustrated. This scenario is of interest for a signal environment in urban canyon or for indoor applications. The results highlight that fading on the signal of interest degrades the acquisition performance.

The results discussed before are in line with the expectations and could even seem trivial. It is however important to note that the analytical tool that has been developed,

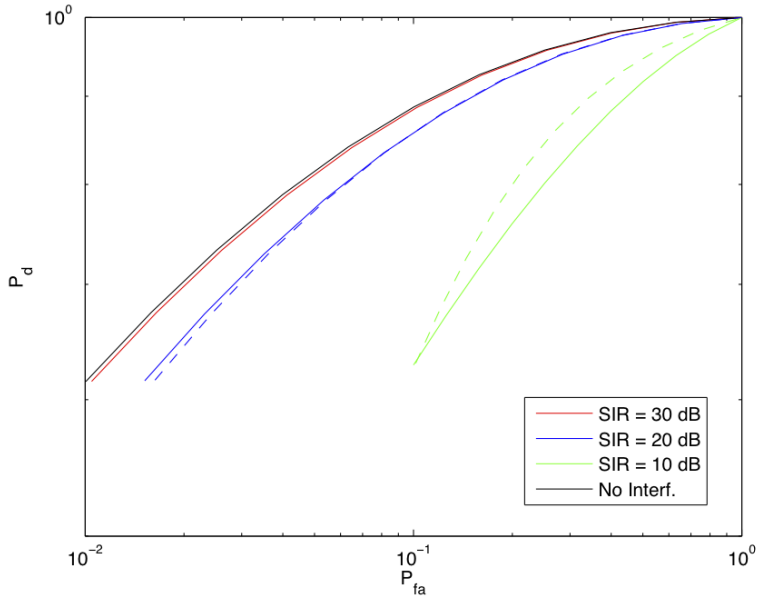

Figure 12: fading for different SIR

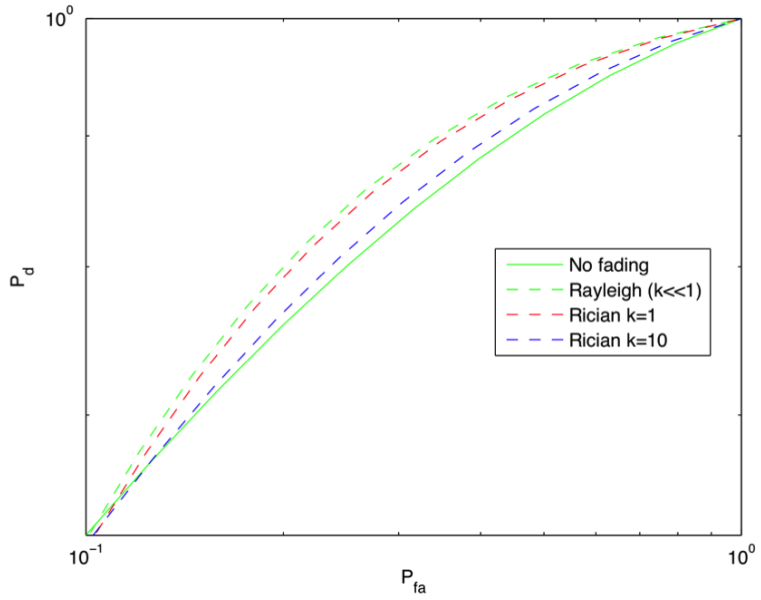

Figure 13: Effects of different fading distributions

enables a quantitative assessment of the impact of fading on the acquisition process. Different fading models can be tested and worst cases can be identified.

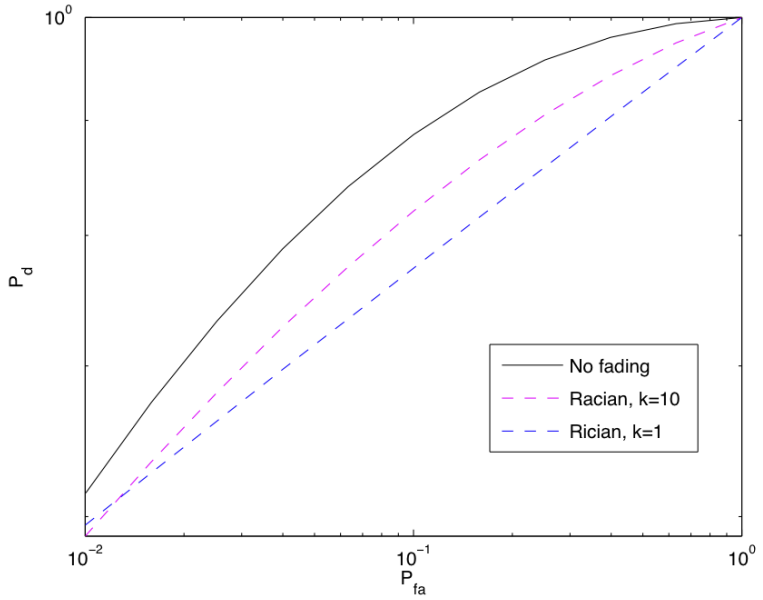

Figure 14: fading effect on GNSS signal

3.5.3 Changing the Decision Statistic

In what follows, an analytical approach is proposed to calculate the probability of detection using the ratio of maximum correlation values. As in Section 3.5.2, the method allows to take into account the effects of fading on the GNSS signal as well as on interfering signals. In ANNEX A, a mathematical expression is derived to calculate the probability of detection in case the ratio of correlation peaks is used as decision variable. An expression is derived for the characteristic function of the decision variable. Applying the inversion theorem, an expression can be found of the probability of detection.

In order to validate the theoretical model, analytical results have been compared with simulation results. Monte Carlo simulations have been executed on the acquisition in two distinct scenarios. Figure 15 shows the impact of the cross-correlation terms as a function of N_{sat} for different signal-to-noise ratio (SNR) values. Every satellite gives a contribution to the decision variable. The presence of other several other satellites can thus be conceived as an increase of the noise floor, which results in a decrease of the acquisition performance. These results demonstrate a good fit between theoretical analysis and simulation, which supports the validity of the mathematical analysis and the correctness of the different approximations made. It can be observed that the cross-correlation terms related to the presence of other satellites have a considerable impact on the probability of detection. By adding more satellites in view, the corresponding increase of the noise floor leads to a deterioration of the probability of detection.

In Figure 16 the theoretical and the simulated probability of detection have been

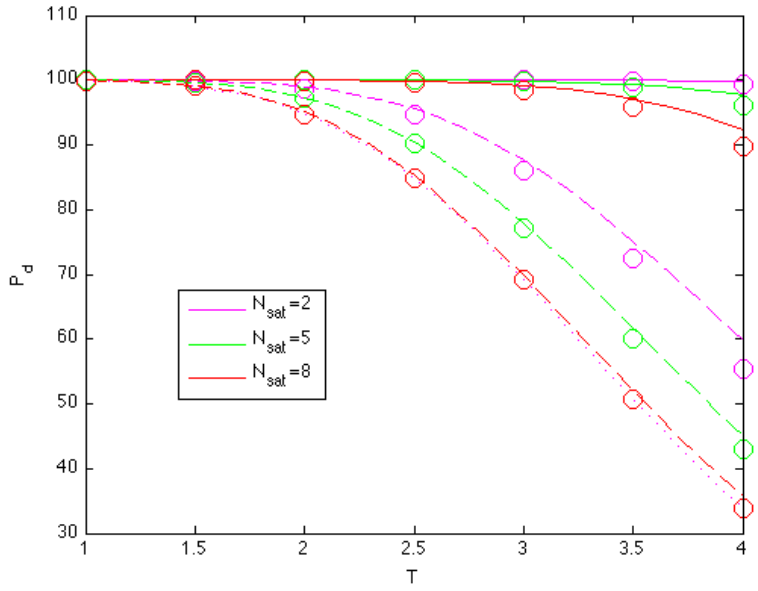

Figure 15: Theoretical results (lines) and simulation results (circles) of the cross-correlation impact on the probability of detection. The SNR values of the decision variable are 18 dB (solid lines) and 15 dB (dashed lines).

compared in presence of DVB-T interference, for different values of the signal-to-interference ratio (SIR). The signal-to-interference ratio (SIR) is defined as $SIR = \frac{C}{\rho P_I}$. The analytical and simulated probability of detection agree well, underlining the validity of the theoretical model. It can be noted that the probability of detection is clearly vulnerable to the presence of interference. Yet, we dispose of a tool that could be used to determine a minimum required DVB-T transmitter distance, corresponding with a minimum probability of detection.

3.5.4 Concluding Remarks

In this section, we discussed the impact of different types of interference on the acquisition performance. The acquisition performance is usually assessed by means of ROC curves. The main achievement is the development of analytical tools to assess how interference impacts the acquisition performance for different types of interference and for different implementations of the acquisition process. For white noise a theoretical model has been discussed and the impact of the signal quality C/N_0 has been presented in terms of the ROC curves. For CWI, a simulation analysis has been executed and for different system parameters the impact on the ROC curves has been quantified. The simulation results show that the impact of CWI is most harmful when the tone falls together with the strongest line of the GNSS PRN code, and moreover the performance reduction has been

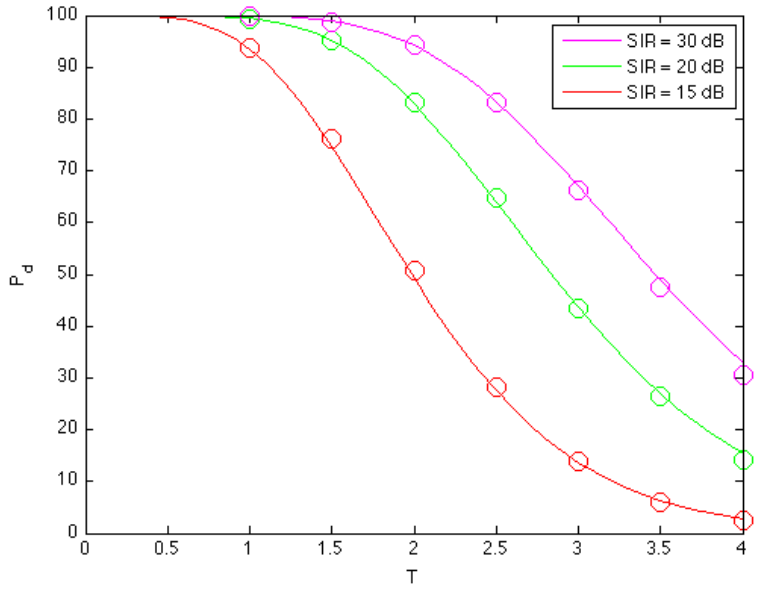

Figure 16: Theoretical results (solid lines) and simulation results (circles) of the DVB-T impact on the probability of detection.

quantified. The acquisition performance has also been studied for longer integration times. Most of the attention has been given to the scenario DVB-T interference. First, it has been shown that a DVB-T signal, or its second and third harmonic, are equivalent to white noise. We demonstrated that the contribution to the decision statistic originating from DVB-T signals or its harmonics have the same distribution as the contribution of white noise. The spectral separation coefficient has been introduced in order to analyse the different impact of DVB-T interference on GPS and Galileo. It has been demonstrated that Galileo and GPS have almost equal robustness with regard to DVB-T. The acquisition performance reduction has been quantified in function of the signal-to-interference ratio. Further, the effects of fading have been added to the analysis. First, fading has been considered on the interfering signals. Different fading distributions have been considered and it has been shown that fading on the interfering signals improves the acquisition performance. Moreover, the performance improvement has been quantified. Fading with respect to the GNSS signals deteriorates the acquisition performance. Finally, we discussed the use of a different decision statistic, where the maximum correlation value is referred to the second highest correlation value. For this decision statistic, probability of false alarm is independent of the noise power spectral density. An expression is proposed for the probability of detection. The results generated by the theoretical analysis and Monte Carlo simulations demonstrate a good fit. Overall, this study yielded several analytical and simulation tools that could be applied to determine minimum distances to

interferers, that guarantee a minimum acquisition performance.

4 Experimental Results

The objective of the measurement analysis is to evaluate the interference effects caused by unintentional interference sources on both professional and commercial GPS L1 receivers. Initially, we begin the experimental study by considering the presence of a CWI signal, which corresponds to the simplest case since it is modelled by a single tone. The impact of a CWI signal on a GPS receiver is widely addressed in the literature [6]. Nevertheless, this type of interference is analysed in this work for comparison with wideband interference scenarios. Furthermore, the situation in which the CWI arrives at the GPS receiver in different burst times, referred to as PCWI, is also evaluated in this section. Finally, a 3^{rd} harmonic of a DVB-T signal is employed in the experimental study in order to evaluate the wideband interference effects on the system quality and positioning metrics of the GPS L1 receivers.

A block diagram of the laboratory test bed for an unintentional interference evaluation on GPS L1 receivers is depicted in Figure 17. The instruments and components employed in the test bed are listed and described as follows:

- GPS L1 antenna.
- Bandpass filter and amplifier to condition the GPS received signal.
- Directional coupler. Component from AtlanTec A2023-6 with 6 dB attenuation and operating in the frequency band $0.5 - 2$ GHz.
- GPS Splitter model AS 41-2P from Aucon with 3 dB losses.
- Attenuator of 30 dB.
- DC Block unit.
- Tektronix 3408A Real-Time Spectrum Analyser with frequency range from DC to 8 GHz.
- Agilent E8267D PSG Vector Signal Generator to generate the 3^{rd} harmonic of a DVB-T signal.
- Tektronix AFG3102 Arbitrary Function Generator to modulate the PCWI signal. It allows the pulse repetition time and the duty cycle of the pulsed interference signal to be set.
- GPS L1 Receivers. Two professional receivers (referred to as PRO1 and PRO2 in this work) and two mass market receivers (MM1 and MM2) have been employed in the test bed in order to assess the interference effects on the C/N0 and position variance metrics.

- A PC Workstation is used to control the measurement campaigns, the generation of the DVB-T interference signal in baseband and to record the measured metrics to be processed offline. The latest functionality is achieved by parsing the information, which is captured by using the dedicated software of each particular receiver.

Next, the interference effects on the C/N0 and variance position metrics of the GPS L1 receivers are presented according to the type of interference source.

4.1 Continuous Wave Interference

The measurement results are obtained by following the procedure outlined in this section. First, the CWI signal is generated by the PSG Vector Signal Generator at five possible centre frequencies. These selected centre frequencies are $f_i = f_c$, $f_i = f_c + f_d + f_1$, $f_i = f_c + f_d + f_2$, $f_i = f_c + 511$ KHz and $f_i = f_c + 1.023$ MHz where $f_c = 1.57542$ GHz is the centre frequency of the GPS L1 signal, f_d is the doppler frequency of the satellite in-view, f_1 is the frequency corresponding to the maximum PSD value of the PRN code and f_2 represents the frequency value of the second maximum PSD value of the PRN code. The values of f_d, f_1 and f_2 are dynamically obtained in the PC workstation for each satellite in view by running a MATLAB script. The RF interference signal is obtained from the PSG Vector Signal Generator by changing the power levels from -60 dBm to -25 dBm with steps of 5 dBm. Therefore, forty different scenarios are generated corresponding to eight power levels and five centre frequencies of the CWI signal.

Subsequently, the measured metrics are represented as a function of the interference-to-noise ratio (INR), which is calculated as the ratio between the maximum value of the interference PSD and the noise floor. An estimated noise floor value of -112 dBm/Hz is measured at the Spectrum Analyser as shown in Figure 18. Note that, in order to obtain the maximum PSD level of the interference signal, the signal-to-noise ratio (SNR)

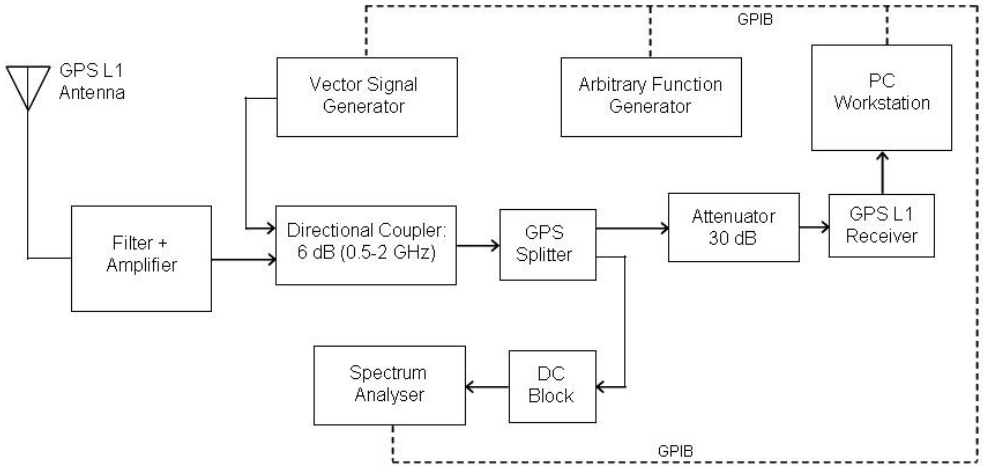

Figure 17: Block diagram of the Test Bed for the interference study on GPS L1 receivers

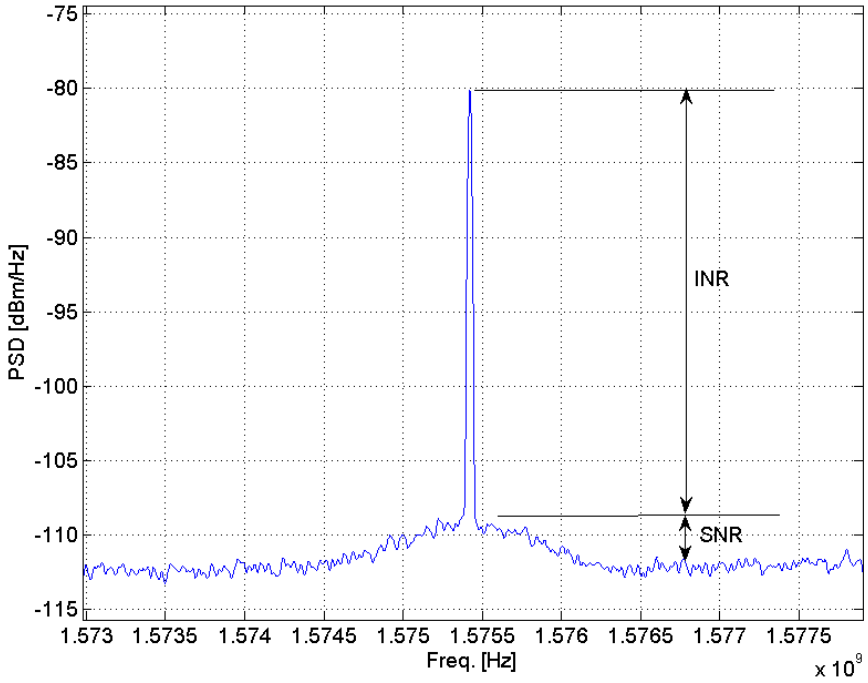

Figure 18: Measured PSD of the GPS L1 and CWI signal

has been taken into account. The main reason for using INR values instead of received power levels is to omit unknown power losses from electronics and connectors embedded in the test bed. The C/N0 and position values are recorded in real time using the dedicated software for each receiver. In both receivers, a value per second of the C/N0 and position is measured. The duration of each particular measurement scenario is set to 120 seconds. The reason for selecting this time duration is linked to the tradeoff between selecting a large duration in order to obtain an accurate value of the averaged metrics and a short value that maintains the same elevation of the targeted satellites (for C/N0 values) during the entire measurement process. Furthermore, the measured values are post-processed offline by parsing the generated output files. The estimated C/N0 values are obtained by considering three satellites in-view with high (HE), medium (ME) and low (LE) elevations.

Finally, the system quality, in the presence of CWI interference, is evaluated in terms of C/N0 and position variance performances.

4.1.1 C/N0 Performance Analysis

The performances of the measured C/N0 as a function of the INR for the PRO1 receiver are plotted in Figure 19. In this scenario, a satellite that presented a high elevation dur-

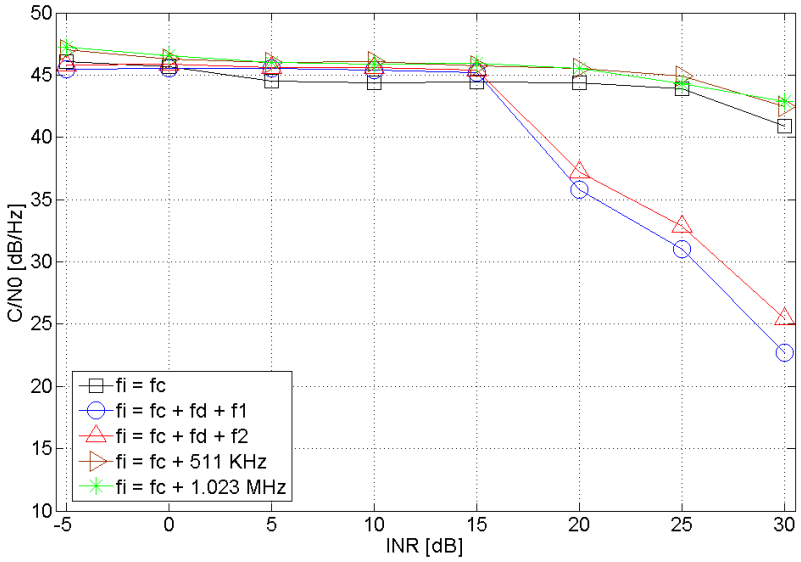

Figure 19: C/N0 measured at the PRO1 receiver of a HE satellite as a function of the INR in the presence of CWI.

ing the experimental process is considered. The measurement results show that when the centre frequency of the CWI signal is aligned with the frequency component corresponding to the maximum of the code PSD (f_1), the C/N0 considerably decreases for INR values larger than 15 dB. In this situation, a C/N0 degradation of approximately 12 dB is measured when INR $=$ 25 dB with respect to the interference-free case. This phenomenon is practically identical when the CWI centre frequency is chosen to be $f_i = f_c + f_d + f_2$. The C/N0 performances as a function of the INR for a system that employs the MM1 receiver are presented in Figure 20 under the same aforementioned scenario. It is noticeable that the C/N0 levels of the professional receiver (PRO1) shown in Figure 19 are approximately 6 dB higher with respect to the mass marked (MM1) receiver in the situation of low interference power (INR $<$ 5 dB). This is due to the fact that both receivers use different tracking estimation algorithms. The measurement results in Figure 20 illustrate that the MM1 receiver loses its tracking when the CWI jammer is transmitting at the worst line or second worst line frequencies and INR $>$ 25 dB. The last C/N0 value that the receiver is capable of measuring prior to losing lock is represented by a filled marker in the figures.

Next, the C/N0 performances of a low elevation satellite and considering the four GPS L1 receivers (PRO1, PRO2, MM1 and MM2) are evaluated when $f_i = f_c + f_d + f_1$, as shown in Figure 21. The measurement results show that PRO1 and MM2 receivers are capable of tracking the satellite for INR $\leq$ 25 dB and INR $\leq$ 30 dB respectively. Conversely, PRO2 and MM1 receivers are less robust when the interference power is large and they lose lock for values of INR $>$ 15 dB.

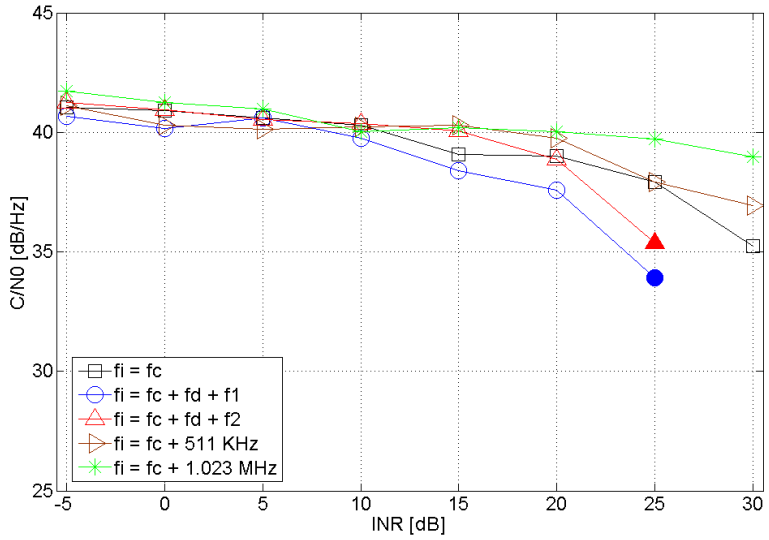

Figure 20: C/N0 measured at the MM1 receiver of a HE satellite as a function of the INR in CWI presence.

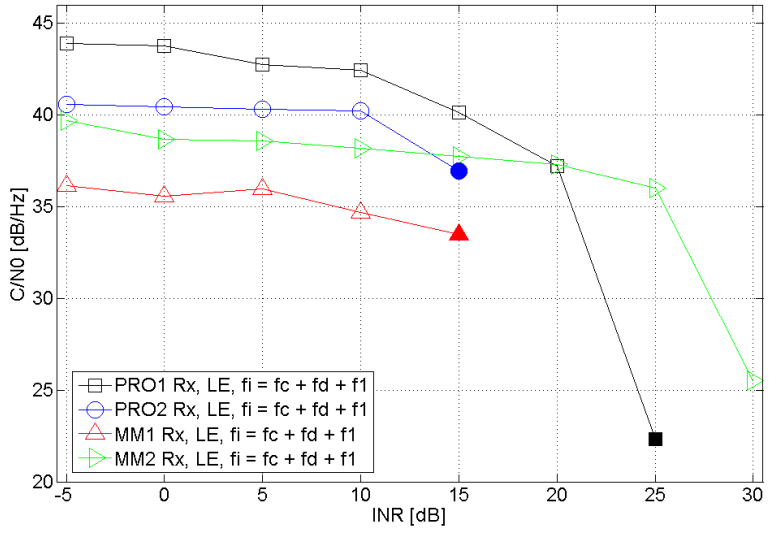

Figure 21: C/N0 measured at the PRO1, PRO2, MM1 and MM2 receivers of a LE satellite as a function of the INR in the presence of a CWI signal with $f_i = f_c + f_d + f_1$.

Finally, the C/N0 performances for both PRO1 and MM1 receivers are provided in Figure 22 when $f_i = f_c + f_d + f_1$. In this scenario, three satellites in-view with different elevations (HE,ME and LE) are considered. The measurement results show that for large values of INR (INR $= 25$ dB) the C/N0 performance degradation of the LE satellite is larger than 15 dB with respect to the low interference situation (INR ≤ 0 dB) when the PRO1 receiver is employed. It is also noticeable that the MM1 receiver behaves slightly better than the PRO1 receiver when $20 \leq$ INR ≤ 25 dB.

Further measurement results are presented in the Annex B.

4.1.2 Position Variance Performance Analysis

The variance of the position, measured at the PRO1 GPS L1 receiver, as a function of the INR is shown in Figure 23 in the presence of a CWI with $f_i = f_c + f_d + f_1$, $f_i = f_c + 511$ KHz or $f_i = f_c + 1.023$ MHz. The measurement results illustrate the interference effects on the Earth Centered Earth Fixed (ECEF) cartesian coordinates. The results show that the position variance is constant for all the INR levels when $f_i = f_c + 511$ KHz and $f_i = f_c + 1.023$ MHz. The position variance slightly increases when INR ≥ 20 dB for a $f_i = f_c + f_d + f_1$ CWI signal. Nevertheless, this increase in variance is not very significant since, in the case of CWI presence, only one satellite is jammed and the position is obtained by using an optimization technique (i.e. least square method, kalman filter, etc.), which employs several satellites, to solve an overdetermined problem.

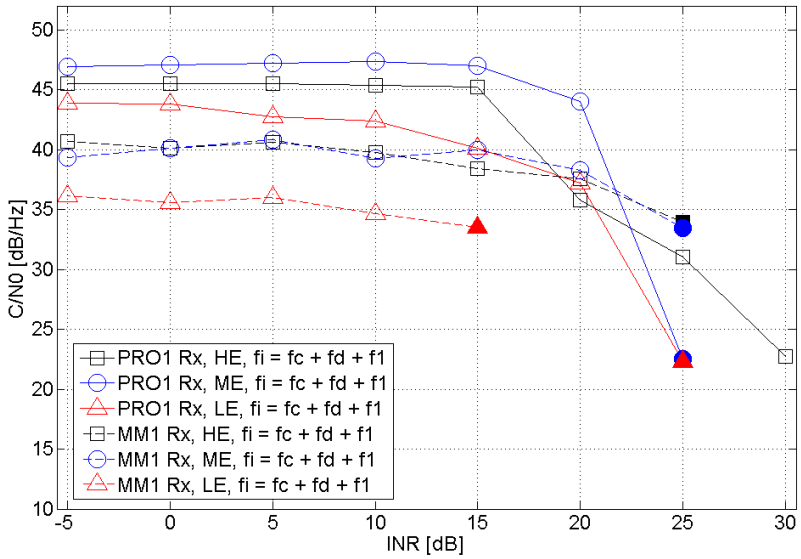

Figure 22: C/N0 measured at the PRO1 and MM1 receivers of HE, ME and LE satellites as a function of the INR in the presence of a CWI signal with $f_i = f_c + f_d + f_1$.

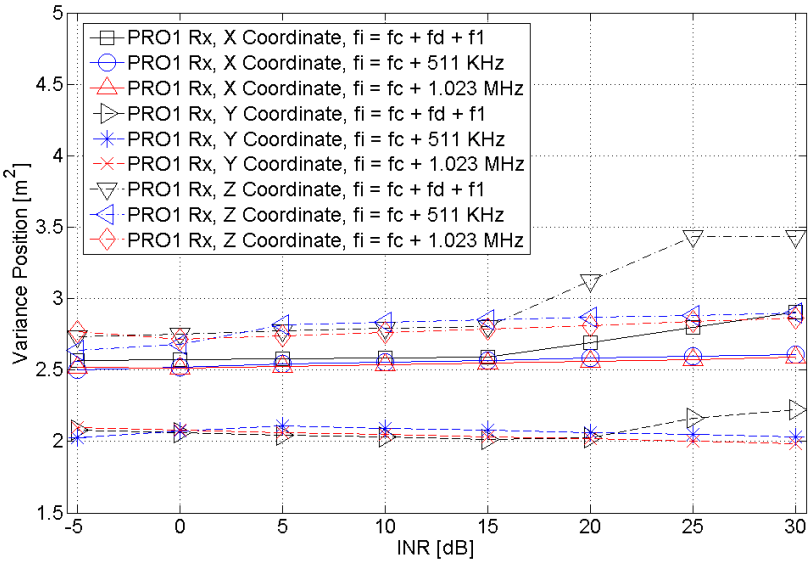

Figure 23: Variance position measured at the PRO1 receiver of a HE satellite as a function of the INR in the presence of CWI.

4.2 Pulse Continuous Wave Interference

The test bed configuration and the measurements methodology used for the evaluation of the PCWI effects on the GPS L1 receivers are the same as the CWI ones with the difference that an Arbitrary Function Generator is employed in the test bed, which allows the PCWI signal to be modulated in terms of pulse waveform, amplitude, duty cycle (DC) and pulse repetition time (PRT). In the next set of measurements, a PRT value of 2 ms is employed. Next, the performance analysis of the signal quality in terms of the C/N0 and position variance is provided.

4.2.1 C/N0 Performance Analysis

First, the performance of the measured C/N0 as a function of the INR is evaluated for a satellite in high elevation and using the PRO1 receiver. Five centre frequencies of the interference signal are employed as in the case of CWI. Also, a value of DC $= 10\%$ is chosen in this scenario. The results are plotted in Figure 24 and show that the C/N0 performance degradation, when the PCWI centre frequency is $f_i = f_c + f_d + f_1$, is minimal (less than 3 dB) for INR ≤ 25 dB values with respect to the interference-free case. However, a C/N0 loss of approximately 10 dB is measured when INR $= 30$ dB. Nevertheless, this value is considerably lower than the 25 dB measured when the interference is CWI. Note that a CWI signal corresponds to a PCWI signal with a DC $= 100\%$. Considering the same scenario, the C/N0 performance using the MM1 receiver is plotted in Figure 25. In this

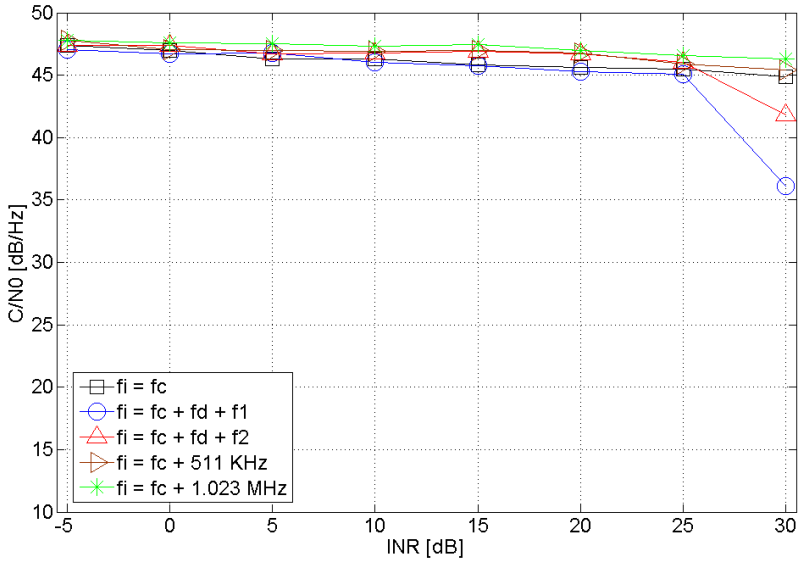

Figure 24: C/N0 measured at the PRO1 receiver of a HE satellite as a function of the INR in the presence of PCWI with DC $= 10\%$.

situation, the C/N0 performance degradation, with respect to the non-interference scenario, is also approximately 10 dB when INR $= 30$ dB. It is also observable that the C/N0 waterfall curves have approximately identical behavior for $f_i = f_c + f_d + f_1$, $f_i = f_c + f_d + f_2$ and $f_i = f_c$. This is due to the frequency width of the real interference signal and the fact that the maximum and the second maximum of the PRN code PSD are close to each other and also close to f_c.

Next, the C/N0 performances of all four receivers are evaluated for a satellite in low elevation and a PCWI signal transmitting at $f_i = f_c + f_d + f_1$, as shown in Figure 26. The measurement results show that all receivers can combat the interference effects for INR ≤ 25 dB values. When the interference level is high (INR $= 30$ dB), receivers PRO1 and MM2 suffer 15 dB and 10 dB C/N0 losses with respect to the low interference case. The other two receivers, PRO2 and MM1, lose lock under these conditions.

Subsequently, the C/N0 performances of three satellites in high, medium and low elevations for both PRO1 and MM1 receivers when $f_i = f_c + f_d + f_1$ are depicted in Figure 27. The results illustrate that both receivers are capable of tracking the satellites when the interference level is high (INR $= 30$ dB) except for the MM1 when the tracking satellite is in low elevation.

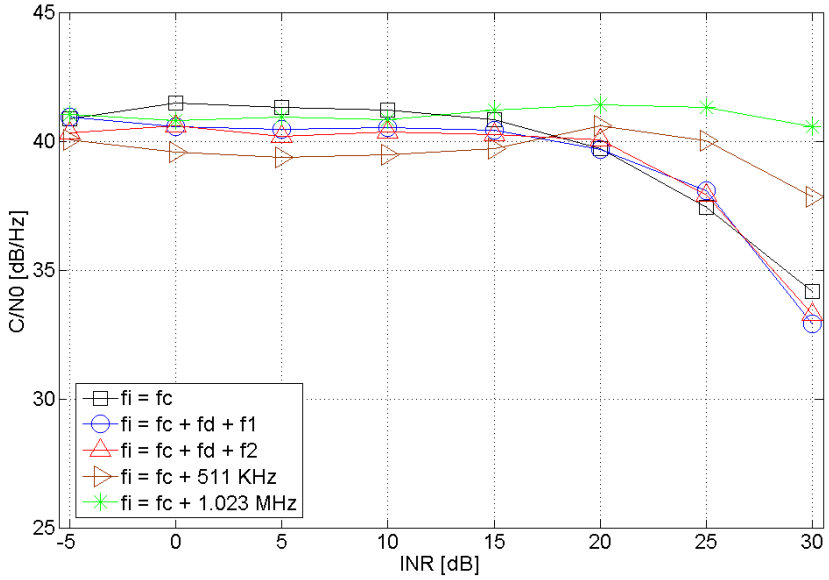

Figure 25: C/N0 measured at the MM1 receiver of a HE satellite as a function of the INR in the presence of PCWI with DC $= 10\%$.

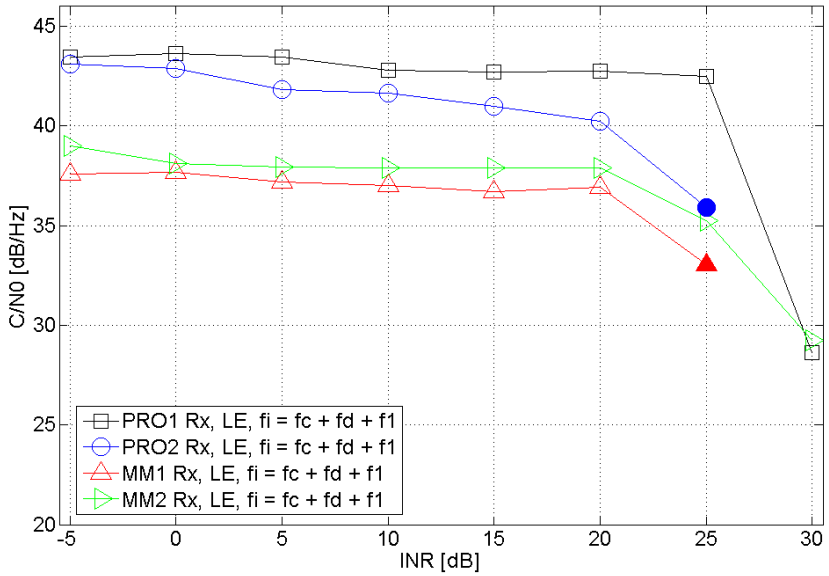

Figure 26: C/N0 measured at the PRO1, PRO2, MM1 and MM2 receivers of a LE satellite as a function of the INR in the presence of a CWI signal with $f_i = f_c + f_d + f_1$ and DC $= 10\%$.

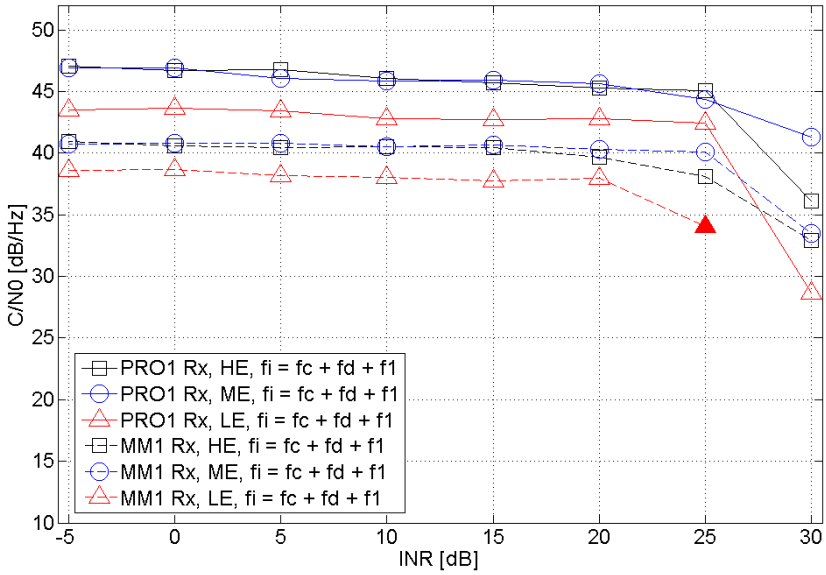

Figure 27: C/N0 measured at the PRO1 and MM1 receivers of HE, ME and LE satellites as a function of the INR in the presence of a CWI signal with $f_i = f_c + f_d + f_1$ and DC $= 10\%$.

Finally, the interference effects, caused by choosing different DC values, on the C/N0 of a low elevation satellite are evaluated for PRO1 and MM1 receivers, shown in Figure 28 and Figure 29 respectively. In the case of a PRO1 receiver, the satellite is tracked for values of DC $< 20\%$ when INR $= 30$ dB. Conversely, the MM1 receiver cannot track satellites in LE when DC $< 10\%$ for a value of INR $= 30$ dB. Further measurement results are provided in the Annex B.

4.2.2 Position Variance Performance Analysis

The variance of the position, measured at the PRO1 GPS L1 receiver, as a function of the INR is shown in Figure 30 in the presence of a PCWI with DC $= 10\%$ and $f_i = f_c + f_1$, $f_i = f_c + 511$ KHz or $f_i = f_c + 1.023$ MHz. The measurement results show that the interference with low duty cycle does not cause any disturbance to the positioning of the receiver, even when the centre frequency is $f_i = f_c + f_1$.

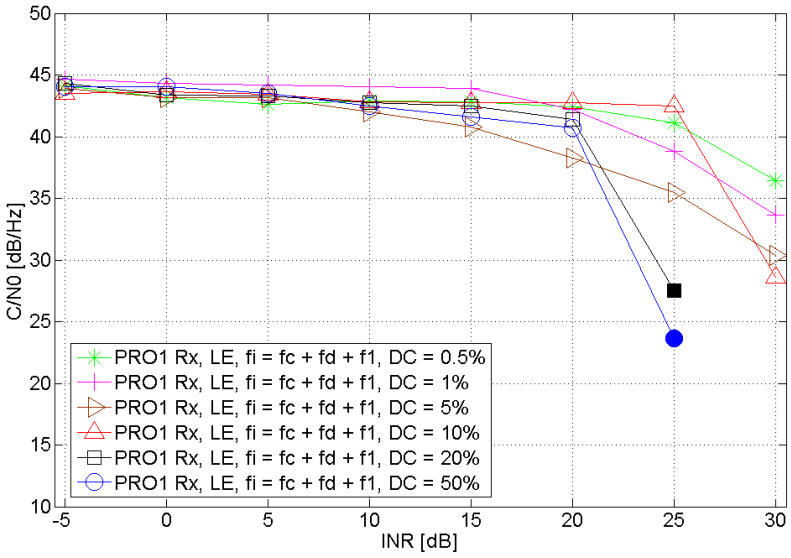

Figure 28: C/N0 measured at the PRO1 receiver of a LE satellite as a function of the INR in the presence of a CWI signal with $f_i = f_c + f_d + f_1$.

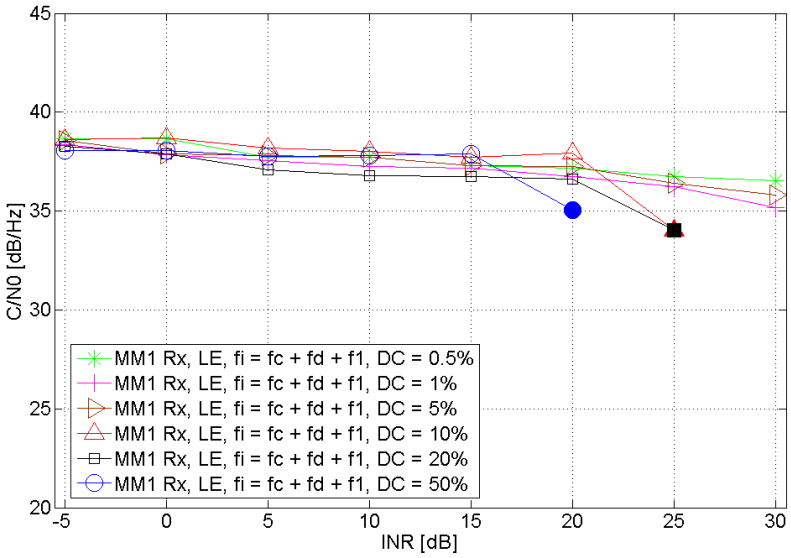

Figure 29: C/N0 measured at the PRO1 receiver of a LE satellite as a function of the INR in the presence of a CWI signal with $f_i = f_c + f_d + f_1$.

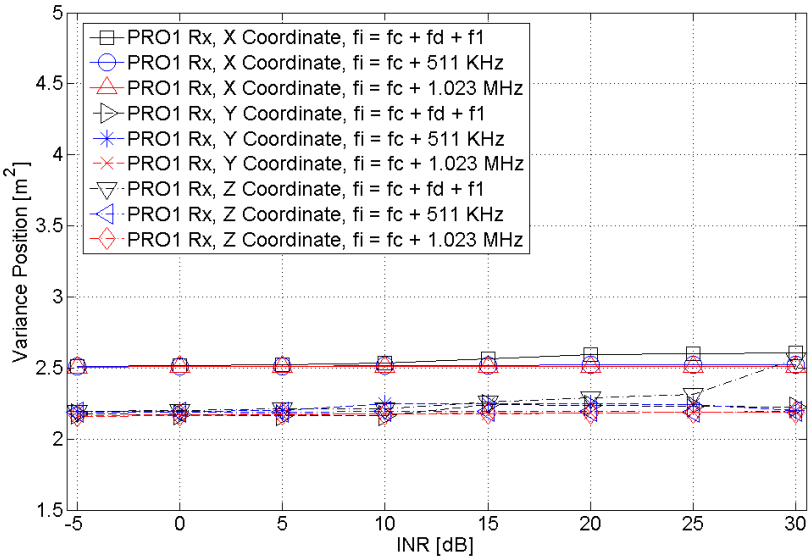

Figure 30: Variance position measured at the PRO1 receiver of a HE satellite as a function of the INR in the presence of CWI with DC $= 10\%$.

4.3 DVB-T Harmonics Interference

The 3rd harmonic of the DVB-T signal is transmitted in a conducted modality at a centre frequency $f_i = f_c$, with $f_c = 1.57542$ GHz, or at $f_i = f_c + 511$ MHz. The up-converted interference signal is obtained from the PSG Vector Signal Generator by changing the power levels from -45 dBm to 0 dBm in steps of 5 dBm. Therefore, eighteen different scenarios are produced corresponding to nine power levels and two centre frequencies of the interference signal. The measured metrics are also represented as a function of the INR. In contrast to the CWI and PCWI, the wideband interference when $f_d = f_c$ affects all the satellites in-view independent of the doppler values, as shown in Figure 31.

Next, the performance analysis of the signal quality in terms of the C/N0 and position variance is provided.

4.3.1 C/N0 Performance Analysis

The measured C/N0 values are obtained by considering three satellites in-view with high, medium and low elevations. The waterfall curves of the C/N0, as a function of the INR, for the PRO1 receiver are shown in Figure 32. Initially, the results show that the C/N0 performance degradation of all satellite elevations when INR $= 25$ dB and $f_i = f_c$ is approximately 13 dB with respect to the low interference situation (INR < 0 dB). Similarly, this C/N0 performance loss is 10 dB when $f_i = f_c + 511$ KHz. Analogously, the same C/N0 performance evaluation is conducted by considering the MM1 receiver as presented in

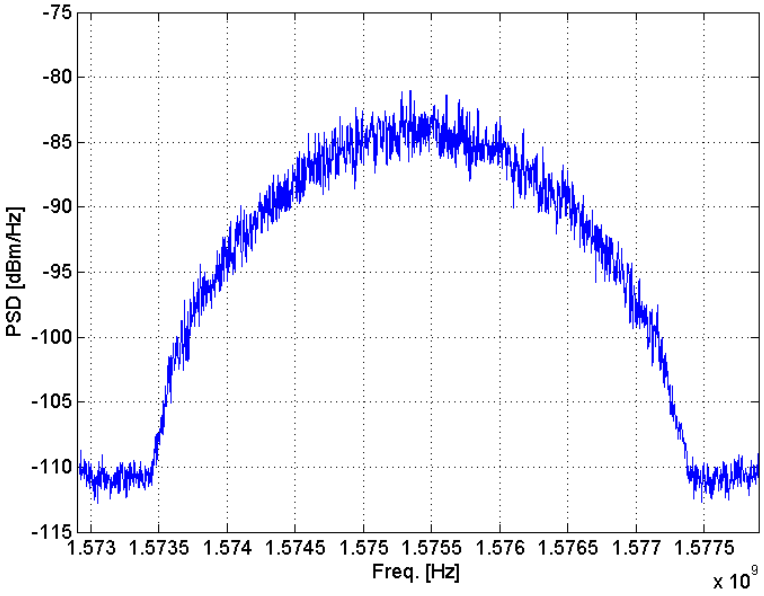

Figure 31: Measured PSD of the GPS L1 and the 3rd harmonic of the DVB-T signal

Figure 33. Now, in the situation of high power interference level, the C/N0 performance of the MM1 receiver decreases slower than the C/N0 of the PRO1 receiver for both centre frequency interference cases. The C/N0 performance degradation, with respect to the low interference situation, when INR $= 25$ dB and $f_i = f_c$ is approximately 7 dB for the MM1 receiver. Similarly, the C/N0 degradation is only 4 dB when $f_i = f_c + 511$ KHz.

Finally, the measured C/N0 of a satellite in low elevation as a function of the INR for all the four GPS L1 receivers is illustrated in Figure 34. The measurement results show that the PRO2 receiver loses lock when INR > 15. In a situation with high levels of interference (INR $= 25$ dB) the PRO1 and MM1 receivers with $f_i = f_d$ present a C/N0 degradation of approximately 5 dB with respect to $f_i = f_c + 511$ KHz. This performance degradation is larger (approximately 15 dB) when the MM2 receiver is employed.

Further measurement results are provided in the Annex B.

4.3.2 Position Variance Performance Analysis

The variance of the position, measured at the PRO1 GPS L1 receiver, as a function of the INR is shown in Figure 30 in the presence of a DVB-T 3rd harmonic signal with centre frequency at $f_i = f_c$ or $f_i = f_c + 511$ KHz. In contrast to the CWI and PCWI, the 3rd harmonic of the DVB-T signal causes larger variations in the positions when INR > 10 dB. Now, the interference signal affects all the satellites in-view and therefore it is present in all the equations used by the optimizing technique when calculating the receiver position.

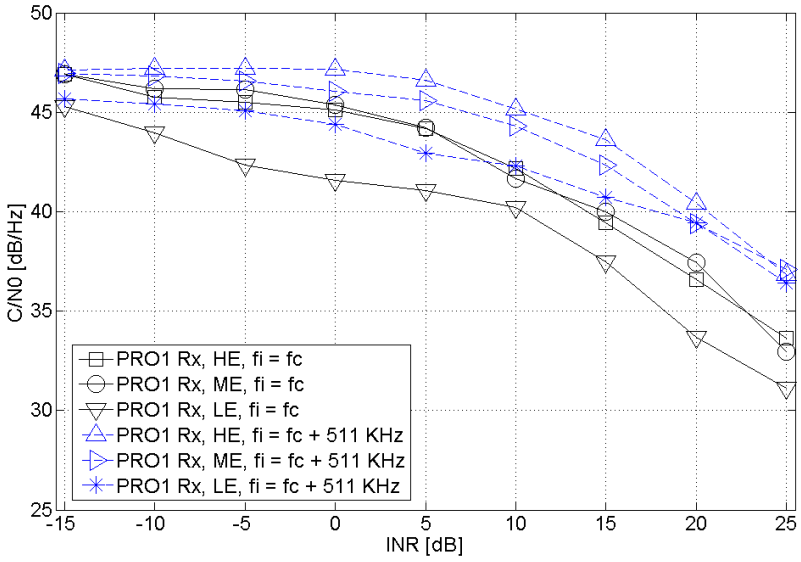

Figure 32: C/N0 measured at the PRO1 receiver of HE, ME and LE satellites as a function of the INR in the presence of a DVB-T 3rd harmonic interference signal with $f_i = f_c$ or $f_i = f_c + 511$ KHz.

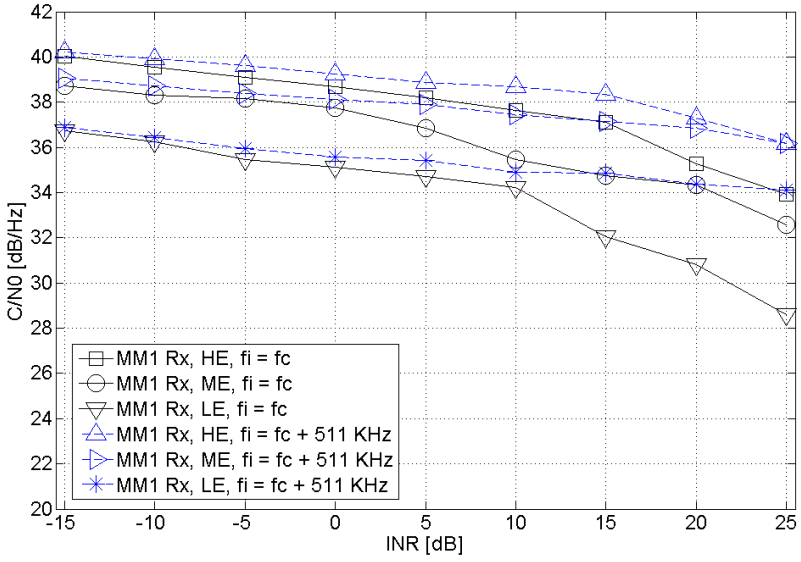

Figure 33: C/N0 measured at the MM1 receiver of HE, ME and LE satellites as a function of the INR in the presence of a DVB-T 3rd harmonic interference signal with $f_i = f_c$ or $f_i = f_c + 511$ KHz.

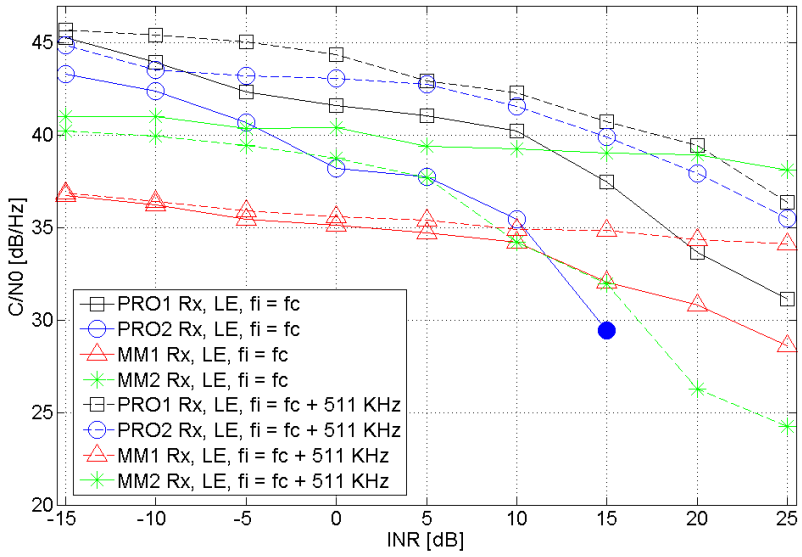

Figure 34: C/N0 measured at the PRO1, PRO2, MM1 and MM2 receivers of a LE satellite as a function of the INR in the presence of DVB-T 3rd harmonic interference signal with $f_i = f_c$ or $f_i = f_c + 511$ KHz.

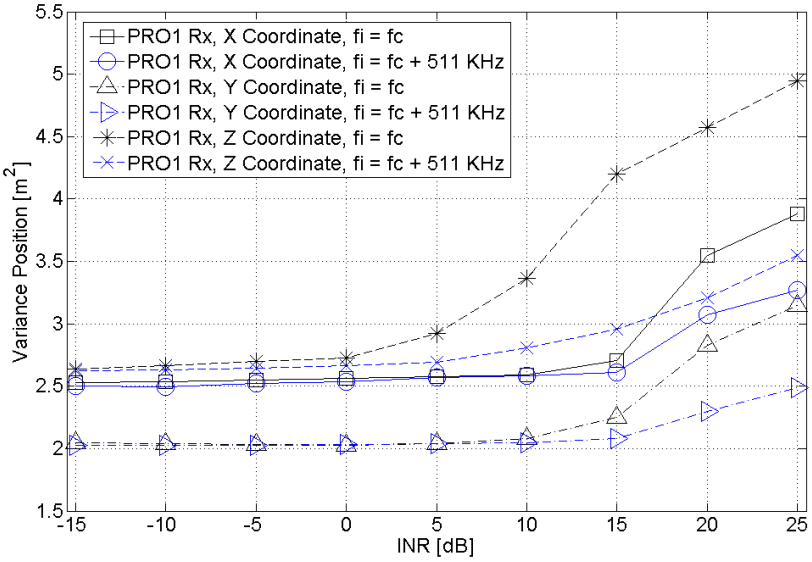

Figure 35: Variance position measured at the PRO1 receiver of a HE satellite as a function of the INR in the presence of DVB-T 3rd harmonic interference signal with $f_i = f_c$ or $f_i = f_c + 511$ KHz.

4.4 Concluding Remarks

Firstly, the measured C/N0 performances of a GPS L1 satellite, in the presence of CWI, PCWI or the 3rd harmonic of a DVB-T signal, as a function of the INR were evaluated in this section for different professional and commercial receivers. The measurement results showed that when the interference is CW and with values of INR $\geq$ 20 dB, the C/N0 performance degradation is noticeable only if $f_i = f_c + f_d + f_1$ or $f_i = f_c + f_d + f_2$. In these scenarios, the C/N0 degradation of a satellite in HE, with respect to the interference-free situation, is approximately 10 dB and 5 dB for the PRO1 and MM1 receivers respectively. The C/N0 performances of the four GPS receivers (PRO1, PRO2, MM1 and MM2) were compared for different satellite elevations and centre frequencies of the CWI signal. The results illustrate that the PRO1 and MM2 receivers offer a higher stability and sensitivity of C/N0 as the interference power levels increase. Conversely, the other two receivers, PRO2 and MM1, provide higher position accuracy.

Next, the resulting effect on the C/N0 caused by selecting different duty cycle values of the PCWI was addressed. The measurement results showed that the C/N0 performance degradation of a HE satellite is lower than 3 dB when INR $=$ 20 dB and $f_i = f_c + f_d + f_1$ for both PRO1 and MM1 receivers if DC $\leq$ 20%.

In the aforementioned situations (CWI and PCWI), the impact of the interference on the C/N0 performance was shown to be relevant only if the centre frequency of the interference tone is aligned with the maximum PSD values of the PRN code. This frequency alignment was achieved in the measurement campaigns by adaptively changing the interference centre frequency according to the measured doppler of the satellite in-view. In real applications, in the context of unintentional interference, the interference source does not track the doppler of the satellite in observation. Thus, this scenario corresponds to the case of having an arbitrary value of the f_i, as for example $f_i = f_c + 511$ KHz. In this case, the measurement results showed that the impact of the CWI and PCWI on the C/N0 performance is negligible (less than 3 dB) when the interference power is large.

On the contrary, a wideband signal, such as the 3rd harmonic of a DVB-T signal, that occupies all of the GPS L1 band over the entire time, interferes with all satellites in-view independently of their doppler values. This C/N0 performance degradation was shown in the measurement results for two values of the centre frequency, $f_i = f_c$ and $f_i = f_c + 511$ KHz. The estimated C/N0 performance degradation of a satellite in HE, with respect to the interference-free situation, and using the PRO1 receiver was measured as 10 dB and 7 dB for $f_i = f_c$ and $f_i = f_c + 511$ KHz respectively. These values are clearly larger than the 2 dB obtained for CWI with $f_i = f_c + 511$ KHz under the same conditions.

Finally, the variance of the position performances as a function of the INR were measured by using the PRO1 receiver and considering the three types of interference sources. The measurement results showed that the position variance in the presence of CWI or PCWI is practically constant. Conversely, the 3rd harmonic of the DVB-T signal causes larger variations in the positions when INR $>$ 10 dB. This is due to the fact that the DVB-T harmonic interference signal affects all the satellites in-view and therefore it is present

in all the equations used by the optimizing technique when calculating the receiver position.

5 Simulation Results: Tracking

The main objective of the simulation study is to validate the experimental results previously provided in section 4. Since no complete information about the implementation of the receivers employed in the measurement study is provided by the manufacturers, the development of a complete GPS simulator provides a flexible approach for assessing the interference impacts on the different stages of the receiver chain. Thus, the simulator allows the behavior of the GPS receiver to be studied in the presence of an unintentional interference for different acquisition methods, control loop implementations, values of the bandwidth filter, values of the integration time, etc.

The most significant simulation results, in terms of tracking performance of the GPS L1 receiver in the presence of external interference signals, are presented in this section. The tracking performance is evaluated through the analysis of the estimated carrier-to noise ratio (C/N0) and error vector magnitude (EVM) metrics under different types of interference sources.

5.1 Tracking Metrics

Two tracking metrics have been considered in this work to evaluate the tracking performance. The first metric, the estimated C/N0, provides fundamental information about the quality of the received signal in critical environments. In particular, the C/N0 values are good indicators of the behavior of the different control loops that integrate the tracking process. The estimated C/N0 is obtained in this simulation study by using a moment method (MM) algorithm [14]. The MM method uses the second and fourth moments of the n $-$ *th* received constellation point in order to estimate the carrier strength and the noise spectral density. The expressions of the second and fourth moments are given by $M_2 = \mathbb{E}\{r_c[n]^2\}$ and $M_4 = \mathbb{E}\{r_c[n]^4\}$ respectively. Thus, the estimated C/N0 values are computed as

$$\frac{C}{N_0} = 10\log_{10}\left(\frac{\sqrt{2M_2^2 - M_4}}{\left(M_2 - \sqrt{2M_2^2 - M_4}\right)W_e}\right) \tag{27}$$

where W_e is the equivalent noise bandwidth. The other metric employed in this work is the EVM. The EVM, also called the receive constellation error, accounts for the error distance between the received constellation data point and its ideal value in the case of high signal-to-noise ratio and interference-free situations. Both metrics, CN0 and EVM, provide the same information since they are inversely proportional. The advantage of using EVM with respect to the most commonly used metric C/N0 is that EVM is a faster parameter to estimate. The EVM values are calculated from

$$EVM = \frac{\frac{1}{N}\sum_{n=1}^{N} |r_{op}[n] - r_c[n]|^2}{\frac{1}{N}\sum_{n=1}^{N} |r_{op}[n]|^2}, \quad (28)$$

where $r_{op}[n]$ represents the optimum received constellation point.

5.2 Test Scenarios

The performance of the tracking method is evaluated considering the presence of three different types of interference signals. These interference sources are classified as narrowband interference (including the cases of continuous wave interference (CWI) and pulse continuous wave interference (PCWI)), and wideband interference resulting from third order harmonics of a DVB-T signal. The most significant interference scenarios and the main simulation parameters are described in Table 1.

5.3 Simulation Analysis

5.3.1 Continuous Wave Interference

We begin this section by analysing the tracking performances of the GPS L1 receiver in the presence of a CWI signal. Without loss of generality, the signal of interest coming from the satellite with PRN code 15, whose power spectrum density (PSD) is plotted in Figure 36, has been considered in this study. The expression of the CWI signal is given by

$$i_{cwi}(t) = \sqrt{2P_i} cos(2\pi f_i t + \phi_i), \quad (29)$$

where P_i is the interference signal power, f_i is the center frequency of the signal and ϕ_i is the phase, which follows a random distributed variable on $[0, 2\pi)$. The center frequency of the interference signal is chosen as $f_i = f_{IF} + f_\delta$, where f_{IF} is the intermediate frequency set in the GPS L1 receiver and f_δ is a frequency shift, whose value depends on the PSD of the PRN code. Five different values of f_δ have been selected in this analysis. The most critical value, $f_\delta = f_1$, is the one in which the interference tone and maximum value of the code PSD are aligned causing the largest interference impact when Doppler effects are not present. Another significant value is $f_\delta = f_2$, which corresponds to the second peak of the code PSD. Finally, three arbitrary values have been considered, $f_\delta = 0$, half of the main lobe of the code PSD ($f_\delta = 511$ KHz) and the full lobe or first null ($f_\delta = 1.023$ MHz).

The C/N0 performances are computed as a function of the signal-to-interference ratio, $SIR = P_s/P_I$, where P_s and P_I are the power of the GPS L1 signal and the interference power respectively, both measured after the front-end receiver filter. The five aforementioned centre frequency values of the CWI signal are considered as shown in Figure 37. The simulation parameters in this scenario are defined in Table 1 for Exp.1.

Exp	Interf. Source	SIR [dB]	Interf. Freq. [KHz]	Interf. Param.	C/N0 [dB/Hz]	Notes
1	CWI	10 to -30	(i) f_{IF} (ii) $f_{IF}+f_1$ (iii) $f_{IF}+f_2$ (iv) $f_{IF}+511$ (v) $f_{IF}+1023$	-	45	Estimated C/N0 and EVM vs SIR
2	CWI	0	(i) f_{IF} (ii) $f_{IF}+f_1$ (iii) $f_{IF}+f_2$ (iv) $f_{IF}+511$ (v) $f_{IF}+1023$	-	30 to 60	Estimated C/N0 and EVM vs C/N0
3	CWI	-10	(i) f_{IF} (ii) $f_{IF}+f_1$ (iii) $f_{IF}+f_2$ (iv) $f_{IF}+511$ (v) $f_{IF}+1023$	-	30 to 60	Estimated C/N0 and EVM vs C/N0
4	CWI	-20	(i) f_{IF} (ii) $f_{IF}+f_1$ (iii) $f_{IF}+f_2$ (iv) $f_{IF}+511$ (v) $f_{IF}+1023$	-	30 to 60	Estimated C/N0 and EVM vs C/N0
5	PCWI	10 to -30	(i) f_{IF} (ii) $f_{IF}+f_1$ (iii) $f_{IF}+f_2$ (iv) $f_{IF}+511$ (v) $f_{IF}+1023$	DC $=10\%$ PRT $=2$ ms	45	Estimated C/N0 and EVM vs SIR
6	PCWI	10 to -30	(i) f_{IF} (ii) $f_{IF}+f_1$ (iii) $f_{IF}+f_2$ (iv) $f_{IF}+511$ (v) $f_{IF}+1023$	(i) DC $=0.5,1,5,10$ $20,50$ [%] (ii) PRT $=2$ [ms]	45	Estimated C/N0 and EVM vs DC
7	PCWI	10 to -30	(i) f_{IF} (ii) $f_{IF}+f_1$ (iii) $f_{IF}+f_2$ (iv) $f_{IF}+511$ (v) $f_{IF}+1023$	(i) DC $=10\%$ (ii) PRT $=1,2,4,5$ $10,20$ [ms]	45	Estimated C/N0 and EVM vs PRT
8	DVB-T	10 to -30	f_{IF}	(i) 3^{rd} Harmonic (ii) AWGN Interf.	45	Estimated C/N0 and EVM vs SIR
9	DVB-T	0,-10,-30	f_{IF}	(i) 3^{rd} Harmonic (ii) AWGN Interf.	30 to 60	Estimated C/N0 and EVM vs C/N0

Table 1: Main simulation parameters of a GPS L1 receiver under the presence of interference.

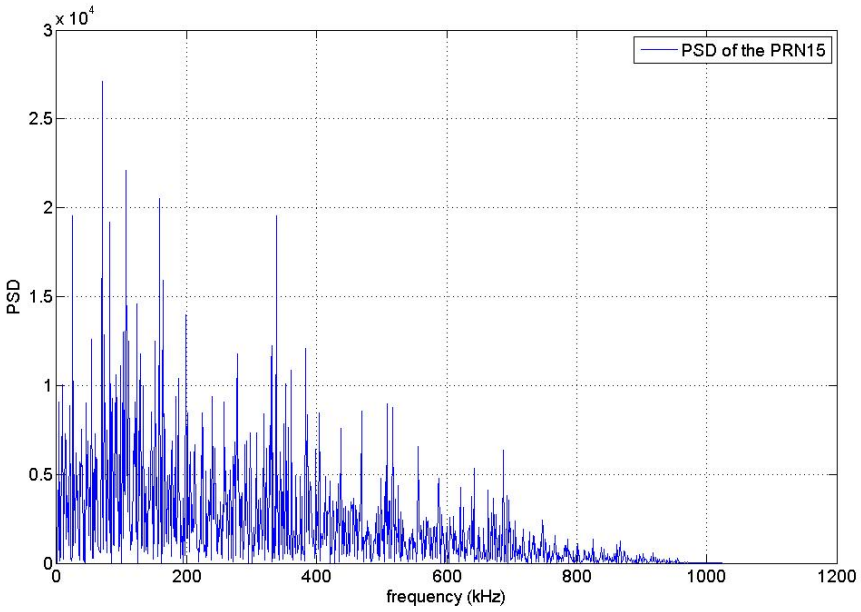

Figure 36: PSD of the PRN code 15.

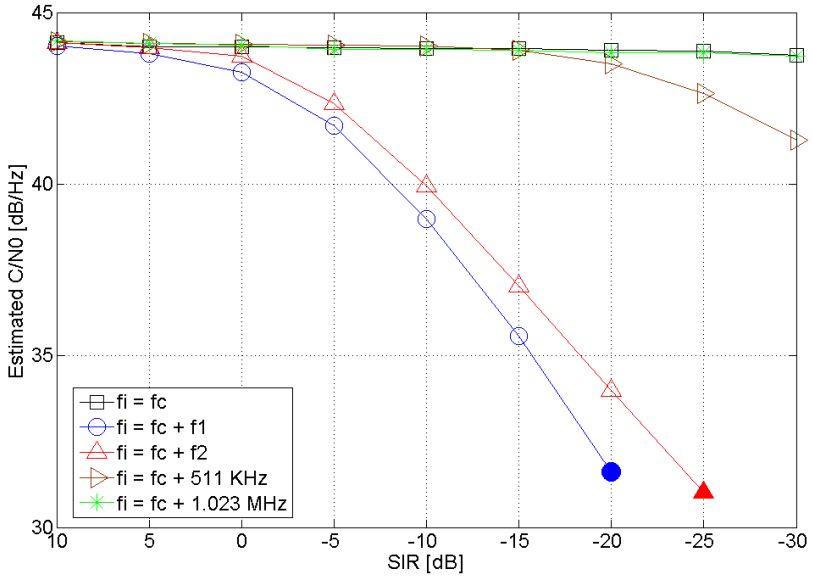

Figure 37: Estimated C/N0 performance as a function of the SIR of a CWI signal, which parameters are defined in scenario Exp.1 of Table 1.

The simulation results show that the performance degradation of the estimated C/N0 is larger than 10 dB when SIR $= -20$ dB for both $f_\delta = f_1$ and $f_\delta = f_2$ scenarios. In the cases of $f_\delta = 0$, $f_\delta = 511$ KHz and $f_\delta = 1.023$ MHz, the C/N0 performance degradation with respect to the interference-free scenario is negligible. For larger interference power levels, SIR < -20 dB, the GPS L1 receiver loses lock of the signal. The C/N0 value measured at the receiver prior to losing lock is plotted with a colour filled marker in Figure 37.

In the following simulation scenarios (Exp.2, Exp.3 and Exp.4), the estimated C/N0 performances are evaluated as a function of the generated C/N0 in the simulator, called here C/N0 input, for a fixed SIR value. Initially, the SIR is set to a low value of 0 dB corresponding to the Exp.2 scenario of Table 1. The simulation results show that the interference effects on the estimated C/N0 are negligible even in the situation of $f_\delta = f_1$, as shown in Figure 38. It is also observable that the relationship between estimated C/N0 and C/N0 input is linear until a value of approximately 50 dB. Above this value, the estimated C/N0 increases slowly as the C/N0 input increases tending to a ceiling value of approximately 56 dB. This saturation behavior is due to the capabilities of the MM tracking algorithm [15].

Furthermore, the C/N0 performances are analyzed when the SIR increases to a -10 dB value (scenario Exp.3), as illustrated in Figure 39. In this case, the performance degradation caused by the interference signals with $f_\delta = f_1$ and $f_\delta = f_2$ is significantly large for high values of C/N0 input. In particular, the estimated C/N0 when $f_\delta = f_1$ decreases approximately 5 dB with respect to the interference-free case for a C/N0 input value of 45 dB.

Finally, the tracking metrics are evaluated in the presence of an interference signal with a very large power level corresponding to a SIR $= -20$ dB, as described in scenario Exp.4 of Table 1. In this situation, the C/N0 performance degradation for $f_\delta = f_1$ and $f_\delta = f_2$ interference signals with respect to the interference-free case are 12 dB and 10 dB respectively, as shown in Figure 40. It is also noticeable that the estimated C/N0 curves for both $f_\delta = f_1$ and $f_\delta = f_2$ CWI signals saturate for values of C/N0 > 40 dB providing an estimated C/N0 ceiling value of 36 dB.

The simulation analysis of the EVM tracking metric in the presence of a CWI signal are provided in the Annex C.

5.3.2 Pulse Continuous Wave Interference

A PCWI signal is considered in the following set of simulations. The analytical expression of the PCWI signal is given by

$$i_{pi}(t) = \sqrt{2P_i} \sum_{n=1}^{+\infty} cos(2\pi f_c t + \phi_i) q\left(\frac{t - nP}{T_p}\right), \tag{30}$$

where $q(t)$ is a rectangular pulse signal with unitary energy value, P is the pulse repetition time (PRT) and T_p is the pulse duration, also called duty cycle (DC). The relationships between the estimated C/N0 and the SIR corresponding to the scenario Exp.5 of Table 1

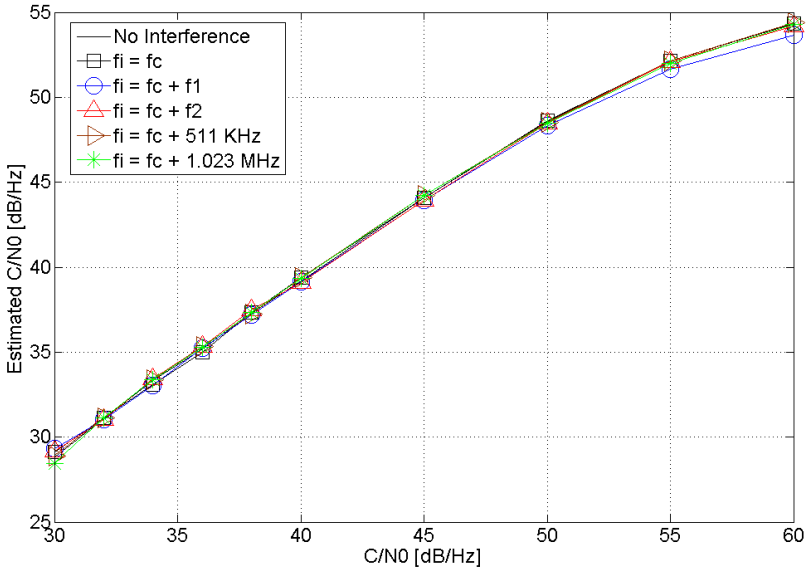

Figure 38: Estimated C/N0 performance as a function of the C/N0 input for a CWI signal with SIR $= 0$ dB, which parameters are defined in scenario Exp.2 of Table 1.

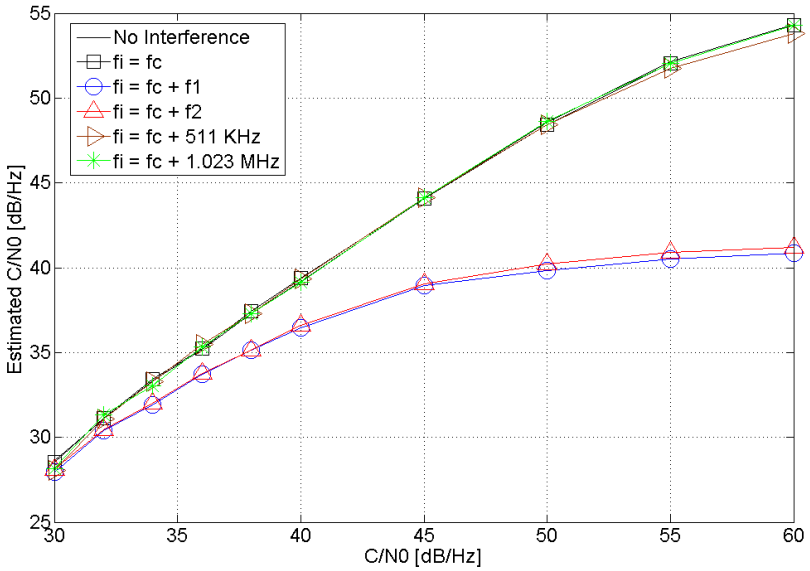

Figure 39: Estimated C/N0 performance as a function of the C/N0 input for a CWI signal with SIR $= -10$ dB, which parameters are defined in scenario Exp.3 of Table 1.

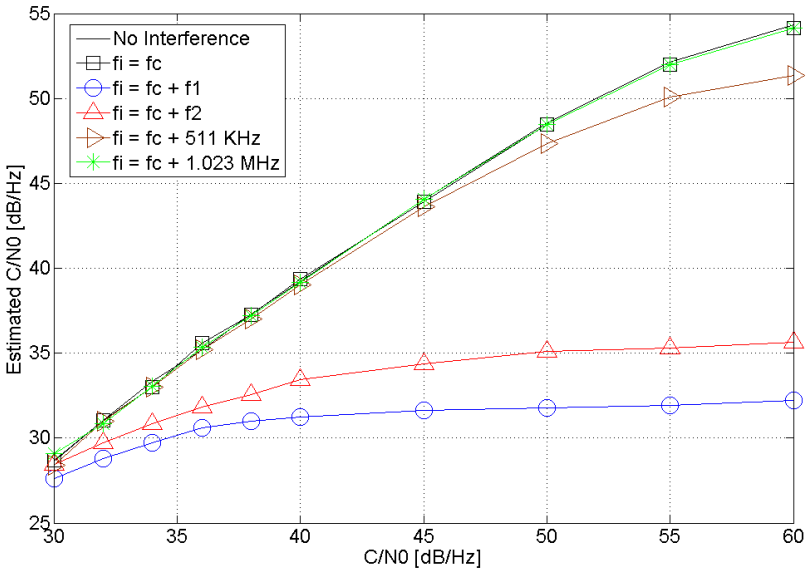

Figure 40: Estimated C/N0 performance as a function of the C/N0 input for a CWI signal with SIR $= -20$ dB, which parameters are defined in scenario Exp.4 of Table 1.

are plotted in Figure 41 for the five centre frequencies defined in the CWI section. As predicted, the interference effects on the C/N0 performances are lower than the CWI case since DC $= 10\%$. Note that a CWI signal corresponds to a PCWI signal with DC $= 100\%$. In this scenario, the C/N0 performance degradation when $f_\delta = f_1$ is less than 5 dB for values of SIR ≥ -15 dB, with respect to the minimum interference case ($f_\delta = 1.023$ MHz)

Subsequently, the estimated C/N0 waterfall curves are plotted as a function of the duty cycle (Exp.6) in Figure 42 for a large interference level, SIR $= -20$ dB. The simulation results show that if the duty cycle of the interference signal is chosen to be below 5%, the degradation of the C/N0 performances is lower than 6 dB for any interference centre frequency value.

Finally, the C/N0 performances as a function of the PRT are provided in Figure 43 for the simulation scenario defined in Exp.7 of Table 1. The results show that the performance degrades as the PRT increases.

A simulation analysis of the EVM tracking metric in the presence of a PCWI signal is provided in the Annex C.

5.3.3 DVB-T Harmonics Interference

Finally, the last interference source considered in this simulation work corresponds to the 3rd harmonic of a DVB-T signal. The harmonics are present in the GPS L1 frequency

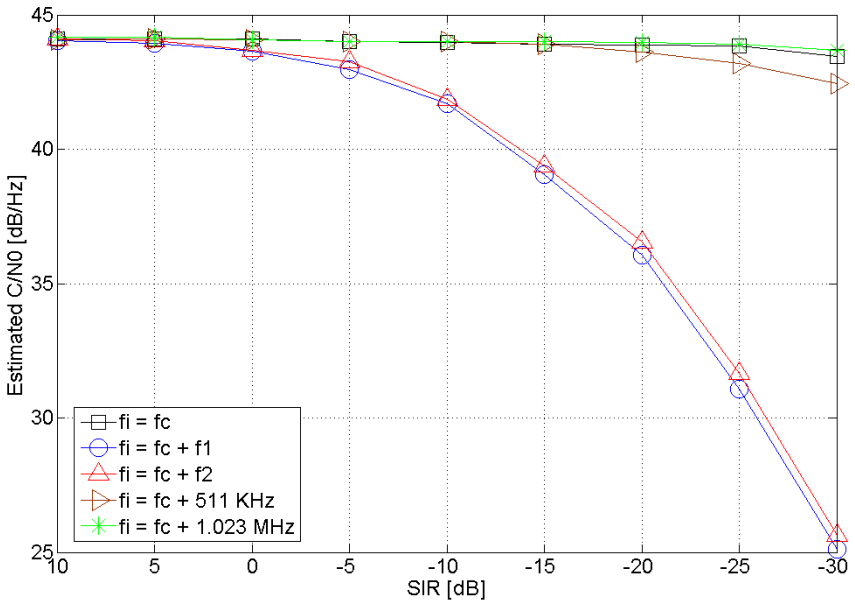

Figure 41: Estimated C/N0 performance as a function of the SIR of a PCWI signal, which parameters are defined in scenario Exp.5 of Table 1.

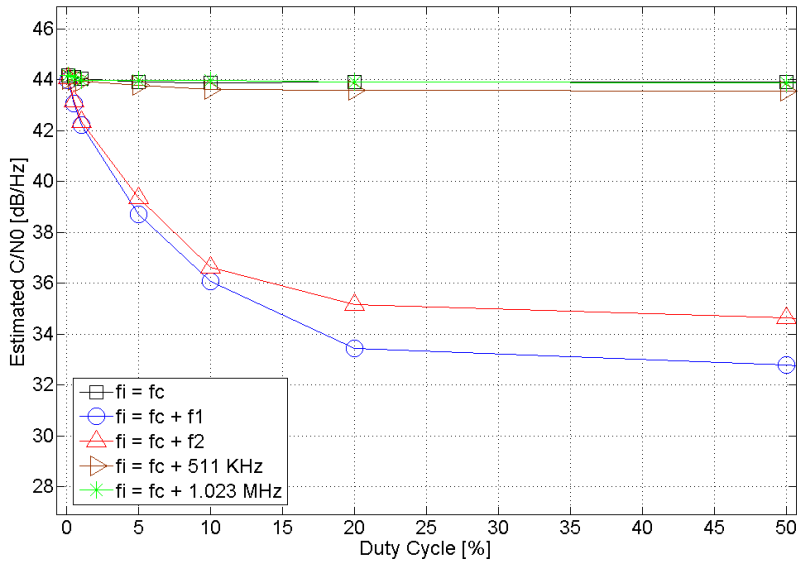

Figure 42: Estimated C/N0 performance as a function of the Duty Cycle of a PCWI signal with SIR $= -20$ dB ,which parameters are defined in scenario Exp.6 of Table 1.

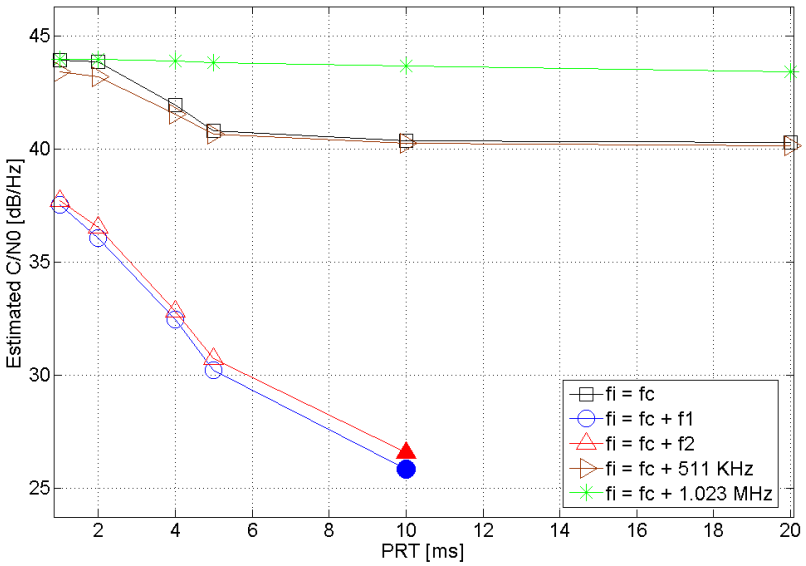

Figure 43: Estimated C/N0 performance as a function of the Pulse Repetition Time of a PCWI signal with SIR $= -20$ dB ,which parameters are defined in scenario Exp.7 of Table 1.

band due to the electronic malfunctioning of the DVB-T transceivers caused by the non-linear behavior of the amplifiers. The DVB-T employs an orthogonal frequency-division multiplexing (OFDM) signalling structure with 1705 sub-carriers ($2k$ mode version). The simulated DVB-T signal in this analysis has 7 MHz bandwidth and operates in the UHF-IV ($470 - 582$ MHz) band producing 3rd harmonics. The analytical expression for the n-th harmonic signal is written as

$$i_{dvbt}(t) = \sqrt{2P_i}\left(\Re\left\{e^{j2\pi f_h t}\sum_{k=0}^{Nsc-1} d_k e^{j2\pi(k-N_{sc}/2)(t-\Delta)/T_U}\right\}\right)^n, \tag{31}$$

where $f_h = nf_c$ is the center frequency of the n-th harmonic signal, f_c is the center frequency of the DVB-T signal and N_{sc} is the total number of sub-carriers (2048 including zero padding). The parameters d_k, Δ and T_U in (31) represent the modulated data, the guard interval duration and the inverse of the carrier spacing respectively. Two modulation schemes, QPSK and 64-QAM, are considered in this analysis.

The PSD of a DVB-T signal and its third harmonic are depicted in Figure 44. It can be observed that the bandwidth of the signal increases proportional to the order of the harmonic, such as $W = n \times 7$ MHz. It is also noticeable that the separation between spectral lines decreases when the order of the harmonic increases.

The probability distribution function (PDF) of the in-phase and the quadrature contributions of the DVB-T 3rd harmonic signal, which uses a QPSK and a 64-QAM modulation techniques, on the decision variable are plotted in Figure 45(a) and Figure 45(b) respec-

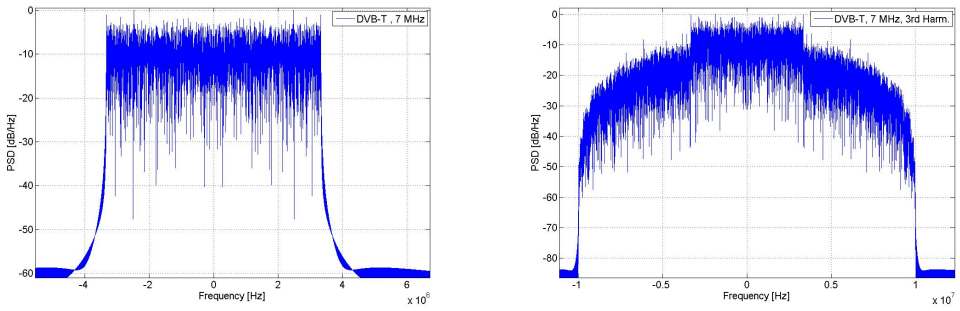

(a) DVB-T PSD (b) 3rd harmonic DVB-T PSD

Figure 44: PSD of the DVB-T signal and its 3rd harmonic

tively. At a first glance, it is noticeable that the interference contribution to the decision variable is Gaussian for both modulation schemes.

Subsequently, the estimated C/N0 performances as a function of the SIR are analyzed in this section by considering two types of interference signals. These interferers are the the 3rd harmonic of a DVB-T signal and an Additive White Gaussian Noise (AWGN) signal, whose values are described in Exp.8 of Table 1. Initially, the simulation results depicted in Figure 46 show that the estimated C/N0 performance of the DVB-T 3rd harmonic, as previously predicted, behaves identical to a Gaussian noise for both QPSK and 64-QAM modulation schemes. The performance reduction with respect to the interference-free case is 3 dB and 10 dB for SIR $= -20$ dB and SIR $= -30$ dB respectively, when the C/N0 input is 45 dB.

Furthermore, the estimated C/N0 performances as a function of the generated C/N0 are presented in the following analysis for several values of SIR. In particular the SIR values are 0 dB, -10 dB, -15 dB, -20 dB, and -30 dB,, as described in Exp.9 of Table 1.

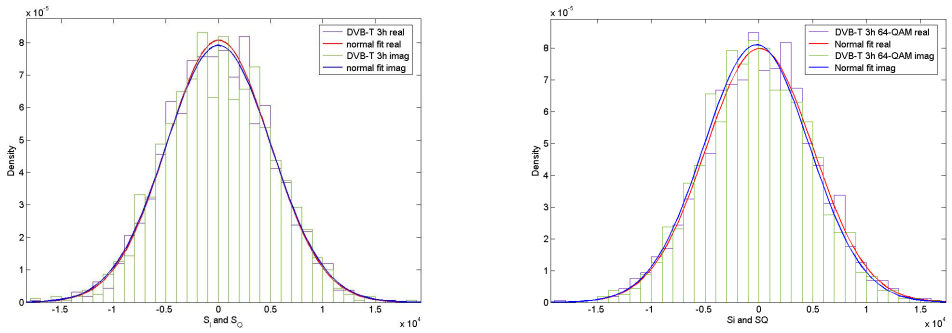

(a) QPSK Modulation (b) 64-QAM Modulation

Figure 45: PDF of the IQ components form the QPSK and 64-QAM modulated DVB-T 3rd harmonic interference signal.

The simulation results plotted in Figure 47 illustrate that when C/N0 $\leq$ 45 dB, the GPS L1 receiver can combat the effects of the DVB-T 3rd harmonic interference if SIR ≥ -20 dB. However, in the situation of SIR $= -30$ dB, the degradation of the estimated C/N0 with respect to the interference-free scenario is approximately 9 dB when the C/N0 $=$ 45 dB.

The previous simulations illustrate the reduction of the signal quality as a function of the signal-to-interference ratio. The interference power that is perceived at the receiver depends on the transmission power and on the distance with regard to the DVB-T base station. The Effective Isotropically Radiated Power (EIRP) of the DVB-T third harmonic is calculated as $EIRP = P_t G_t$, where P_t and G_t represents the transmitted power and the transmitter antenna gain, respectively. Considering a free space path loss model, the SIR can be derived from

$$\text{SIR} = \frac{P_s \left(\frac{4\pi fd}{c}\right)^2}{\text{EIRP}\, G_r} \tag{32}$$

with G_r the receiver antenna gain and c the speed of light. The parameters P_s, f and d of expression (32) are the GNSS received signal power, the interference central frequency and the distance between the interferer and the victim receiver. In Figure 48, the SIR is illustrated as a function of the EIRP and the distance d. This simulation tool allows to determine the minimum distance that corresponds with a guaranteed signal quality.

The simulation analysis of the EVM tracking metric in the presence of both AWGN and DVB-T 3rd harmonic interference signals are presented in the Annex C.

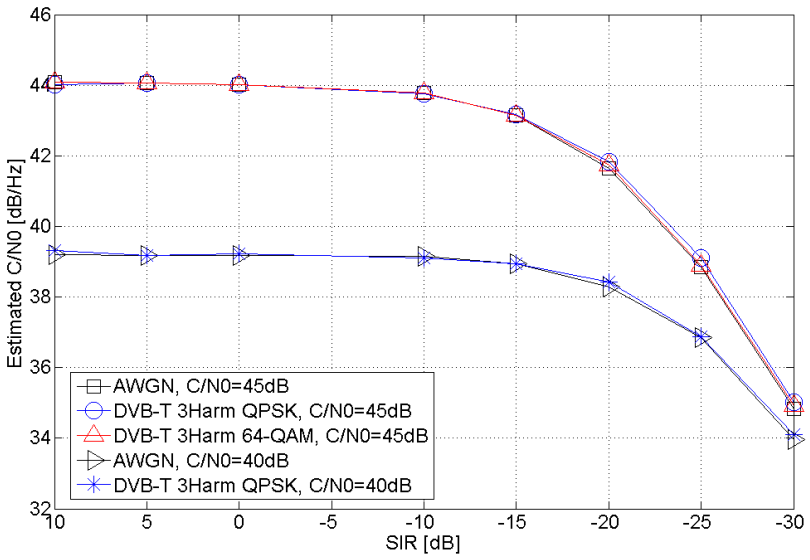

Figure 46: Estimated C/N0 performance as a function of the SIR of AWGN and DVB-T 3rd harmonic interference signals, which parameters are defined in scenario Exp.8 of Table 1.

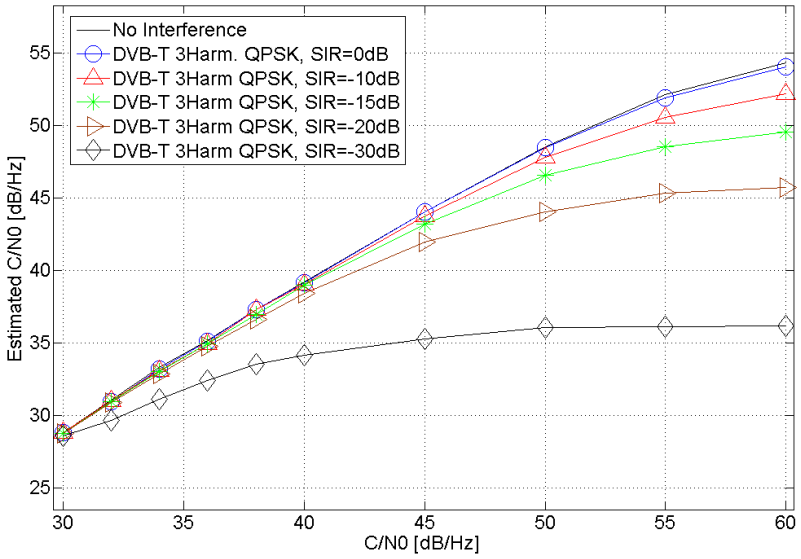

Figure 47: Estimated C/N0 performance as a function of the C/N0 for AWGN and DVB-T 3rd harmonic interference signals, which parameters are defined in scenario Exp.9 of Table 1.

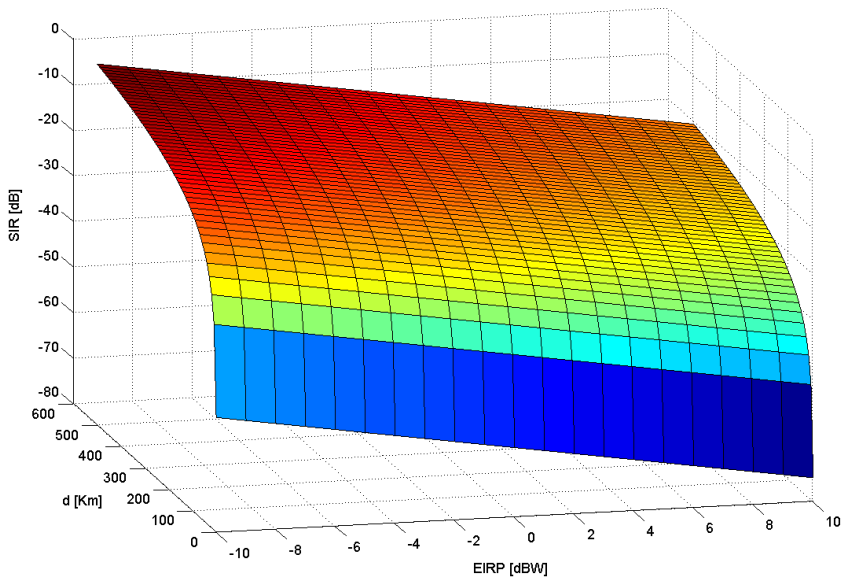

Figure 48: Reduction of the SIR as a function of (i) the distance between DVB-T interferer and victim receiver and (ii) the EIRP of the DVB-T third harmonic

5.4 Concluding Remarks

The estimated C/N0 performances of a GPS L1 satellite, in the presence of CWI, PCWI or the 3^{rd} harmonic of a DVB-T signal, as a function of the SIR or the generated C/N0 were evaluated in this section by means of a simulation analysis. Firstly, the simulation results showed that the performance degradation of the estimated C/N0 when CWI is present, with respect to the interference-free situation, is larger than 10 dB when SIR $= -20$ dB and $f_i = f_c + f_1$. However, in the situation of an arbitrary selection of the f_i (for example, $f_i = f_c + 511$ KHz), the C/N0 degradation due to high interference effects is lower than 3 dB. This is in accordance with the experimental results obtained in section 4.1. Also, in the same scenario, it is observable that the simulation receiver loses lock when SIR < -20 dB. This SIR is equivalent to an approximate value of INR > 15 dB. Thus, the sensitivity of the simulation receiver is in good agreement with the PRO2 receiver used in the experimental work.

Subsequently, the estimated C/N0 performance is evaluated in the presence of a PCWI signal with different values of DC. The simulation results showed that if the DC is below 10%, the interference effects on the C/N0 are negligible. This result is also in concordance with the observations obtained in the experimental study of section 4.2.

Finally, the estimated C/N0 performances as a function of the SIR were analyzed by considering two types of interference signals. These interferers are the the 3^{rd} harmonic of a DVB-T signal and an Additive White Gaussian Noise (AWGN) signal. The simulation results proved the theoretical findings in section 3, that the 3^{rd} harmonic of a DVB-T interference contribution to the decision variable is Gaussian independently of the modulation scheme of the original DVB-T signal.

6 Summary

The main objective of this report was to assess the impact of unintentional interference on GNSS receivers. The overall scope was to perform an impact assessment of unintentional radio frequency interference on critical infrastructures relying on GNSS-services. Unintentional interference is a high probability event. In this report, different scenarios of unintentional interference were selected, covering white noise, CWI, pulsed CWI and DVB-T. The impact of the different types of unintentional interference has been evaluated on the acquisition and the tracking process, involving theoretical analysis, simulation and experimental work.

The probabilistic nature of the acquisition problem suggests to evaluate the performance of the acquisition process by means of an analytical approach or by simulations. The main achievement of this part is the development of analytical tools to assess how interference impacts the acquisition performance for different types of interference and for different implementations of the acquisition process. For CWI, the simulation results show that the impact of CWI is most harmful when the tone falls together with the strongest line of the GNSS PRN code, and moreover the performance reduction has been quantified. Most of the attention has been given to the scenario of DVB-T interference. First, it has been shown that the impact of a DVB-T signal, or its second and third harmonic, is equivalent to the impact of white noise. Further, the effects of fading have been added to the analysis. It has been shown that fading on the interfering signals improves the acquisition performance, while fading with respect to the GNSS signals deteriorates the acquisition performance.Different fading distributions have been considered, as well as different decision statistics. Overall, this analysis of the acquisition process yielded several analytical and simulation tools that allow to determine minimum distances to interferers, which correspond with a minimum acquisition performance.

The interference effects have also been evaluated on both professional and commercial GPS L1 receivers. For CW interference, the performance degradation is mainly noticeable when the frequency falls together with the strongest spectral lines of the GNSS PRN code. For $\mathrm{INR} \geq 20\mathrm{dB}$, the C/N_0 degradation with respect to the interference-free situation, can vary between 5 and 10 dB, depending on the type of receiver. For PCWI, the measurements show that for $\mathrm{INR} = 20\mathrm{dB}$, interference falling together with one the highest spectral line and duty cycles smaller than 20 %, the C/N_0 degradation is lower than 3 dB. Interference originating from DVB-T is a wideband signal and interferes with all satellites in view. The variance of the position has been observed for the different types of interference. CWI and PCWI do not impact the variance of the position calculation, whereas the third harmonic of DVB-T causes a larger variance, since all satellites are effected by the wideband interference.

Since no implementation details are known about the commercial and the professional receivers, it is often difficult to draw concise conclusions. Therefore, additional simulations have been performed that allow to have complete control on all the parameters of

the signal and the receiver. The same interference scenarios have been simulated as for the experimental work. The trends observed for the experimental work are found back in the simulation results.

ANNEX A: Peak Ratio Decision Statistic

The acquisition of the GNSS signal is achieved when the decision variable S surpasses a defined threshold

$$S > T, \tag{33}$$

where T is the threshold and S is the decision variable defined as

$$S = \frac{S_1}{S_2}. \tag{34}$$

The variables S_1 and S_2 are the two maximum values chosen in the search space $\bar{S}$, composed of elements $S[\tau, f_d]$, as explained in 3.4.3. Without loss of generality, the doppler frequency is assumed to be known. Therefore, the search space loses its dependency of the doppler frequency and can be considered one-dimensional over the codephase. The variable $S[\tau] \in \bar{S}$ can now be written as

$$S[\tau] = \left| \frac{1}{N} \sum_{n=1}^{N_{\text{sat}}} \sqrt{C} h_n R_n[\tau] e^{-j\phi_n} + S_i[\tau] + S_n[\tau] \right|^2, \tag{35}$$

where N_{sat} is the number of satellites in view, h_n is the fading affecting the n^{th} satellite signal[1], $R_n[\tau]$ is the cross-correlation function between the code under search and the code of the nth satellite and $S_n[\tau]$ is a complex Gaussian random variable with power spectral density $\sigma^2_{S_n} = N_0/(2T_{\text{per}})$.

In order to calculate the probability of detection, we need to know the probability density function (pdf) of the decision variable S, and hence, of the variables S_1 and S_2. Since we consider a case with relatively strong satellite signals, we assume that $S_1 = \max\{\bar{S}\}$ yields the correct code phase τ_1 of the code under search. The r.v. S_1 can be written as

$$S_1 = \left| \sqrt{C} h_1 e^{-j\phi_1} + \underbrace{\sum_{n=2}^{N_{\text{sat}}} \sqrt{C} h_n R_n[\tau_1] e^{-j\phi_n}}_{S_c} + S_i[\tau_1] + S_n[\tau_1] \right|^2 \tag{36}$$

where we have considered that satellite number 1 as the one under search. S_c represents the contribution of the cross-correlation terms to the decision statistic and can be approximated by a complex Gaussian distributed r.v. with

$$\sigma^2_{S_c} = \left[\mathbb{E}\{h_n^2\}(N_{\text{sat}} - 1)\right] \sigma_c^2/2. \tag{37}$$

In other words, in case there are N_{sat} satellites in view, the cross-correlation noise stems from the contribution of $N_{\text{sat}} - 1$ satellites. Conditioning on h_1 the r.v. S_1 features a

[1] We consider the set of $\{h_n\}$ as i.i.d., the averaged fading power $\mathbb{E}\{h_n^2\} = 1$, and the value of h_n constant over the acquisition time.

non-central χ^2 distribution with 2 degrees of freedom and non-centrality parameter $\mu_{S_1} = h_1^2 C$. The second maximum is then chosen among the samples in $\bar{S}^-$ which correspond to $\bar{S}$, with exclusion of the sample corresponding to the autocorrelation peak. $\bar{S}^-$ is composed of i.i.d random variables that follow a central χ^2 distribution with two degrees of freedom, i.e. an exponential distribution with $\lambda = \frac{1}{2\sigma^2_{\text{tot}}}$, where $\sigma^2_{\text{tot}} = \sigma^2_{S_c} + \sigma^2_{S_i} + \sigma^2_{S_n}$.[2] It can be shown that $S_2 = \max\{\bar{S}^-\}$ follows a generalized exponential distribution with probability density function[16]

$$f_{S_2}(x) = \lambda(N-1)e^{-\lambda x}(1-e^{-\lambda x})^{(N-2)}. \tag{38}$$

We redefine now the decision variable of (34) as

$$\tilde{S} = S_1 - TS_2, \tag{39}$$

and as a consequence, acquisition is successful when

$$\tilde{S} > 0. \tag{40}$$

By using the inversion theorem, the probability of detection conditioned on h_1 can be expressed as

$$P_{\text{d}|\,h_1} = \mathbb{P}\left\{\tilde{S} > 0 | \, h_1\right\} = \frac{1}{2} + \frac{1}{\pi}\int_0^\infty \mathfrak{Re}\left\{\frac{\Psi_{\tilde{S}}(-js) - \Psi_{\tilde{S}}(js)}{js}\right\} ds, \tag{41}$$

where $\Psi_{\tilde{S}}(js)$ is the characteristic function (CF) of the variable $\tilde{S}$. The CF of the decision variable has the following expression

$$\Psi_{\tilde{S}}(js) = \mathbb{E}\left\{e^{js\tilde{S}}\right\} = \mathbb{E}\left\{e^{js(S_1 - TS_2)}\right\}. \tag{42}$$

Conditioning on h_1, the CF of the variable $\tilde{V}$ can be written as

$$\Psi_{\tilde{S}|\,h_1}(js) = \frac{1}{1-2js\sigma^2_{\text{tot}}} \exp\left(\frac{jsh_1^2 C}{1-2js\sigma^2_{\text{tot}}}\right) \Psi_{S_2}(-jsT), \tag{43}$$

where $\Psi_{S_2}(js)$ is the CF of the r.v. S_2. Taking the expectation over h_1, (43) simplifies to

$$\Psi_{\tilde{S}}(js) = \frac{1}{1-2js\sigma^2_{\text{tot}}} \Psi_{h_1^2}\left(\frac{jsC}{1-2js\sigma^2_{\text{tot}}}\right) \Psi_{S_2}(-jsT), \tag{44}$$

where $\Psi_{h_1^2}$ is the CF of the fading power. The CF of the generalized exponential distribution can be expressed as

$$\Psi_{S_2}(js) = \frac{\Gamma(N)\Gamma(1-\frac{js}{\lambda})}{\Gamma(N-\frac{js}{\lambda})}. \tag{45}$$

Unfortunately, the CF of the r.v. S_2 is not convenient for numerical integration, since the Gamma function diverges to infinity in the integration interval of (41). However, recently the generalized exponential function has been demonstrated to provide a good approximation of the Gamma distribution [17]. In this case, the opposite approach is applied

[2] We consider negligible the contribution of the autocorrelation

and we assign to the random variable S_2 a Gamma distribution as a good approximation of the generalized exponential distribution. The Gamma distribution is defined by two parameters k and θ. In order to estimate the parameters of the Gamma distribution, we impose the equivalence of the first two moments of the Gamma distribution with the first two moments of X_2. Mean and variance of a Gamma distribution are expressed as

$$\mu_G = k\theta \text{ and } \sigma_G^2 = k\theta^2, \tag{46}$$

while for S_2 we have

$$\mu_{S_2} = \frac{1}{\lambda}\left[\psi(N) - \psi(1)\right] \text{ and } \sigma_{S_2}^2 = \frac{1}{\lambda^2}\left[\psi\prime(1) - \psi\prime(N)\right], \tag{47}$$

where $\psi(x)$ and $\psi\prime(x)$ are the digamma and the polygamma function, respectively. Therefore, we have

$$\theta = \frac{\left[\psi(N) - \psi(1)\right]^2}{\psi\prime(1) - \psi\prime(N)}, \tag{48}$$

and

$$k = \lambda\frac{\psi(N) - \psi(1)}{\psi\prime(1) - \psi\prime(N)}. \tag{49}$$

Finally, the CF of $\tilde{S}$ can be obtained by inserting the CF of the Gamma distributed r.v. S_2 in (44)

$$\Psi_{\tilde{S}}(js) = \frac{1}{1 - 2js\sigma_{\text{tot}}^2}\Psi_{h_1^2}\left(\frac{jsC}{1 - 2js\sigma_{\text{tot}}^2}\right)(1 + jsT\theta)^{-k}, \tag{50}$$

Now we dispose of an expression of the CF of $\tilde{(S)}$ and consequently, the probability of detection can be calculated by numerical integration of (41). The results are further reported in Section 3.5.3.

ANNEX B: Measurement Results

A comprehensive display of the measured C/N0 as a function of the INR for GPS L1 satellites in the presence of CWI, PCWI or the 3rd harmonic of a DVB-T signal is provided in this annex. The measured C/N0 performances, for CWI evaluation purposes, of high elevation (HE) and low elevation (LE) satellites are provided in Figures 49-56. Subsequently, the C/N0 curves in the presence of a PCWI signal are provided in this section for different duty cycle values (DC $= 0.5\%$, DC $= 1\%$, DC $= 5\%$, DC $= 10\%$, DC $= 20\%$ and DC $= 50\%$) when using the PRO1 receiver (Figures 57-68) or the MM1 receiver (Figures 71-82). Furthermore, the C/N0 performances in the presence of a PCWI with DC $= 10\%$ are depicted in Figures 69-70 and Figures 82-83 for PRO2 and MM2 receivers respectively. Finally, the measured C/N0 waterfall curves impaired by a DVB-T 3rd harmonic signal are plotted in Figures 83-88 for all four GPS receivers.

The most significant results of the measurement campaign are summarised in the following tables. It was observed during measurements and simulation analysis that, under specific conditions, the GPS L1 receivers lose lock (LL) when the interference levels increase. The corresponding estimated C/N0 value prior to the loss of lock (i.e. sensitivity of the receiver) is measured as approximately 30 dB in this work. In the following analysis, the INR values obtained when the receiver sensitivity is fixed to C/N0 $= 30$ dB are presented in Table 2 for CWI. Note that the maximum value of INR used in the measurements is 30 dB. The simulation results show that the MM1 receiver loses lock before obtaining a measured C/N0 $= 30$ dB value for both HE and LE satellites. The maximum INR value that the PRO1 receiver is capable of tolerating when $f_i = f_c + f_1$ is 26 dB and 22.5 dB for HE and LE satellites respectively. Under the same conditions, when the MM2 receiver is employed, these INR values are > 30 dB and 27.5 dB for HE and LE respectively. These results show that the MM2 receiver possesses the highest sensitivity. Conversely, the PRO2 receiver loses lock prior to reaching a C/N0 $= 30$ dB when the satellite is in low elevation.

Subsequently, the INR values corresponding to a sensitivity of C/N0 $= 30$ dB are presented in Table 3 for the situation of a PCWI with DC $= 10\%$. Note that for lower values of DC (DC $= 0.5\%$, DC $= 1\%$ and DC $= 5\%$), an $INR > 30$ dB is always obtained for all satellite elevations and centre frequencies of the PCWI signal, as shown in Figures 57-62 and Figures 71-76. The measurement results show that an INR $> 30\%$ is measured for all receivers when a satellite is in high elevation. However, PRO2 and MM1 receivers lose lock before the critical C/N0 $= 30$ dB value when the satellite is in LE. Furthermore, the same analysis is repeated in Table 4 for values of DC $= 20\%$ and DC $= 50\%$ when PRO1 and MM1 receivers are employed. The measurement results show that the PRO1 receiver combat better the interference effects when the receiver is operating at its sensitivity level than the MM1 receiver.

Finally, the same analysis is applied to the case of 3rd harmonic of the DVB-T signal interference, as shown in Table 5. It can be observed that the INR values for a sensitivity

		PRO1 Rx	PRO2 Rx	MM1 Rx	MM2 Rx
HE	$f_i = f_c + f_1$	26.0	24.2	LL	> 30
	$f_i = f_c + f_2$	27.0	24.3	LL	> 30
	$f_i = f_c$	> 30	> 30	> 30	> 30
	$f_i = f_c + 511$ KHz	> 30	> 30	> 30	> 30
	$f_i = f_c + 1.023$ MHz	> 30	> 30	> 30	> 30
LE	$f_i = f_c + f_1$	22.5	LL	LL	27.5
	$f_i = f_c + f_2$	23.2	LL	LL	29.8
	$f_i = f_c$	> 30	> 30	> 30	> 30
	$f_i = f_c + 511$ KHz	> 30	LL	> 30	> 30
	$f_i = f_c + 1.023$ MHz	> 30	> 30	> 30	> 30

Table 2: INR values for a sensitivity level of C/N0 $= 30$ dB in the situation of CWI.

of C/N0 $= 30$ dB are much lower than in the case of CWI. As an example of this, a value of INR $= 17$ dB is required for LE satellite when using the MM2 receiver, while INR $= 27.5$ dB was measured in the CWI with $f_i = f_c + f_1$ case.

		PRO1 Rx	PRO2 Rx	MM1 Rx	MM2 Rx
HE	$f_i = f_c + f_1$	> 30	> 30	> 30	> 30
	$f_i = f_c + f_2$	> 30	> 30	> 30	> 30
	$f_i = f_c$	> 30	> 30	> 30	> 30
	$f_i = f_c + 511$ KHz	> 30	> 30	> 30	> 30
	$f_i = f_c + 1.023$ MHz	> 30	> 30	> 30	> 30
LE	$f_i = f_c + f_1$	29.0	LL	LL	29.0
	$f_i = f_c + f_2$	29.3	> 30	> 30	> 30
	$f_i = f_c$	> 30	> 30	> 30	> 30
	$f_i = f_c + 511$ KHz	> 30	> 30	> 30	> 30
	$f_i = f_c + 1.023$ MHz	> 30	> 30	> 30	> 30

Table 3: INR values for a sensitivity level of C/N0 $= 30$ dB in the situation of PCWI with $(DC) = 10\%$.

		DC = 20%		DC = 50%	
		PRO1 Rx	**MM1 Rx**	**PRO1 Rx**	**MM1 Rx**
HE	$f_i = f_c + f_1$	> 30	> 30	27.5	LL
	$f_i = f_c + f_2$	> 30	> 30	> 30	LL
	$f_i = f_c$	> 30	> 30	> 30	> 30
	$f_i = f_c + 511$ KHz	> 30	> 30	> 30	> 30
	$f_i = f_c + 1.023$ MHz	> 30	> 30	> 30	> 30
LE	$f_i = f_c + f_1$	24.0	LL	23.5	LL
	$f_i = f_c + f_2$	LL	> 30	24.0	LL
	$f_i = f_c$	> 30	> 30	> 30	> 30
	$f_i = f_c + 511$ KHz	> 30	> 30	> 30	> 30
	$f_i = f_c + 1.023$ MHz	> 30	> 30	> 30	> 30

Table 4: INR values for a sensitivity level of C/N0 $= 30$ dB in the situation of PCWI with $(DC) = 20\%$ and $(DC) = 50\%$.

		PRO1 Rx	**PRO2 Rx**	**MM1 Rx**	**MM2 Rx**
HE	$f_i = f_c$	> 30	> 30	> 30	18.5
	$f_i = f_c + 511$ KHz	> 30	> 30	> 30	> 30
LE	$f_i = f_c$	> 30	14.5	22.0	17.0
	$f_i = f_c + 511$ KHz	> 30	> 30	> 30	> 30

Table 5: INR values for a sensitivity level of C/N0 $= 30$ dB in the situation of DVB-T 3^{rd} harmonic interference.

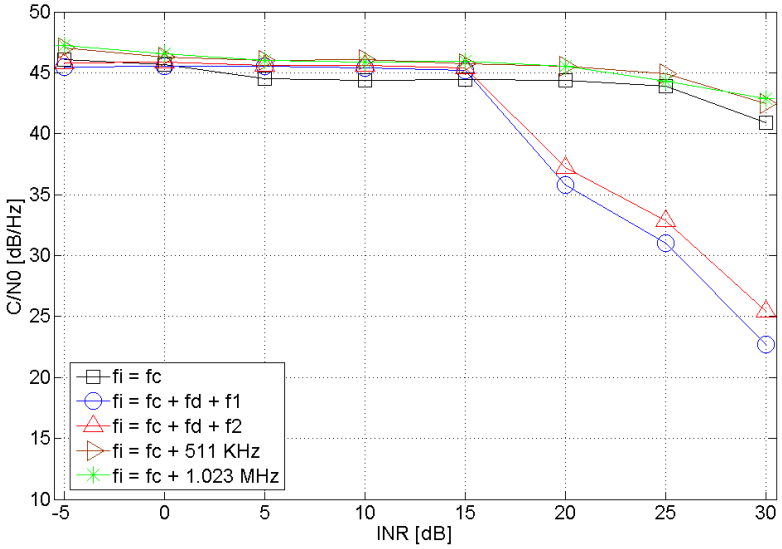

Figure 49: C/N0 measured at the PRO1 receiver of a HE satellite as a function of the INR in the presence of CWI.

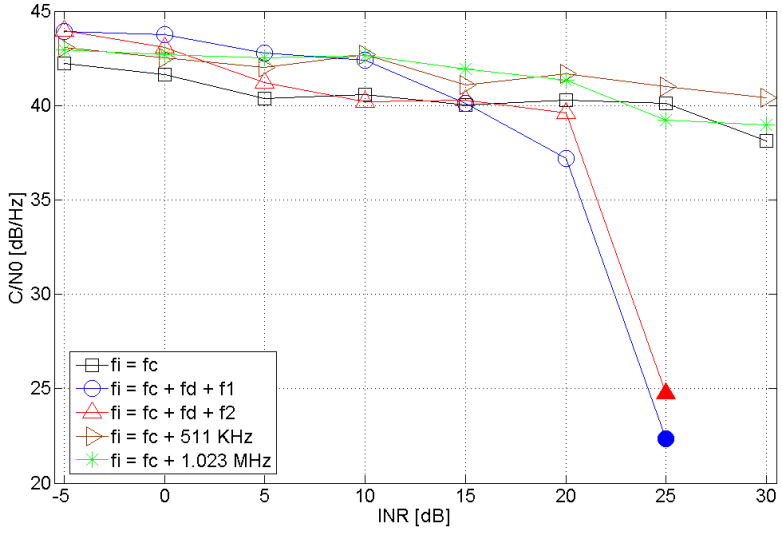

Figure 50: C/N0 measured at the PRO1 receiver of a LE satellite as a function of the INR in the presence of CWI.

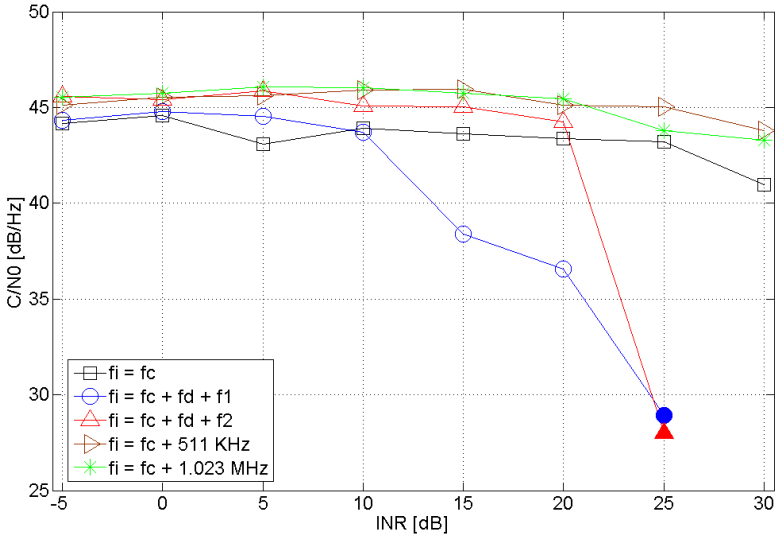

Figure 51: C/N0 measured at the PRO2 receiver of a HE satellite as a function of the INR in the presence of CWI.

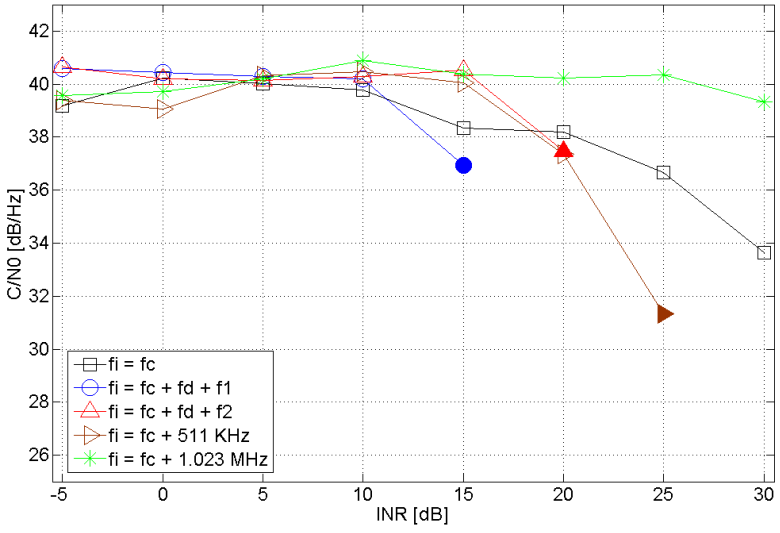

Figure 52: C/N0 measured at the PRO2 receiver of a LE satellite as a function of the INR in the presence of CWI.

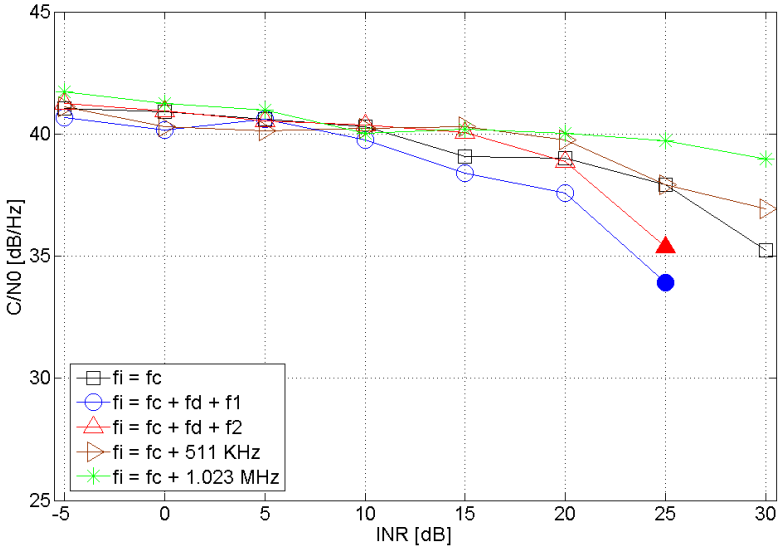

Figure 53: C/N0 measured at the MM1 receiver of a HE satellite as a function of the INR in the presence of CWI.

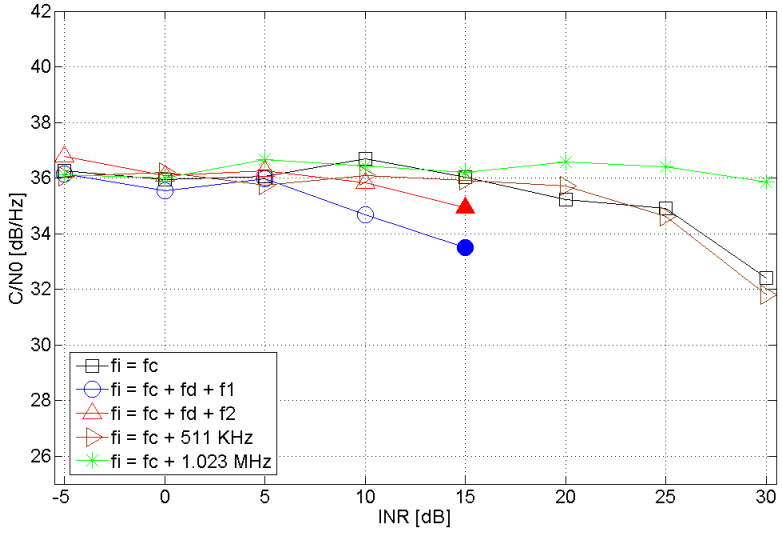

Figure 54: C/N0 measured at the MM1 receiver of a LE satellite as a function of the INR in the presence of CWI.

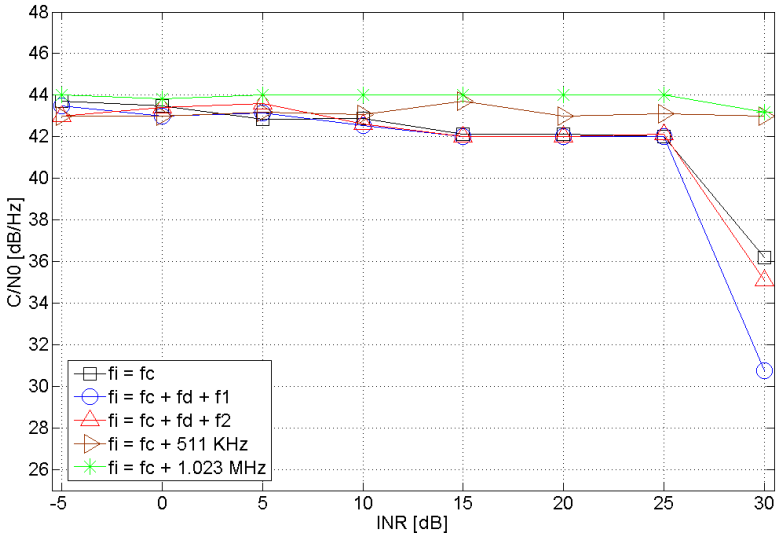

Figure 55: C/N0 measured at the MM2 receiver of a HE satellite as a function of the INR in the presence of CWI.

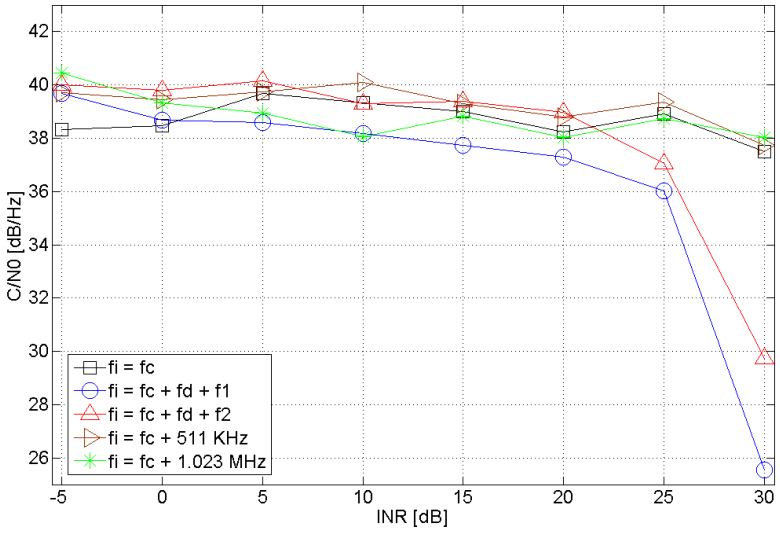

Figure 56: C/N0 measured at the MM2 receiver of a LE satellite as a function of the INR in the presence of CWI.

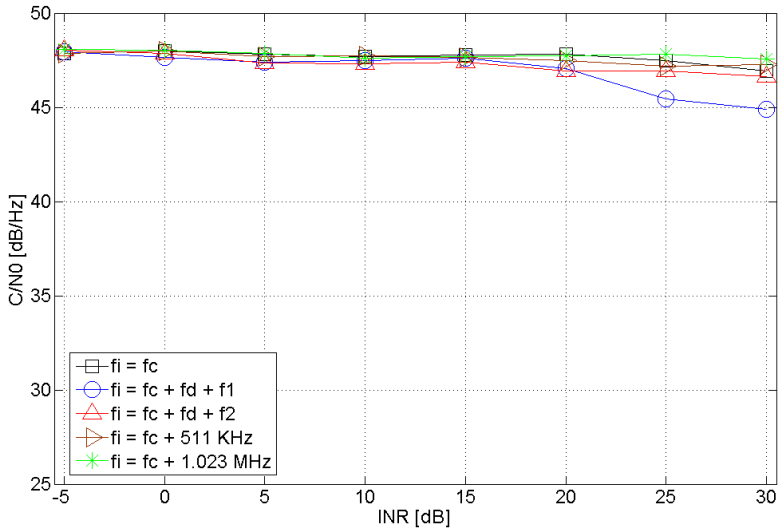

Figure 57: C/N0 measured at the PRO1 receiver of a HE satellite as a function of the INR in the presence of PCWI with DC = 0.5%.

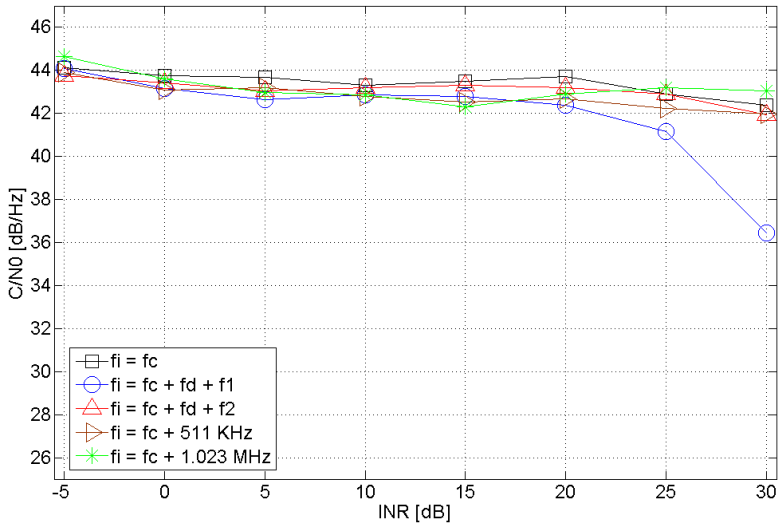

Figure 58: C/N0 measured at the PRO1 receiver of a LE satellite as a function of the INR in the presence of PCWI with DC = 0.5%.

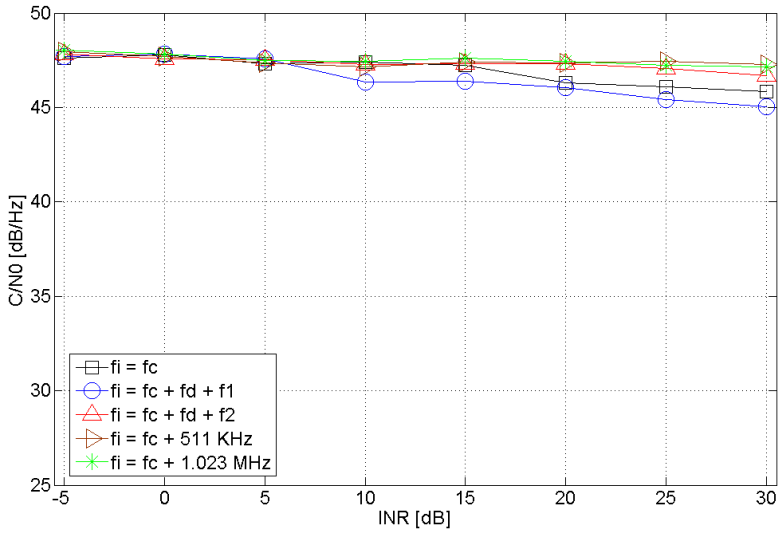

Figure 59: C/N0 measured at the PRO1 receiver of a HE satellite as a function of the INR in the presence of PCWI with DC $= 1\%$.

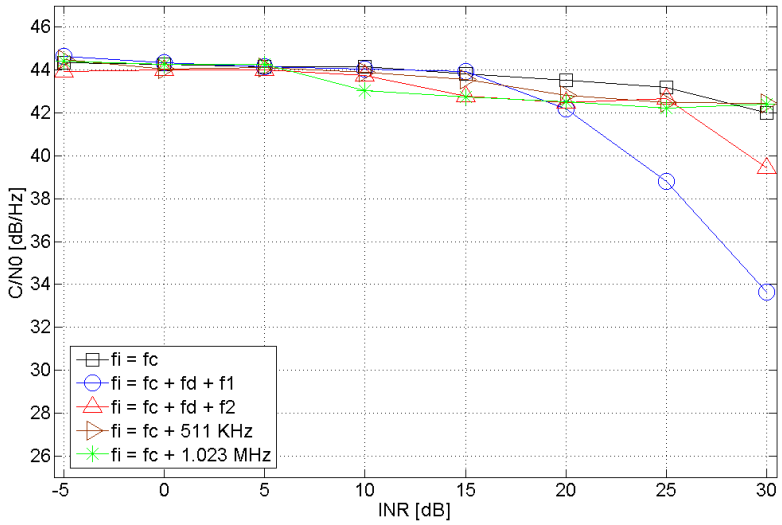

Figure 60: C/N0 measured at the PRO1 receiver of a LE satellite as a function of the INR in the presence of PCWI with DC $= 1\%$.

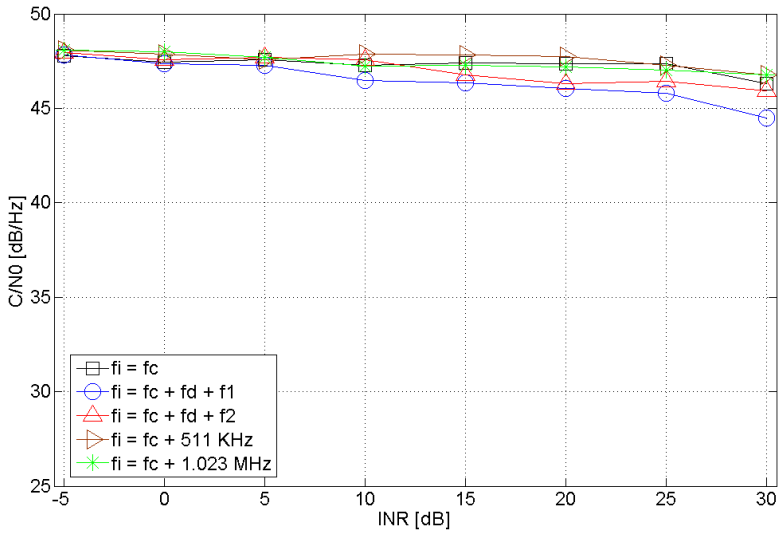

Figure 61: C/N0 measured at the PRO1 receiver of a HE satellite as a function of the INR in the presence of PCWI with DC = 5%.

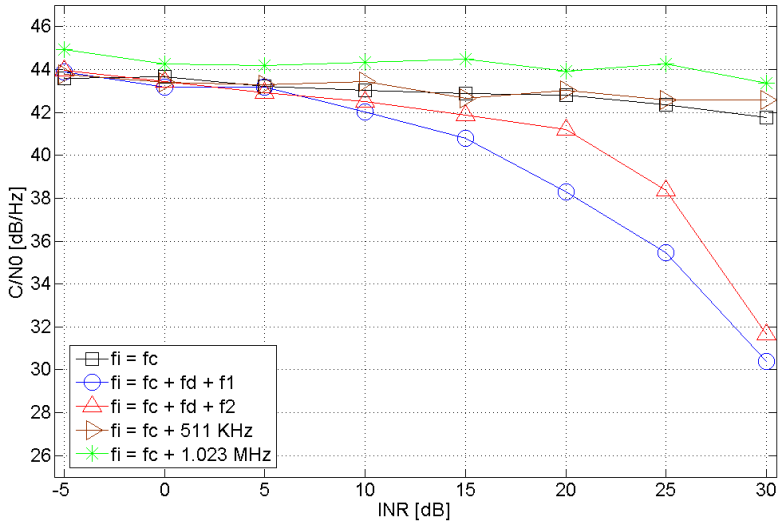

Figure 62: C/N0 measured at the PRO1 receiver of a LE satellite as a function of the INR in the presence of PCWI with DC = 5%.

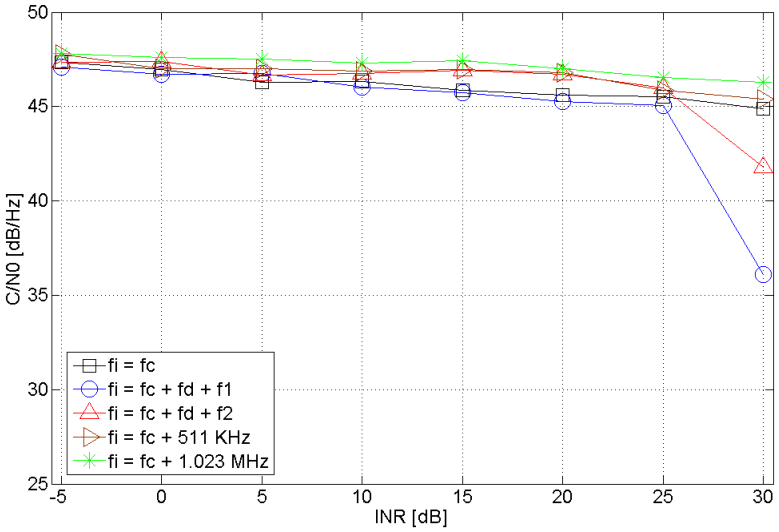

Figure 63: C/N0 measured at the PRO1 receiver of a HE satellite as a function of the INR in the presence of PCWI with DC = 10%.

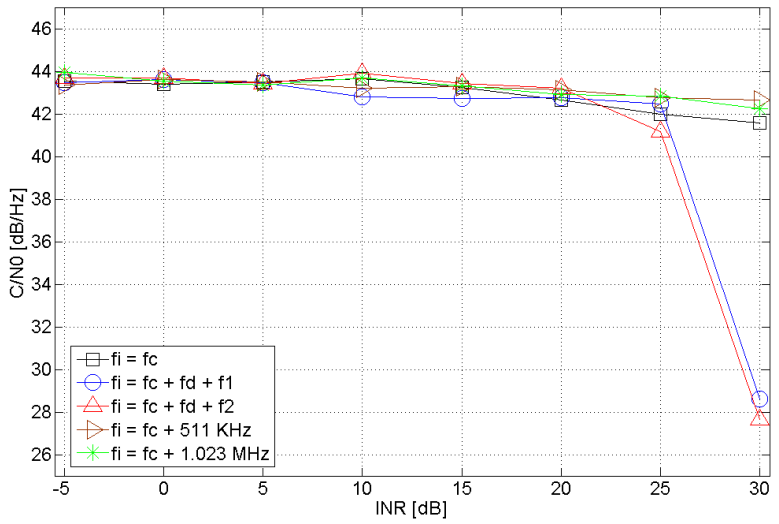

Figure 64: C/N0 measured at the PRO1 receiver of a LE satellite as a function of the INR in the presence of PCWI with DC = 10%.

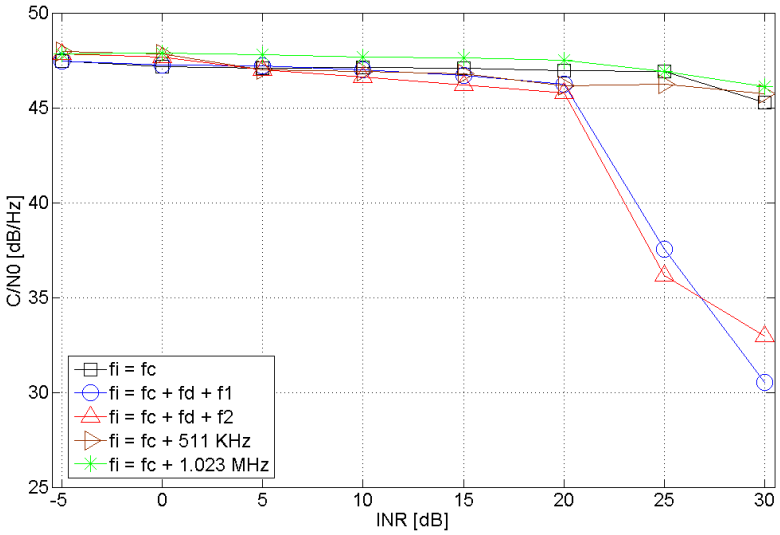

Figure 65: C/N0 measured at the PRO1 receiver of a HE satellite as a function of the INR in the presence of PCWI with DC = 20%.

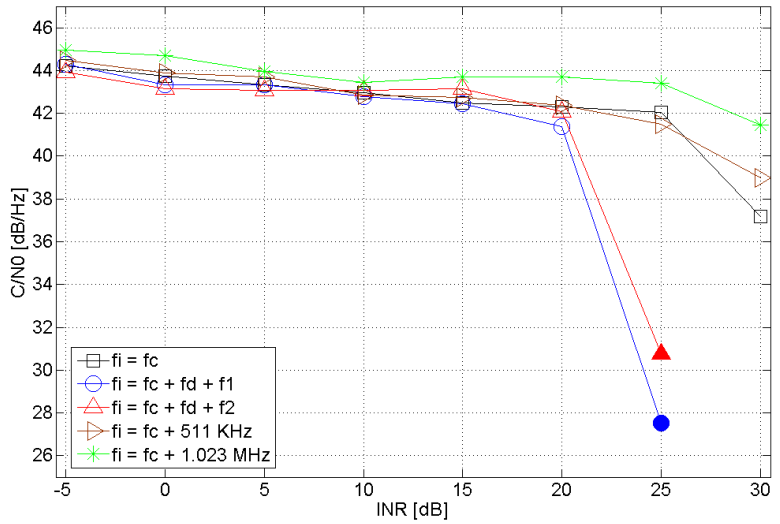

Figure 66: C/N0 measured at the PRO1 receiver of a LE satellite as a function of the INR in the presence of PCWI with DC = 20%.

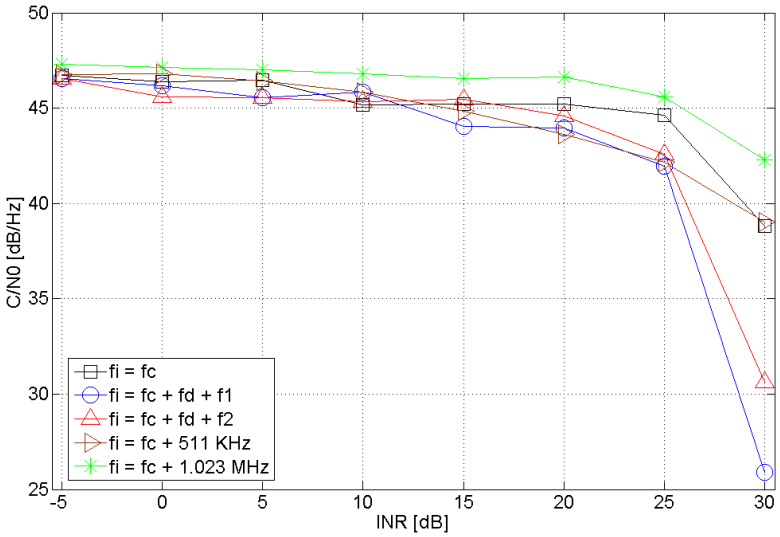

Figure 67: C/N0 measured at the PRO1 receiver of a HE satellite as a function of the INR in the presence of PCWI with DC = 50%.

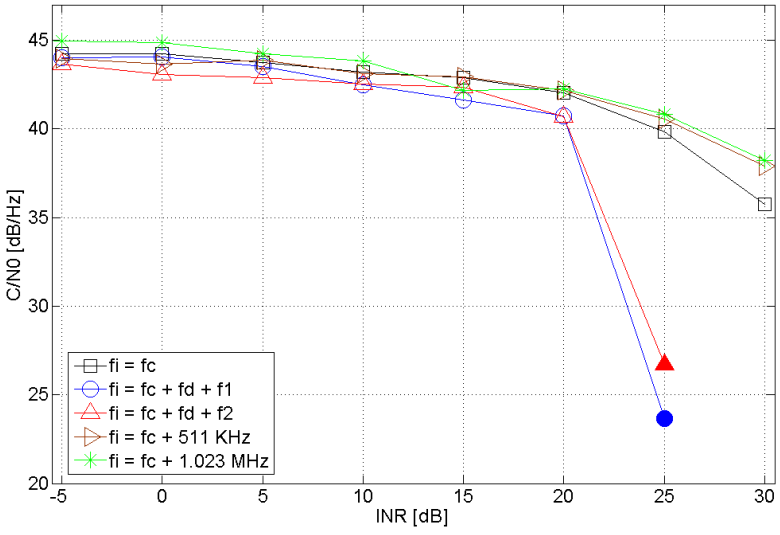

Figure 68: C/N0 measured at the PRO1 receiver of a LE satellite as a function of the INR in the presence of PCWI with DC = 50%.

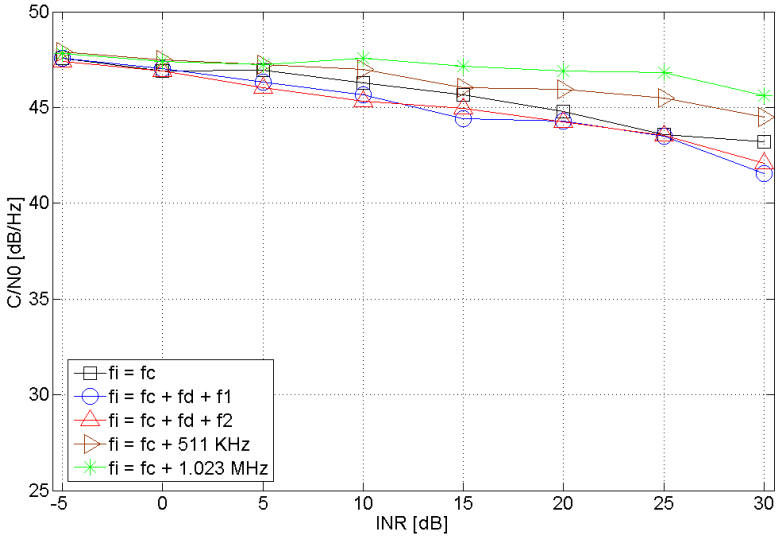

Figure 69: C/N0 measured at the PRO2 receiver of a HE satellite as a function of the INR in the presence of PCWI with DC = 10%.

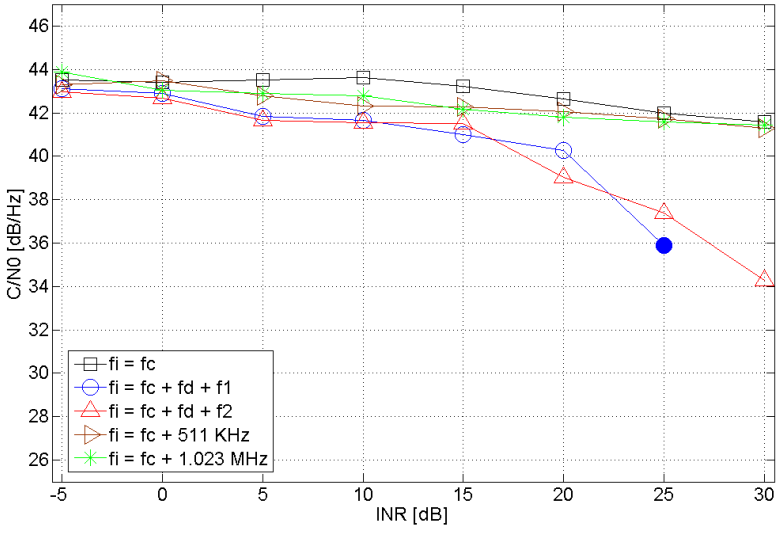

Figure 70: C/N0 measured at the PRO2 receiver of a LE satellite as a function of the INR in the presence of PCWI with DC = 10%.

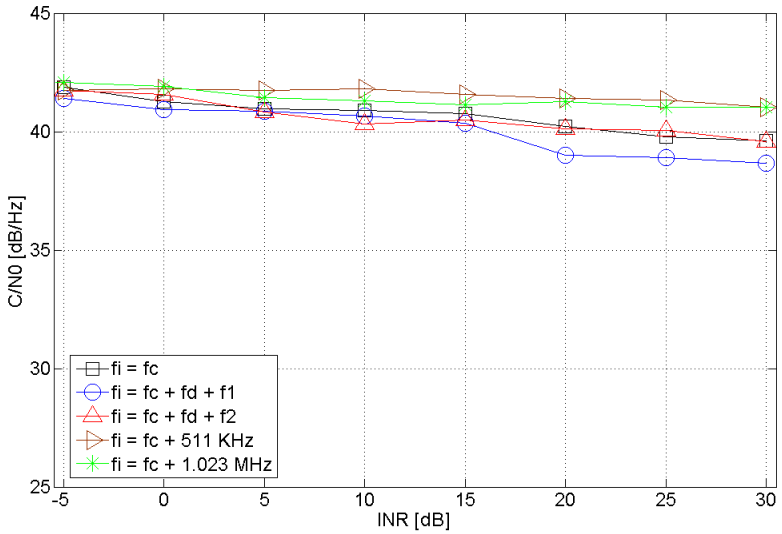

Figure 71: C/N0 measured at the MM1 receiver of a HE satellite as a function of the INR in the presence of PCWI with DC = 0.5%.

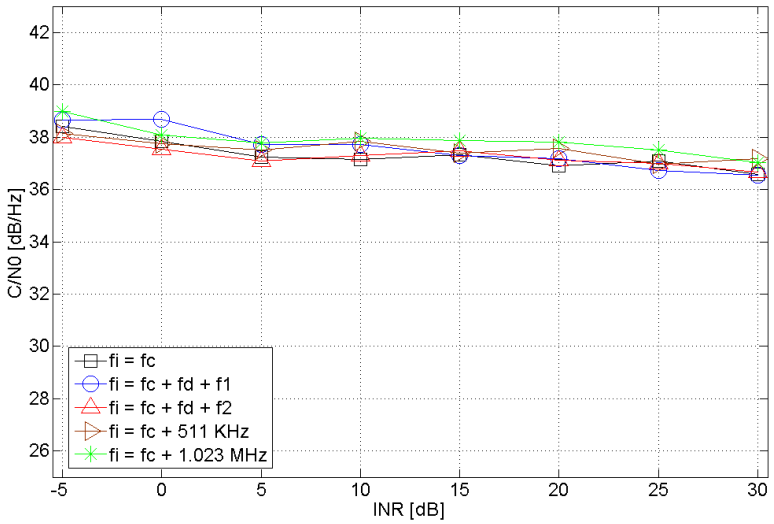

Figure 72: C/N0 measured at the MM1 receiver of a LE satellite as a function of the INR in the presence of PCWI with DC = 0.5%.

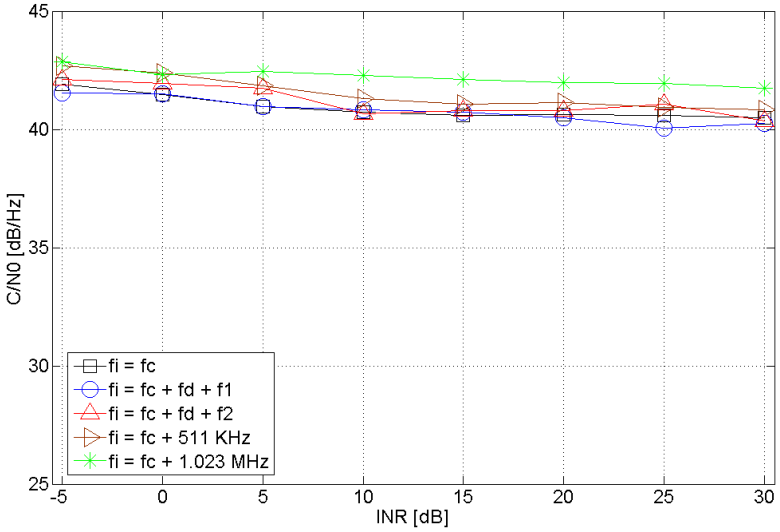

Figure 73: C/N0 measured at the MM1 receiver of a HE satellite as a function of the INR in the presence of PCWI with DC $= 1\%$.

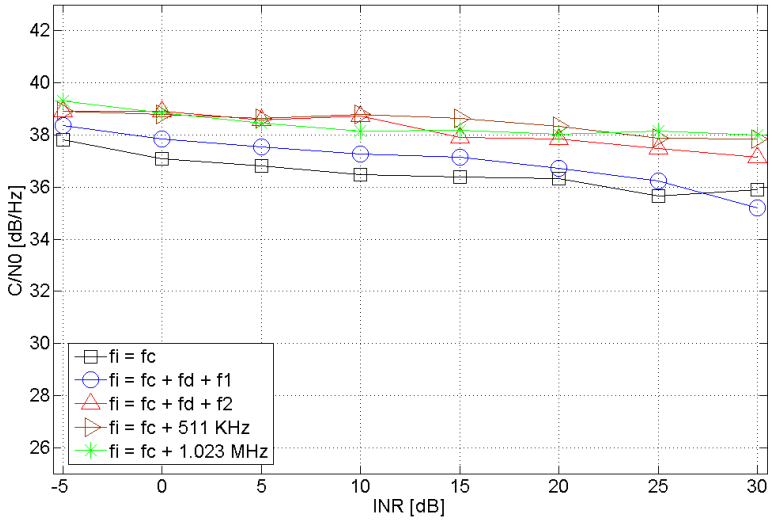

Figure 74: C/N0 measured at the MM1 receiver of a LE satellite as a function of the INR in the presence of PCWI with DC $= 1\%$.

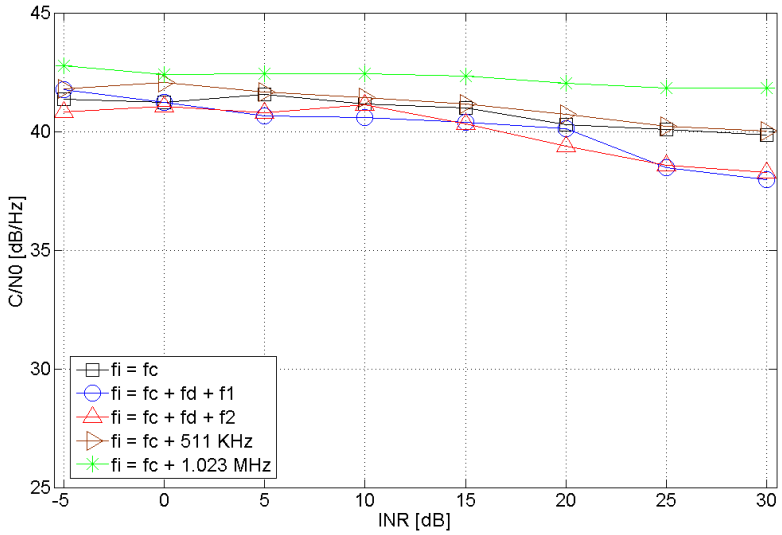

Figure 75: C/N0 measured at the MM1 receiver of a HE satellite as a function of the INR in the presence of PCWI with DC = 5%.

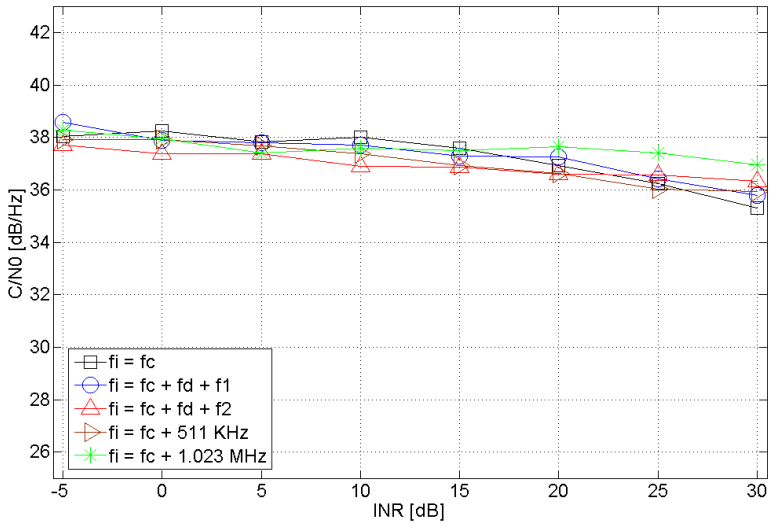

Figure 76: C/N0 measured at the MM1 receiver of a LE satellite as a function of the INR in the presence of PCWI with DC = 5%.

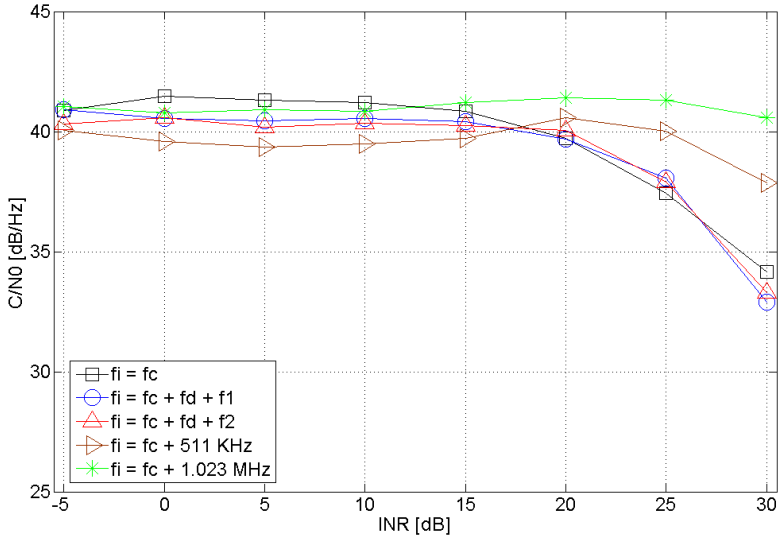

Figure 77: C/N0 measured at the MM1 receiver of a HE satellite as a function of the INR in the presence of PCWI with DC = 10%.

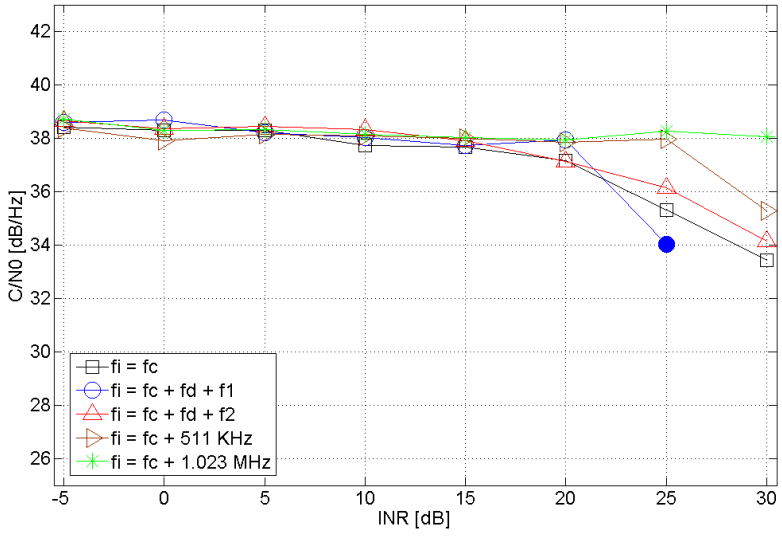

Figure 78: C/N0 measured at the MM1 receiver of a LE satellite as a function of the INR in the presence of PCWI with DC = 10%.

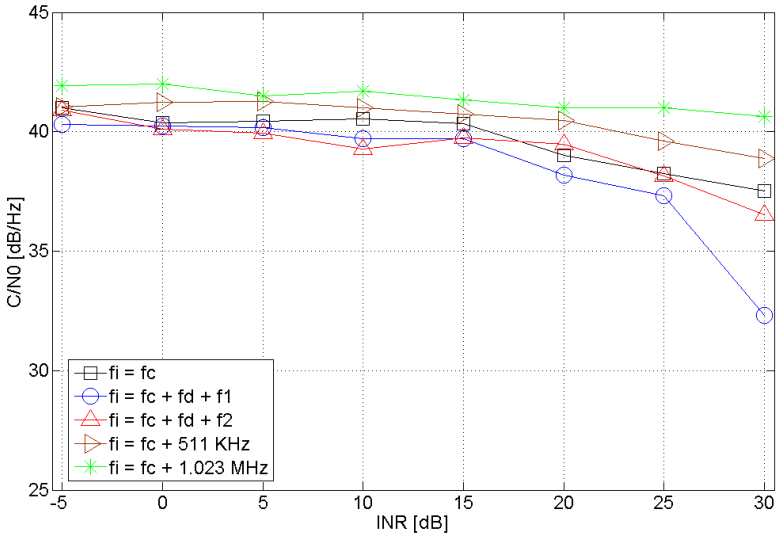

Figure 79: C/N0 measured at the MM1 receiver of a HE satellite as a function of the INR in the presence of PCWI with DC = 20%.

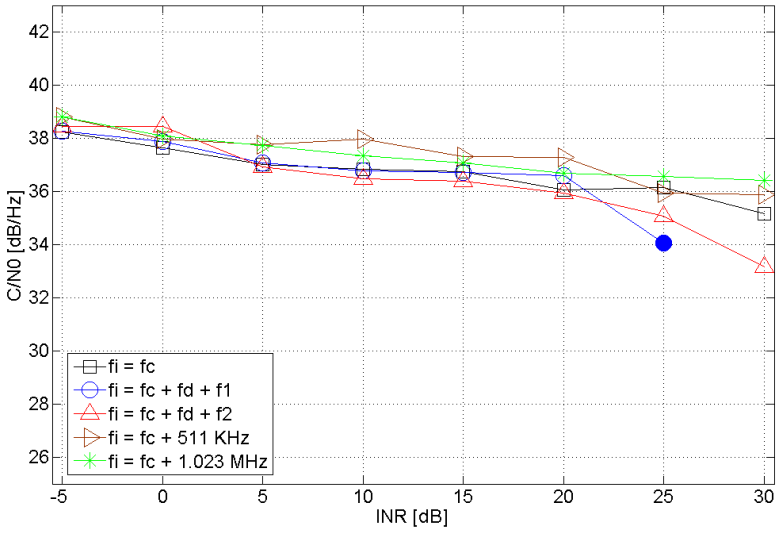

Figure 80: C/N0 measured at the MM1 receiver of a LE satellite as a function of the INR in the presence of PCWI with DC = 20%.

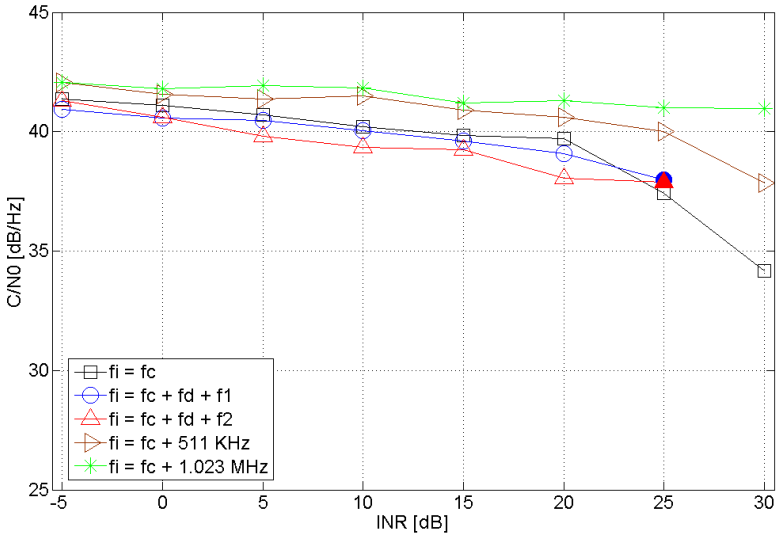

Figure 81: C/N0 measured at the MM1 receiver of a HE satellite as a function of the INR in the presence of PCWI with DC = 50%.

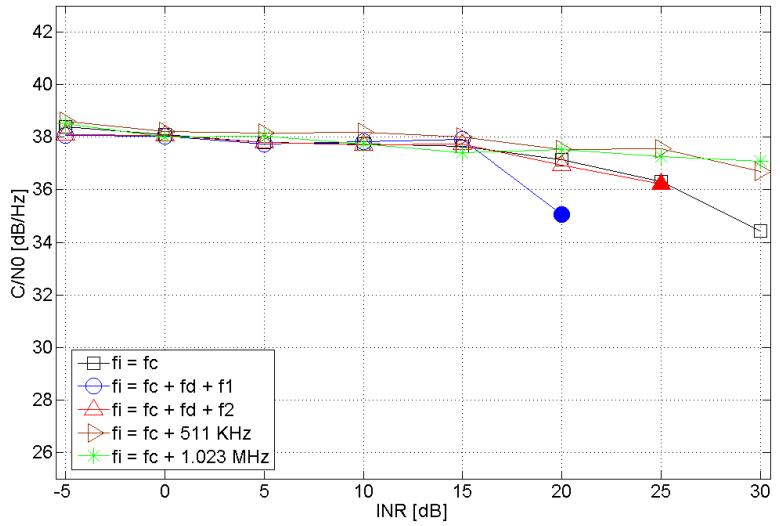

Figure 82: C/N0 measured at the MM1 receiver of a LE satellite as a function of the INR in the presence of PCWI with DC = 50%.

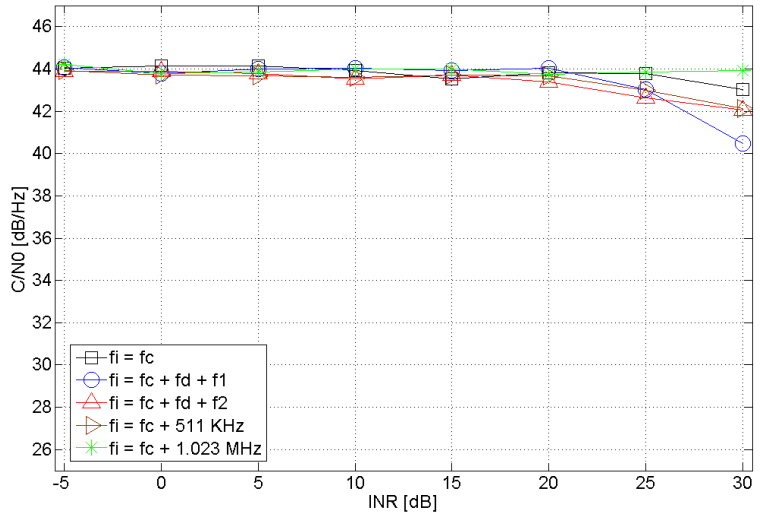

Figure 83: C/N0 measured at the MM2 receiver of a HE satellite as a function of the INR in the presence of PCWI with DC = 10%.

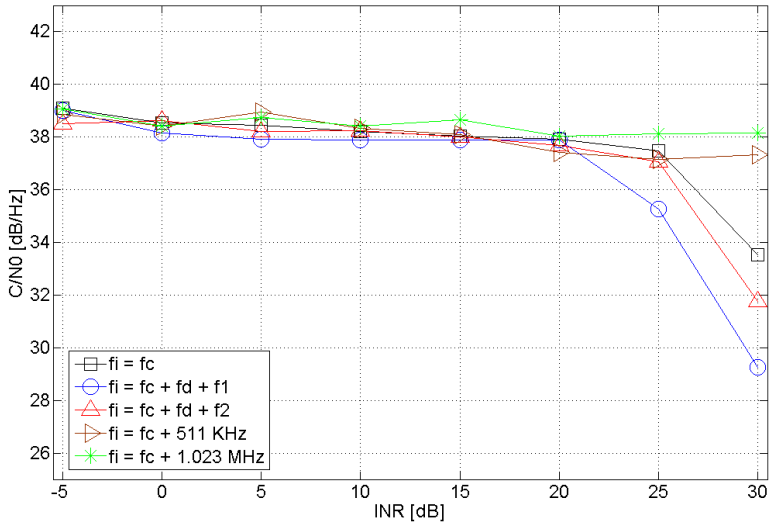

Figure 84: C/N0 measured at the MM2 receiver of a LE satellite as a function of the INR in the presence of PCWI with DC = 10%.

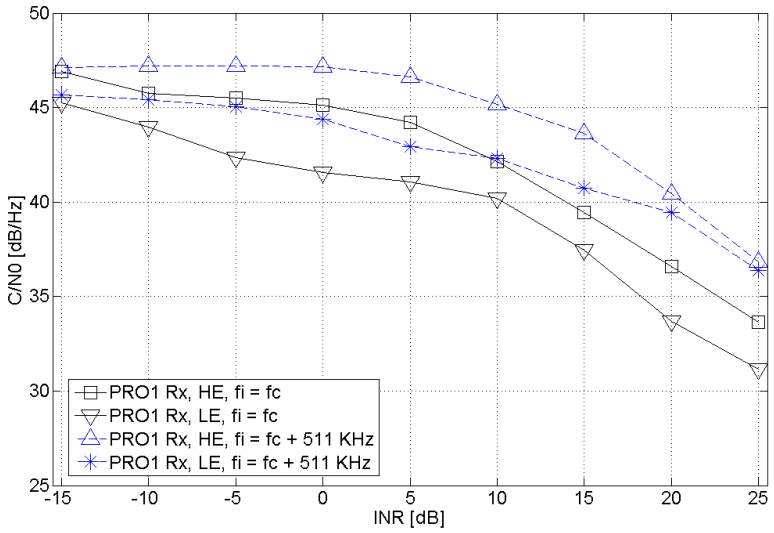

Figure 85: C/N0 measured at the PRO1 receiver of HE and LE satellites as a function of the INR in the presence of a DVB-T 3rd harmonic interference signal with $f_i = f_c$ or $f_i = f_c + 511$ KHz.

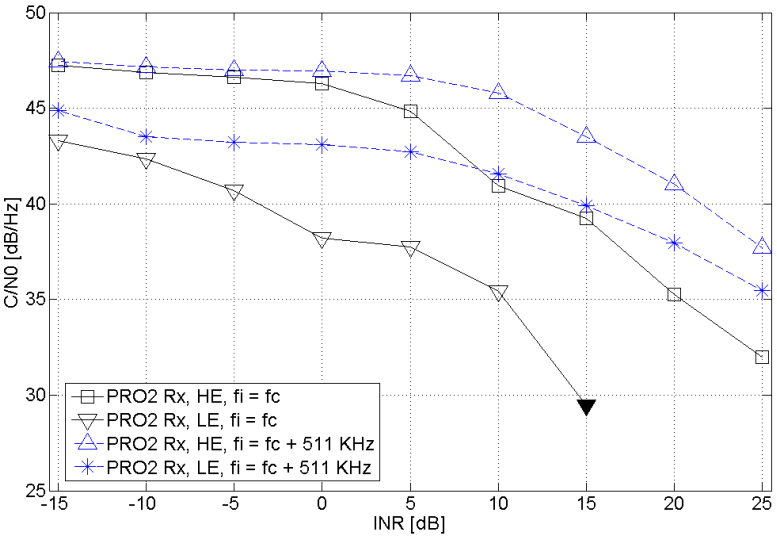

Figure 86: C/N0 measured at the PRO2 receiver of HE and LE satellites as a function of the INR in the presence of a DVB-T 3rd harmonic interference signal with $f_i = f_c$ or $f_i = f_c + 511$ KHz.

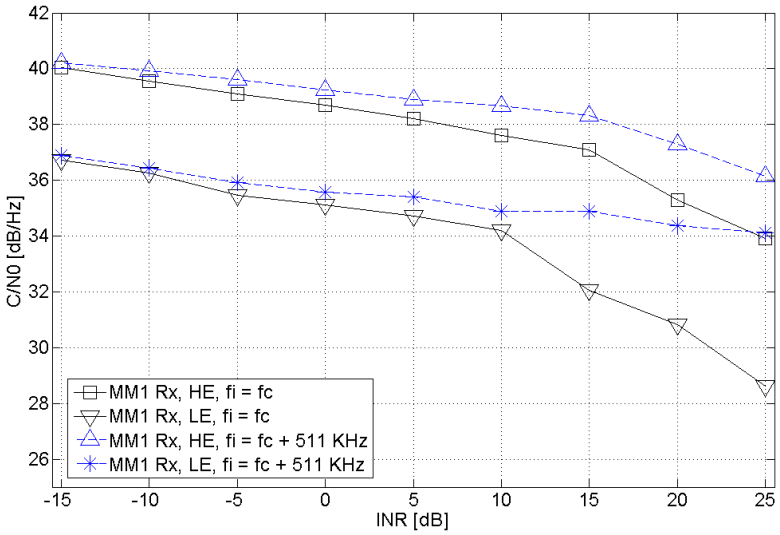

Figure 87: C/N0 measured at the MM1 receiver of HE and LE satellites as a function of the INR in the presence of a DVB-T 3rd harmonic interference signal with $f_i = f_c$ or $f_i = f_c + 511$ KHz.

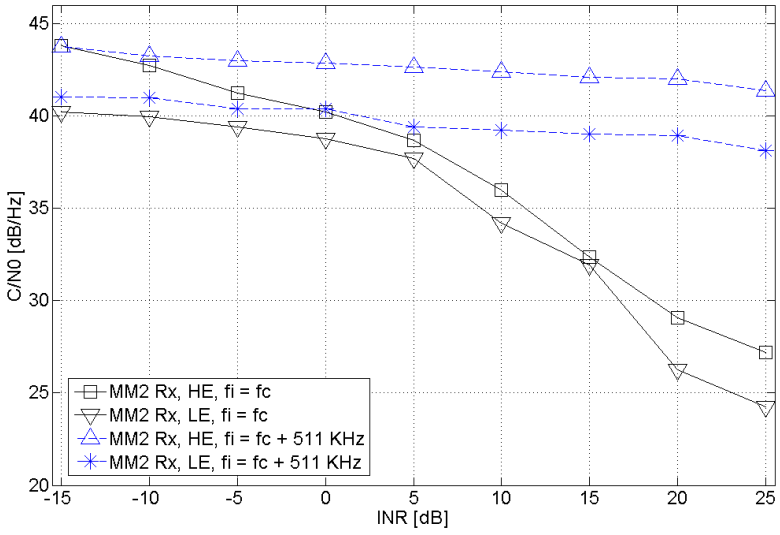

Figure 88: C/N0 measured at the MM2 receiver of HE and LE satellites as a function of the INR in the presence of a DVB-T 3rd harmonic interference signal with $f_i = f_c$ or $f_i = f_c + 511$ KHz.

ANNEX C: Tracking Simulation Results

A comprehensive display of the EVM performance of a GPS L1 satellite in the presence of an external interference is provided in this annex by means of novel simulation results. As described in section 5, three types of interference sources are considered in this work. These are CWI, PCWI and the 3rd harmonic of a DVB-T signal. The simulation scenarios correspond to the ones presented in section 5, except the evaluated tracking metric (estimated C/N0) is replaced by the EVM. Thus, the EVM performances of the GPS L1 receivers in the presence of CWI are plotted from Figure 89 to Figure 92 with simulation parameters defined in scenarios Exp1-Exp4 of Table 1. Subsequently, the PCWI effects on the EVM performance are displayed in Figures 93-95 corresponding to simulation scenarios Exp.5 - Exp.7 of Table 1. Finally, the EVM performance as a function of the SIR in the presence of an AWGN wideband signal and the 3rd harmonic of the DVB-T signal are plotted in Figures 96-97.

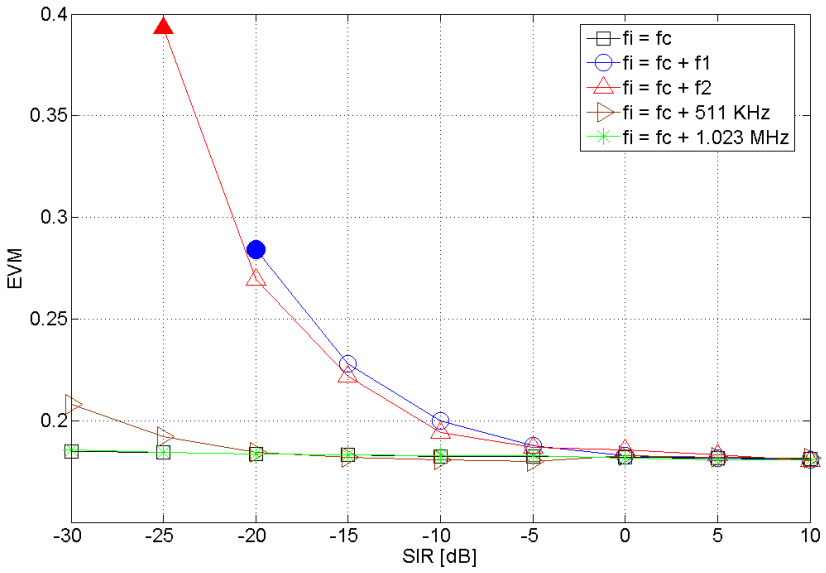

Figure 89: EVM performance as a function of the SIR of a CWI signal, which parameters are defined in scenario Exp.1 of Table 1.

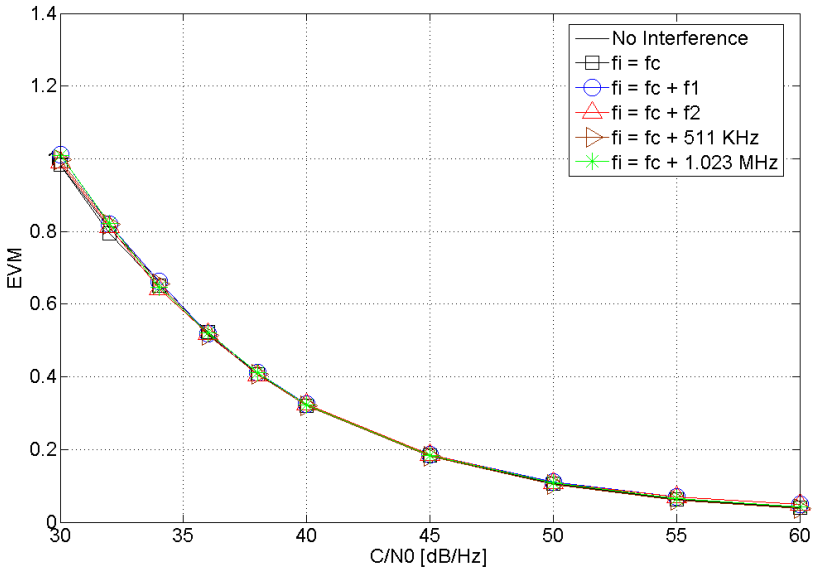

Figure 90: EVM performance as a function of the C/N0 input for a CWI signal with SIR $= 0$ dB, which parameters are defined in scenario Exp.2 of Table 1.

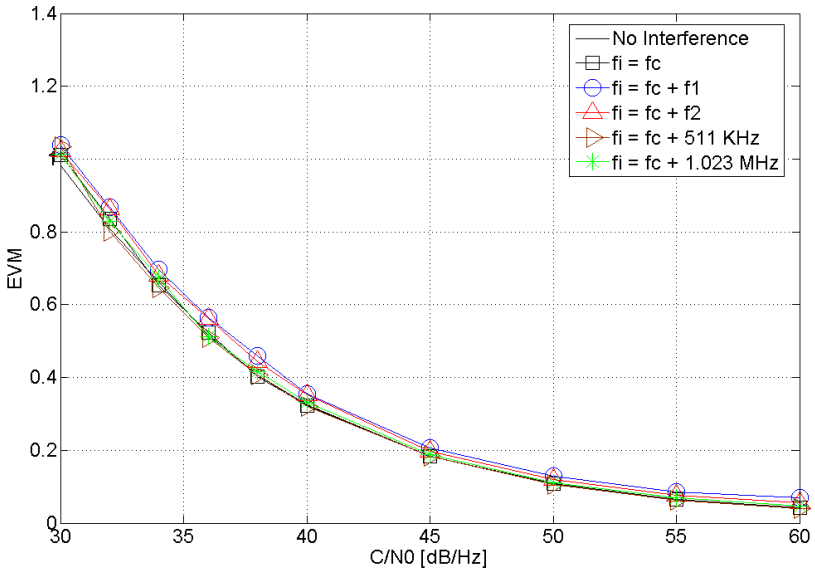

Figure 91: EVM performance as a function of the C/N0 input for a CWI signal with SIR $= -10$ dB, which parameters are defined in scenario Exp.3 of Table 1.

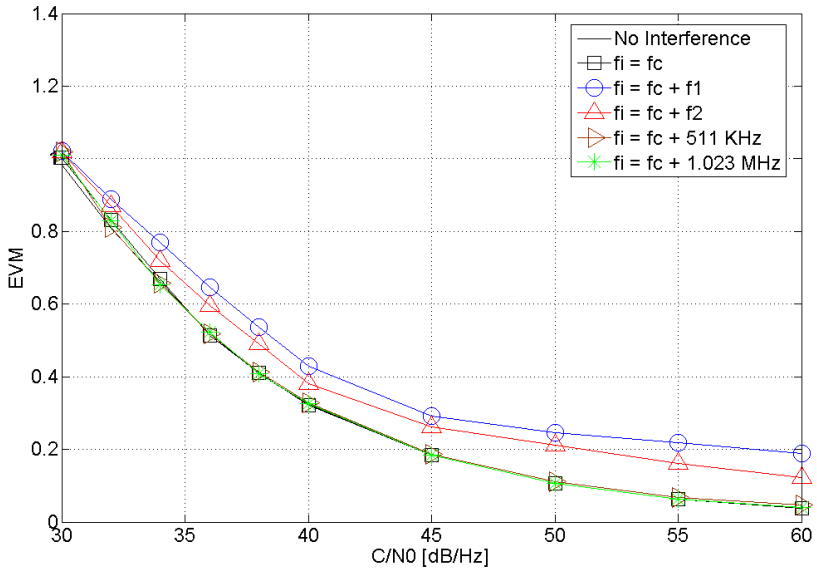

Figure 92: EVM performance as a function of the C/N0 input for a CWI signal with SIR $= -20$ dB, which parameters are defined in scenario Exp.4 of Table 1.

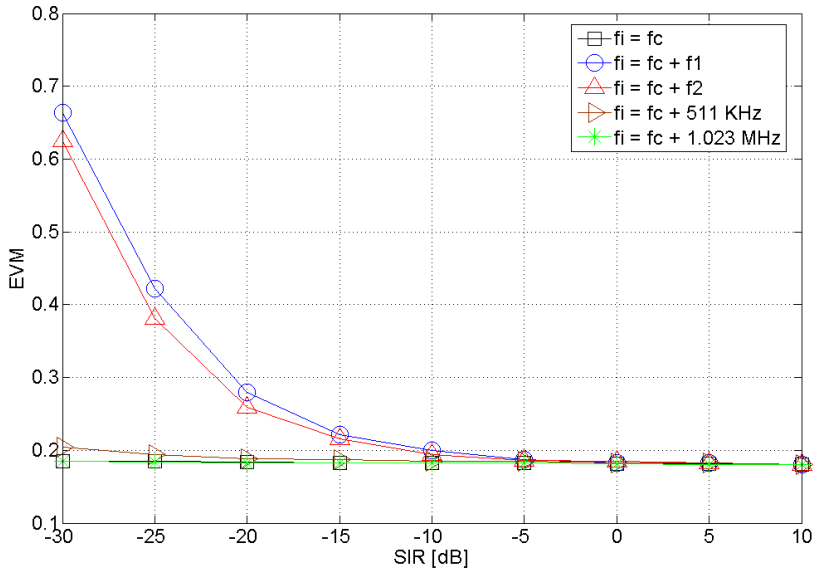

Figure 93: EVM performance as a function of the SIR of a PCWI signal, which parameters are defined in scenario Exp.5 of Table 1.

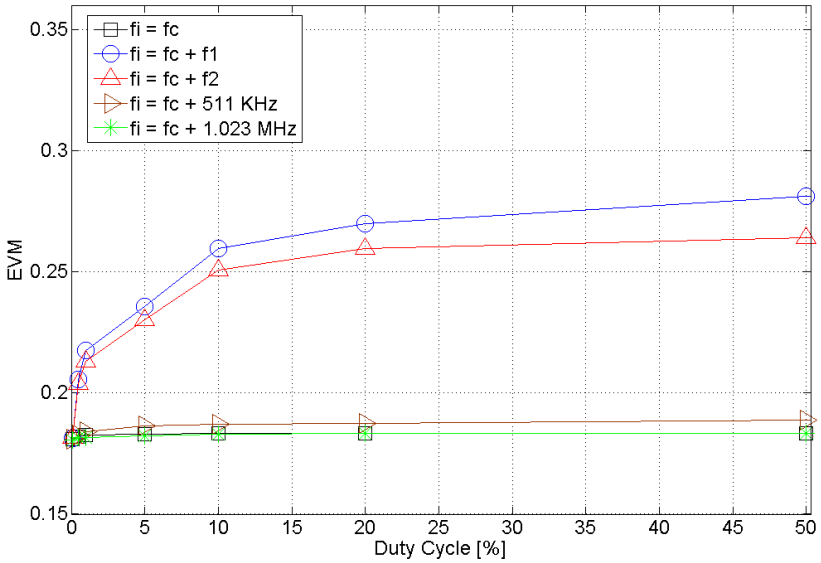

Figure 94: EVM performance as a function of the Duty Cycle of a PCWI signal with SIR $= -20$ dB ,which parameters are defined in scenario Exp.6 of Table 1.

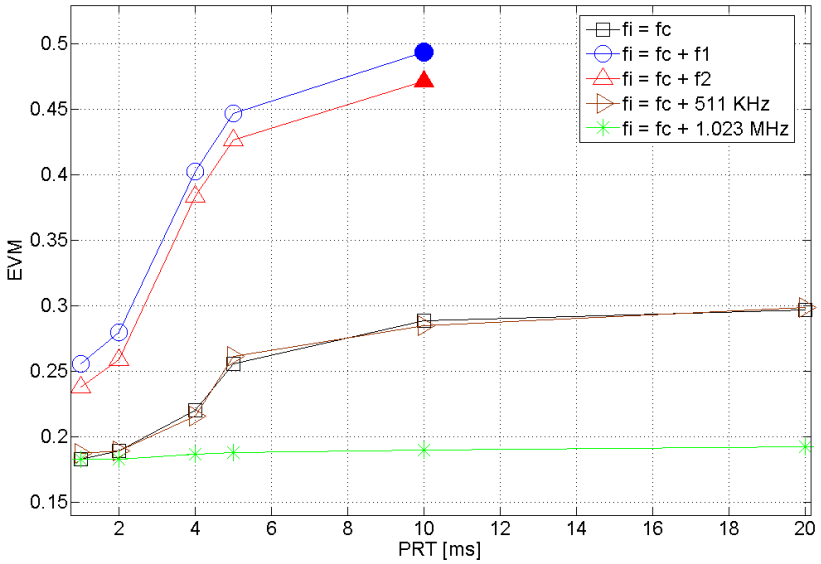

Figure 95: EVM performance as a function of the Pulse Repetition Time of a PCWI signal with SIR $= -20$ dB ,which parameters are defined in scenario Exp.7 of Table 1.

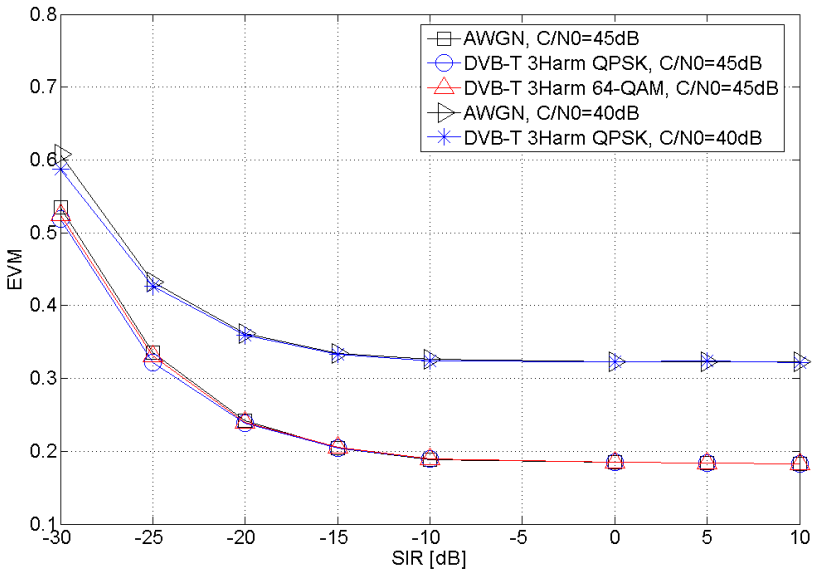

Figure 96: EVM performance as a function of the SIR of AWGN and DVB-T 3rd harmonic interference signals, which parameters are defined in scenario Exp.8 of Table 1.

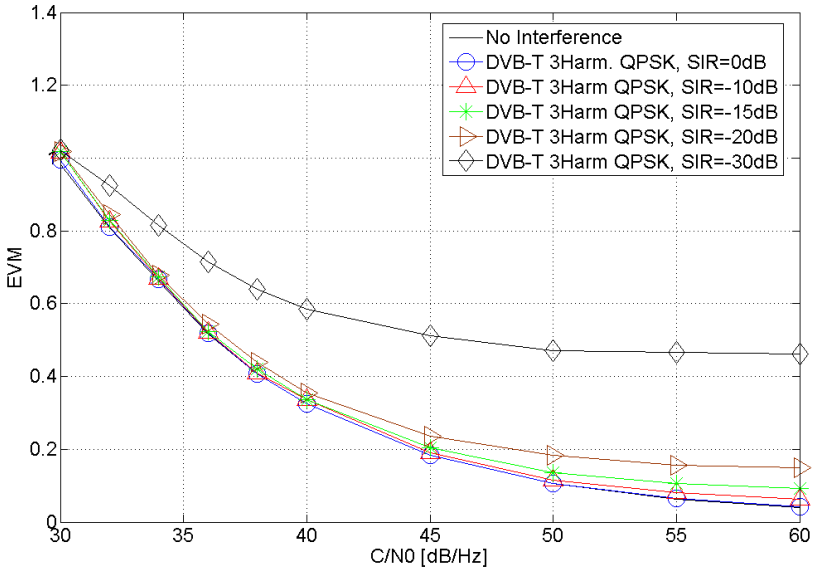

Figure 97: EVM performance as a function of the C/N0 for AWGN and DVB-T 3rd harmonic interference signals, which parameters are defined in scenario Exp.9 of Table 1.

References

[1] U. Kroener. Hardening of GNSS based trackers - final report. Technical report, IPSC-JRC, 2009.

[2] T.E. Humphreys, B.M. Ledvina, M.L. Psiaki, W. O'Hanlon, and P.M. Kintner. Assessing the spoofing threat: Development of a portable GPS civilian spoofer. *proc. ION/GNSS*, September 2008. Savannah, GA.

[3] H.L. Van Trees. *Detection, Estimation, and Modulation Theory - Part1*. Wiley, 2001.

[4] A. Polydoros and C. L. Weber. A unified approach to serial search spread-spectrum code acquisition - part i: General theory. *IEEE Transactions on Communications*, 32(5):542–549, May 1984.

[5] D. Borio. A statistical theory for GNSS signal acquisition. *PhD thesis*, March 2008.

[6] D. Borio. GNSS acquisition in the presence of continuous wave interference. *IEEE Transactions on Aerospace and Electronic Systems*, 46(1):47–60, January 2010.

[7] J. Jung. Implementation of correlation power peak ratio based signal detection method. *ION GNSS*, pages 486–490, Sep. 2004.

[8] K. Borre, D.M. Akos, N. Bertelsen, P. Rinder, and S.H. Jensen. *A Software-Defined GPS and Galileo Receiver: A Single Frequency Approach*. Birkhäuser, 2007.

[9] D. M. Akos, P.-L. Normark, J.-T. Lee, and K. G. Gromov. Low power global navigation satellite system (GNSS) signal detection and processing. *ION GPS*, pages 784–791, Sep. 2000.

[10] ETSI. Digital video broadcasting (DVB); framing structure, channel coding and modulation for digital terrestrial television. *EN 300 744*, 2004-2006.

[11] D. Borio, S. Savasta, and L. Lo Presti. On the DVB-T coexistence with galileo and GPS system. *proc. NAVITEC*, 2006.

[12] J.W. Betz. Effect of narrowband interference on GPS code tracking accuracy. In *Proceedings of ION 2000 National Technical Meeting*, 2000.

[13] J.G. Proakis and M. Salehi. *Digital Communications*. McGraw-Hill International Edition, 2008.

[14] Pauluzzi D. R. and N.C. Beaulieu. A comparison of snr estimation techniques for the AWGN channel. *IEEE Trans. on Communications*, 48(10):1681–1691, October 2000.

[15] M. Falletti E., Pini and Lo Presti L. Low complexity carrier to noise ratio estimators for GNSS digital receivers. *IEEE Trans. On Aerospace and Electronic Systems*, 2009.

[16] R.D. Gupta and D. Kundu. Generalized exponential distribution: existing results and some recent developments. *Journal of Statistical Planning and Inference*, 137(11):3537–3547, 2007.

[17] R.D. Gupta and D. Kundu. Closeness of gamma and generalized exponential distribution. *Communications in statistics. Theory and methods*, 32(4):705–721, 2003.

European Commission

Joint Research Centre – Institute for the Protection and Security of the Citizen
Impact Study of Unintentional Interference on GNSS Receivers
M. Wildemeersch, E. Cano Pons, A. Rabbachin and J. Fortuny Guasch
EC Joint Research Centre, Security Technology Assessment Unit

Luxembourg: Publications Office of the European Union
2010 – 96 pp. – 21 x 29.7 cm
EUR – Scientific and Technical Research series – ISSN 1018-5593
ISBN 978-92-79-19523-5
doi:10.2788/57794

Abstract

This work has been performed in the context of an Administrative Arrangement for DG HOME. The overall scope is to perform an impact assessment of radio frequency (RF) interference on critical infrastructures relying on GNSS-services for timing and synchronization purposes. In WP3, the analysis has been divided into the impact of intentional interference on critical infrastructures presented in WP3.1 and the analysis of unintentional interference, covered in this report. DVB-T has been identied as the most important source of unintentional interference in the GNSS frequency bands and therefore a special attention is paid to this interference source.

The main motivation to assess the performance reduction of receivers due to unintentional interference, is related to the high probability of these events. Unintentional interference stems from out-of-band emissions or spurious transmissions. Four different scenarios have been considered in this work, covering (i) additive white Gaussian noise, (ii) continuous wave interference, (iii) pulsed continuous wave nterference and (iv) interference that stems from the third harmonic of DVB-T transmissions. All these scenarios are highly relevant and are frequently observed in realistic signal conditions. The scenario of DVB-T interference receives most of the attention in this work, since DVB-T has become the most widely adopted digital terrestrial television broadcasting standard in the world. Harmonics of the DVB-T signal could possibly fall together with the GPS L1 or Galileo E1 bands and as such become a threat. DVB-T services are operational in more than 40 countries, with more than 75% of the deployment in Europe. In the coming years, DVB-T is expected to be deployed in more than 100 countries.

In the frame of this work, different tools have been developed to quantify the impact of unintentional interference. First, a laboratory testbed has been set up, that allows to take real GPS L1 signals, combine them with synthetic interfering signals and test the robustness of different commercial and professional receivers. Further, in order to have a full control of the signal characteristics and the implementation details of the receiver, a simulation platform has been developed. This simulation tool generates GNSS as well as interfering signals, and observes consequently the impact on the acquisition or tracking performance for different receiver implementations. Finally, since it is difcult to reach statistical signicance for the acquisition performance, an analytical tool has been developed allowing to evaluate the effects of interference.

This report summarises the relevant results for the four considered scenarios. For the assessment of the acquisition performance the analytical tool and the simulation platform have been used. In order to evaluate the tracking performance, experimental work has been conducted with real receivers and simulations have been performed. For the acquisition, the report quanties how much the probability of detection and the probability of false alarm are affected by the presence of interference. For the tracking, the main result of this report is the quantication of the signal degradation in terms of C=N0 and in terms of the variance of the position solution. In the scenario of DVB-T Page 2 of 94 WP3.2 interference, the degradation of the signal quality has been determined as a function of the DVB-T third harmonic power and the distance between the victim receiver and the DVB-T base station.

The mission of the JRC is to provide customer-driven scientific and technical support for the conception, development, implementation and monitoring of EU policies. As a service of the European Commission, the JRC functions as a reference centre of science and technology for the Union. Close to the policy-making process, it serves the common interest of the Member States, while being independent of special interests, whether private or national.

LB-NA-24742-EN-C

JRC
EUROPEAN COMMISSION

Publications Office

ISBN 978-92-79-19523-5